

G21.042
PAU

CENTRAL LIBRARY
TEZPUR UNIVERSIT
Accession No. T 216
Date 06/03/13

CENTRAL LIBRARY, T. U.
ACC. NO.....

**SYNTHESIS OF CARBON NANOTUBES FROM
PLANT BASED PRECURSORS AND THEIR
APPLICATION IN ORGANIC PHOTOVOLTAIC
CELLS AND BIO-DIESEL STORAGE**

A thesis submitted in partial fulfillment
of the requirements for the degree of
Doctor of Philosophy

Samrat Paul

Registration Number 001 of 2011



School of Engineering

Department of Energy

Tezpur University

May 2012

Abstract

Synthesis of carbon nanotubes from plant based precursors and their application in organic photovoltaic cells and bio-diesel storage

Sustainability of any civilization depends upon its energy resources, and the technological capital for their conversion and conservation. Till present day, the need for energy resources to support healthy and quality life for humankind has shown an ever-increasing trend. The depleting conventional energy resources cannot meet the future energy needs of our country and the world as a whole. This has led to an intensive search to identify new non-conventional renewable energy resources and conversion techniques to transform these resources to useful forms. Solar, wind, biomass, geothermal, ocean wave and tidal are few of the potential energy resources that have been identified. These renewable resources are environment-friendly as compared to the conventional fossil fuel resources. But, renewables have some constraints such as non-equitable distribution throughout the globe, low conversion efficiency and high cost. The “nano” science and technology provides a scope to address many of the multi-dimensional problems related to cost and efficiency of the renewable energy conversion systems and devices. Carbon based nanomaterials like carbon nanotube, carbon nanofibers, carbon nanobeads etc., because of their unique physico-chemical characteristics, have shown immense potential in the development of various energy systems adding a new dimension to the search for better systems and technologies. Carbon nanotube (CNT) is one of the most promising candidates out of all the nanoforms of carbon. But, all the carbon based nanomaterials are synthesized using low molecular weight hydrocarbons precursors derived from petroleum sources. It is the demand of the hour to develop and design techniques which have green origin and which follow green protocols. Thus, ***as a first step, it is endeavoured to look for suitable renewable green precursors for the synthesis of CNT. This forms the first objective of the thesis. The second objective is to synthesize CNTs from the selected plant precursors.*** Few plant based precursors have already been successfully used to synthesize multiwalled carbon nanotube (MWCNT). A number of technologies such as chemical vapour

deposition (CVD), physical vapour deposition (PVD) etc. have been used. Out of these the CVD technique seems to be most appropriate. A CVD system with provision for controlling the input parameters through suitable mechanism is employed for this. Such a system facilitates in the determination of the optimum conditions for synthesis of CNTs having high quality and yield. This is expected to help in achieving the ***third objective of the thesis, which is to optimize the synthesis parameters*** (viz. temperature, flow rate, precursor type used, etc.). It may be noted that renewable precursors consist of a mixture of a number of hydrocarbon molecules. This makes the optimization process for synthesis of CNTs from renewable precursors highly demanding. Hence to reduce the time, effort and resources which are needed in the optimization process a resort to suitable statistical techniques is essential. The optimization process is complemented by characterization of the MWCNTs synthesized under different conditions. Characterization of MWCNTs helps in ascertaining identification of their uniqueness and suitability to different energy applications. It is expected that only a few of them will satisfy the requirements for a particular application. One of the main targets of the thesis is to demonstrate the applicability of these CNTs synthesized from plant precursors in renewable energy systems and applications. Hence ***the final objective of the thesis is to demonstrate the application of MWCNTs synthesized from plant precursors in energy systems*** like organic photovoltaic cells, fuel cell, heterogeneous catalysis etc.

The thesis, consisting of six chapters and four appendices, dwells upon the above mentioned issues in detail as outlined below.

Chapter 1: Introduction

It introduces the theme of the thesis including information about different energy applications of CNTs. It also describes the need and importance of renewable plant based precursors for CNT synthesis.

Chapter 2: Synthesis of MWCNTs from renewable plant based green precursor.

This chapter starts with selection of plant precursors from different parts of north-east India. Few suitable plant varieties were screened on the basis of availability, alternative commercial applications and oil content for carbon nanotube synthesis. In the

next section of the chapter the synthesis of catalyst, and development & modification of the CVD setup for synthesis of CNT from plant precursors are discussed in detail.

The morphology and yield of CNTs synthesized from each precursor is carefully analyzed to sort them out based on suitability of each one of these for a particular application envisaged in the thesis.

Chapter 3: Optimization of process parameters for synthesis of MWCNTs from renewable plant based green precursors using Taguchi Robust Technique.

This chapter is dedicated to refinement of the process of synthesis by optimizing the process parameters like temperature of synthesis, flow rate of carrier gas, catalyst type and precursor type both for improving yield and quality of MWCNT using Taguchi robust technique

Chapter 4: Application of functionalized-MWCNTs in organic photovoltaic cells

The application of MWCNTs synthesized from plant precursors in photovoltaic cells are studied. The chapter also describes a method to cut MWCNTs using simple chemical route.

Finally, the chapter describes the application of the modified MWCNTs in OPVs. The device with functionalized-cut MWCNTs showed best performance.

Chapter 5: Application of antioxidant grafted MWCNTs in biodiesel storage

This chapter discusses a new nanomaterial structure which is engineered to contain a magnetic nanoparticle and an antioxidant attached to a substrate. The idea has a potential to make the antioxidant reusable without affecting the performance of the engine.

This chapter also dwells upon the basics of biodiesel storage issues and analyzes the results of experiments which were designed to investigate the efficacy of the antioxidant material system.

Chapter 6: Conclusion and future work

This chapter concludes about the strengths and discusses about the scope of improvement in the quality and yield of MWCNTs from plant precursors. The prospects of

utilization and application of MWCNTs for energy systems have been discussed. In this work attempts to provide options for application of MWCNT in energy systems have been made. This chapter discusses the future scope of improvement in the energy systems based on CNTs.

Appendix I: Synthesis of CNTs from waste Polypropylene and Polyethylene terephthalate PET products

A method to utilize solid waste products like Polypropylene (PP) and Polyethylene terephthalate (PET) for synthesis of MWCNT has been explained.

Appendix II: Application of MWCNT in Alkaline fuel cell electrode.

It discusses the results of an attempt to use MWCNT in alkaline fuel cell electrode



DECLARATION BY THE CANDIDATE

The thesis entitled "**Synthesis of carbon nanotubes from plant based precursors and their application in organic photovoltaic cells and bio-diesel storage**" is being submitted to the Tezpur University in partial fulfillment for the award of the degree of Doctor of Philosophy in Energy is a record of bonafide research work accomplished by me under the supervision of Dr. S. K. Samdarshi, Professor. Department of Energy, Tezpur University.

All helps received from various sources have been duly acknowledged.

No part of this thesis has been submitted elsewhere for award of any other degree.

Date:

Place: Tezpur

(Samrat Paul)

Department of Energy

Tezpur University

Napaam 784 028

Assam, India.



TEZPUR UNIVERSITY
(A Central University established by an Act of Parliament)
NAPAAM, TEZPUR - 784028
DISTRICT : SONITPUR :: ASSAM :: INDIA

Ph 03712 - 267004
03712 - 267006
Fax 03712 267006
03712 - 267005


e-mail : adm@agnigarh.tezu.ernet.in

CERTIFICATE OF THE SUPERVISOR

This is to certify that the thesis entitled, "**Synthesis of carbon nanotubes from plant based precursors and their application in organic photovoltaic cells and bio-diesel storage**" submitted to the Tezpur University in the department of Energy under the School of Engineering in partial fulfillment for the award of the degree of Doctor of Philosophy in Energy is a record of research work carried out by Mr. Samrat Paul under my personal supervision and guidance. He has complied with all the requirements as laid down in the regulations of Tezpur University for the award of Doctor of Philosophy in Energy (School of Engineering) including course work.

All helps received by him from various sources have been duly acknowledged. No part of this thesis has been reproduced elsewhere for award of any other degree.

Date: 18/05/2012
Place: Tezpur


(Dr. S. K. Samdarshi)
Professor
School of Engineering
Department of Energy
Tezpur University
Napaam 784 028, India



TEZPUR UNIVERSITY


(A Central University established by an Act of Parliament)
NAPAAM, TEZPUR - 784 028
DISTRICT SONITPUR ASSAM INDIA

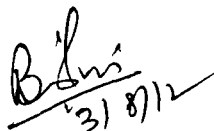
Ph 03712 - 267004
267005
Fax 03712 - 267006
267005
e-mail adm@agnigarh tezu ernet in

Certificate of the External Examiner and ODEC

This is to certify that the thesis entitled "*Synthesis of carbon nanotubes from plant based precursors and their application in organic photovoltaic cells and bio-diesel storage*" submitted by **Mr. Samrat Paul** to Tezpur University in the Department of Energy under the school of Engineering in partial fulfillment of the requirement for the award of the degree of Doctor of Philosophy in Energy has been examined by us on August 03, 2012 and found to be satisfactory

Signature of:


Principal Supervisor


External Examiner

Date. _____

Acknowledgement

I would like to express my deep sense of gratitude to my supervisor Professor. S.K Samdarshi for his inspiring guidance and giving me the opportunity to work in his laboratory. It would have not been possible for me to bring out this thesis without his help, support, and constant encouragement throughout the research work. I am also indebted to family members of my supervisor specially Madam Samdarshi, for their moral support during the work.

I am thankful to Prof. B. Konwar, Department of MBBT to carry out antioxidant potency analysis in his lab. I would remain ever grateful to Dr. R.B Srivastava, Directorate of Life Sciences, DRDO, New Delhi for his valuable suggestions. My sincere thanks goes to Prof. B. Gosh, Director, School for Energy Studies, Jadavpur University, Kolkata for short term training on PVD system in his Lab.

I would like to thank Prof. D. C. Barua, Head, Department of Energy, Prof. D. Deka, Dr. R. Katoki (Assoc. Prof), Dr. D. Bora, (Assoc. Prof.) Mr. S. Mahapatra (Asstt .Prof.) and Mr. P. K. Choudhury (Asstt .Prof.) of Department of Energy, Tezpur University, for their suggestions and discussions during my work. I am grateful to Mr. Tapan borah, (Technical Asstt.) Department of Energy, for his help and suggestions.

I am thankful to my Doctoral Committee members Prof. D. Deka, Department of Energy and Prof A. Kumar, Department of Physics, Tezpur University, for their kind support and encouragement.

I am thankful to Dr. P J Lahkar, Mr. Anuj Chaturvedi, Rangith G. Nair my research colleagues, and Bhiba Boro, Sunny Bhorali, Mr. Rao and Mr. Bhamu, M. Tech students of S&IEM Lab. for their help suggestions and encouragement throughout my research work. I am grateful to Miss Bijumani Rajbongshi, research scholar, S&IEM lab, Department of Energy for her help. I am also thankful to Mr. Birinchi Bora, SRF of S&IEM Lab. for his help. My thanks also go to Mr Saurobh Kr. Karn, fourth year B. Tech. students of Mech. Engg. for his help in fabrication of CVD setup in workshop of Department of Mechanical Engineering .

Also I am very much thankful to staff members, research scholars, M.Tech students of Energy department and my friends and well wishers of this University for their support and encouragement.

My special thanks go to non-teaching staff member of our department, specially Mrs. Pronita S Talukdar, Jogen Das, and others for their timely help during my work,

I would like to thank my friends Dr. J P Saikia, Mr. Alokmani Tripathi, Juthika Boro, Dr. Sudhir Rai, Mr. Rahul Sing Chutia, and many others for their help and support

I am grateful to my parents and my sister and other members of my family for their blessings, love and support. I am thankful to my friend Mahua Gupta Choudhury for her support and encouragement to carry out my work,

Last but not least I would like to thank almighty for everything.

Samrat Paul

Academic acknowledgments

List of publications

1. Ranjith G Nair, Samrat Paul and S K Samdarshi; High UV/visible light activity of mixed phase titania: A generic mechanism. *Solar Energy Materials and Solar Cells (Elsevier)* –95 (2011) 1901-1907
2. Samrat Paul and S K Samdarshi; A green precursor for Carbon Nanotube synthesis. *New Carbon Materials (Elsevier)*- 26 (2011) 85-88.
3. Samrat Paul and S K Samdarshi; Synthesis of carbon microtubes from *cocos nucifera* L. oil. *New Carbon Materials (Elsevier)* -25 (2010) 321-324.
4. Jyoti Prasad Saikia, Samrat Paul, Bolin Kumar Konwar and Sanjoy Kumar Samdarshi; Ultrasonication: enhances the antioxidant activity of metal oxide nanoparticles. *Colloids and Surfaces B: Biointerfaces (Elsevier)* - 79(2010) 521-523.
5. Jyoti Prasad Saikia, Samrat Paul, Bolin Kumar Konwar and Sanjoy Kumar Samdarshi; Nickel oxide nanoparticles: A novel antioxidant. *Colloids and Surfaces B: Biointerfaces (Elsevier)* - 78 (2010) 146-148.
6. Samrat Paul, Jyoti Prasad Saikia, Sanjoy Kumar Samdarshi and Bolin Kumar Konwar; Investigation of antioxidant property of iron oxide particles by 1'-1'diphenylpicryl-hydrazyle(DPPH)method. *Journal of Magnetism and Magnetic Materials (Elsevier)*– 321 (2009) 3621-3623.

Patent

1. R B Srivastava, S K Samdarshi, Samrat Paul, “A process for preparing carbon nanotubes from non-biodegradable polypropylene and polytetraheplelet”. Patent Application No: 430/DEL/2011 of 21.02.2011

Awards and prizes

1. Indian Science Congress Association (ISCA)-Young Scientist Award in Engineering Science Section; 99th Congress of ISCA held at Bhubhaneshwar – 2012 ` *“Polyaniline and functionalized carbon nanotube for novel organic photovoltaic cells”*

2. National Academy of Sciences, India - Swarna Jayanti Puruskar in Physical Sciences Section; 80th Annual session of National Academy of Sciences, India held at Jaipur National University, Jaipur – 2010
“Green synthesis of CNTs and their application in storage of Mesua ferrea oil”
3. Best Poster Presentation Award in Engineering Science section of 96th conference of Indian Science Congress Association (ISCA), held at North-east Hill University (NEHU) Shillong – January 2009
“Effect of aging time in hydrothermal synthesis of iron oxide particles”

Contents

Abstract	i-iv
Declaration and Certificates	v-vii
Acknowledgement	viii-ix
Academic acknowledgements	x-xi
Table of Contents	xii-xv
List of Tables	xvi
List of Figures	xvii-xix
Abbreviations and symbols used	xx-xxi

Chapter	Page No.
1 Introduction	1.1-1.23
1.1 Impact of materials on energy, environment and sustainability	1.1
1.2 Renewable energy resources and potential	1.2
1.3 Carbon nanotube	1.2
1.3.1 Properties of CNT	1.4
1.3.2 Synthesis of carbon nanotubes	1.5
1.4 Application of carbon nanotubes in selected RE technology	1.7
1.4.1 CNT in organic photovoltaic (OPV)	1.7
1.4.2 Bio-energy and biofuels	1.11
1.5 Origin of present work and objectives	1.15
1.6 Summary of the thesis	1.16
References	1.19
2 Synthesis of carbon nanotubes from renewable plant precursors	2.1-2.19
2.1 Introduction	2.1
2.2 Materials and method	2.3
2.2.1 Chemicals and reagents used	2.3
2.2.2 Selection of plant precursor	2.3
2.2.3 Extraction of oil	2.4

2.2.4	Synthesis of Fe ₂ O ₃ nanocatalyst for CNT synthesis	2.4
2.2.5	CVD setup and its modification for plant precursors	2.5
2.2.6	Synthesis and purification of CNT	2.6
2.2.7	Characterization	2.6
2.3	Results and discussion	2.7
2.3.1	Selection of plant precursor and extraction of oil	2.7
2.3.2	Characterization of Fe ₂ O ₃ nanocatalyst	2.8
2.3.3	Modification of CVD setup for plant precursors	2.9
2.3.4	Characterization of CNT synthesized	2.12
2.4	Conclusion	2.14
	References	2.16
3	Optimization of process parameters for synthesis of MWCNTs from renewable plant based green precursors using Taguchi robust method	3.1-3.20
3.1	Introduction	3.1
3.2	Materials and method	3.3
3.2.1	Taguchi robust method	3.3
3.2.2	Process parameters to be optimized	3.5
3.2.3	Design of L9 experiments	3.5
3.2.4	Synthesis of catalyst	3.6
3.2.5	Synthesis of CNT using CVD technique	3.7
3.3	Results and discussion	3.7
3.3.1	L9 experiments	3.7
3.3.2	S/N calculations	3.9
3.3.3	Effect of each parameters	3.9
3.3.4	Yield at best conditions	3.15
3.4	Conclusion	3.17
	References	3.19
4	Application of functionalized and cut-MWCNTs in organic photovoltaic cells	4.1-4.25

4.1	Introduction	4.1
4.2.	Materials and method	4.6
4.2.1.	Chemicals and reagents used	4.6
4.2.2 .	Synthesis of MWCNTs	4.7
4.2.3.	Functionalization and cutting of MWCNTs	4.7
4.2.4.	Synthesis of PANI nanoparticles	4.7
4.2.5.	Composite Preparation	4.9
4.2.6.	Device Fabrication	4.9
4.2.7.	Characterization	4.10
4.2.8.	Characteristics of fabricated solar cell devices	4.11
4. 3.	Results and discussion	4.12
4.3.1.	Characterization of nanoparticles	4.12
4.3.2.	Current-voltage Characteristics of fabricated OPV cell	4.18
4.4	Conclusions	4.21
	References	4.23
5	Application of antioxidant grafted MWCNTs in biodiesel storage	5.1-5.17
5.1	Introduction	5.1
5.2.	Materials and method	5.2
5.2.1.	Chemicals and reagents used	5.2
5.2.2.	Synthesis of metal oxide nanoparticles	5.3
5.2.3.	Synthesis of MWCNTs	5.3
5.2.4.	Proposed design of the heterogenous magnetically separable nanomaterial antioxidant	5.3
5.2.5.	Grafting of BHT in MWCNT	5.4
5.2.6.	Proposed method for antioxidant potency determination for nanoparticles	5.4
5.2.7.	Oxidation stability analysis of biodiesel	5.5
5.3.	Results and discussion	5.7
5.3.1.	Characterization of nanomaterials	5.7
5.3.2.	Antioxidant potency assay	5.12

5.3.3. Oxidation stability analysis	5.13
5.4 Conclusion	5.15
References	5.17
6 Conclusion and future work	6.1-6.3
6.1 Conclusion	6.1
6.2 Future work	6.3
Appendix I	A1.1-A1.6
Appendix II	A2.1-A2.3

List of Tables

Table	Title	Page No.
1.1	Some of the important properties of CNTs	1.5
1.2	Comparison of CNT synthesis techniques	1.6
2.1	Selected plant species along with their oil content, ash content, viscosity and the major fatty acid composition.	2.8
2.2	Yield of CNT from different plant based precursors	2.13
3.1	Different parameters to be optimized for optimum yield.	3.5
3.2	L9 table for precursors with oleic acid as the major fatty acid constituent	3.6
3.3	L9 table for precursors without oleic acid as the major fatty acid constituent	3.7
3.4	S/N ratio for first Taguchi L9 experiment	3.10
3.5	S/N ratio for second Taguchi L9 experiment	3.15
3.6	Effect of parameters of synthesis of CNT for first Taguchi L9 experiment	3.15
3.7	Effect of parameters of synthesis of CNT for second Taguchi L9 experiment	3.16
3.8	Yield of CNT at best conditions for first Taguchi L9 experiment	3.17
3.9	Yield of CNT at best conditions for second Taguchi L9 experiment	3.17
4.1	Different photoactive materials used in OPVs along with reported I-V characteristics and fill factor of the fabricated device	4.3
4.2	Power conversion efficiency, fill factor and gain w.r.t device A	4.20

List of Figures

Figure	Title	Page No.
Figure 1.1	Global potential important RE resources, taken from Peter Milson's report on 'Overview of RE potential in India', (GENI, 2006)	1.3
Figure 1.2	Schematic diagram explaining a hexagonal sheet of graphite 'rolled' to form a carbon nanotube	1.4
Figure 1.3	Number of papers published in scientific journals in the area of OPVs from January 2000 to March 2012 (Search done through ISI, Web of Science)	1.12
Figure 1.4	Number of papers published in scientific journals in the area of biodiesel storage from January 2000 to March 2012	1.13
Figure 2.1	Schematic diagram of CVD unit (1-carrier gas cylinder, 2-gas regulator, 3-manometer, 4-flowmeter, 5- bubbler, 6-quartz tube, 7- 0.5 kW furnace, 8- 5 kW furnace, 9- precursor on quartz boat, 10- catalyst on quartz boat)	2.6
Figure 2.2	XRD analysis of the synthesized iron oxide particles prepared at different temperatures – S1 (450 °C), S2 (550 °C) and S3 (650 °C).	2.9
Figure 2.3	SEM analysis of the synthesized iron oxide particles prepared at different synthesis temperatures, S1 (450 °C), S2 (550 °C) and S3 (650 °C)	2.10
Figure 2.4	TEM image of the iron oxide nanoparticles (S3)	2.10
Figure 2.5	Modified CVD setup (stage-1): a) schematic representation of the setup and b) indigenously modified set up	2.11
Figure 2.6	Modification of CVD setup (stage 2)	2.12
Figure 2.7	SEM micrographs of the CNTs synthesized from plant precursors	2.14
Figure 2.8	TEM micrographs of the CNTs synthesized using plant	2.15

	precursors	
Figure 3.1	Schematic representation of static and dynamic problems by using P-diagram	3.2
Figure 3.2	TEM micrographs for first Taguchi L9 experiments	3.11
Figure 3.3	TEM micrographs for second Taguchi L9 experiments	3.12
Figure 3.4	SAD pattern of synthesized MWCNTs corresponding to first Taguchi experiment for precursors containing oleic acid as major fatty acid composition	3.13
Figure 3.5	SAD pattern of synthesized MWCNTs corresponding to second Taguchi experiment for precursors without oleic acid as their major composition	3.14
Figure 3.6	Graphical representation of average response for each parameter obtained from first L9 experiment	3.16
Figure 3.7	Graphical representation of average response for each parameters obtained from second L9 experiment	3.16
Figure 4.1	Different architecture of OPV device: a) single active layer, b) bi-layer consisting of donor and sceptor molecules and c) dispersed heterojunction of donor and acceptor molecules	4.2
Figure 4.2	Mechanism of CNT-Polymer blend solar cell : a) Schematic of bulk heterojunction along with energy band diagram, and b) Energy band diagram of P3OT based OPV cell	4.4
Figure 4.3	Schematic diagram showing cutting of MWCNTs using HNO_3	4.8
Figure 4.4	Schematic diagram showing functionalization of MWCNTs using H_2SO_4	4.8
Figure 4.5	Schematic representation of the fabricated OPV devices	4.10
Figure 4.6	Potentiostat/galvanostat along with PC control for IV characteristics of fabricated OPV devices	4.11
Figure 4.7	Characterization of MWCNTs synthesized using Sesamum indicum oil (a) SEM micrograph with EDX analysis (inset), (b) TEM micrograph	4.12

Figure 4.8	Effect of ultrasonication in chemically cutting of MWCNT	4.14
Figure 4.9	XRD analysis of MWCNT and fc-MWCNT	4.15
Figure 4.10	FTIR study of fc-MWCNTs and pristine MWCNTs	4.16
Figure 4.11	SAD pattern of a) pristine MWCNTs, and b) fc-MWCNTs	4.17
Figure 4.12	XRD analysis of PANI synthesized using solvent ethanol	4.17
Figure 4.13	SEM micrograph of synthesized PANI nanoparticles	4.18
Figure 4.14	TEM micrograph of synthesized PANI nanoparticles	4.18
Figure 4.15	Current-voltage characteristics of the device A, B, C and D	4.21
Figure 4.16	The energy band diagram of the fabricated device D	4.21
Figure 5.1	Proposed antioxidant nanocomposite	5.4
Figure 5.2	Schematic diagram of Rancimat apparatus.	5.6
Figure 5.3	Photograph of Rancimat apparatus	5.6
Figure 5.4	TEM micrograph of iron oxide nanoparticles synthesized at 650 °C	5.8
Figure 5.5	XRD analysis of iron oxide nanoparticles	5.8
Figure 5.6	TEM micrograph of nickel oxide nanoparticles synthesized at 650 °C (Scale inset = 100 nm)	5.8
Figure 5.7	XRD analysis of nickel oxide nanoparticles	5.9
Figure 5.8	TEM micrograph of cobalt oxide nanoparticles synthesized at 650 °C	5.9
Figure 5.9	XRD analysis of cobalt oxide nanoparticles	5.9
Figure 5.10	TEM image of (a) pristine and (b)BHT grafted MWCNTs	5.10
Figure 5.11	FTIR of BHT, pristine MWCNT and BHT grafted MWCNT	5.11
Figure 5.12	Antioxidant potency assay of synthesized nanoparticles and prepared nanocomposite	5.13
Figure 5.13	Rancimat oxidation stability test of biodiesel, at 110° C	5.14
Figure 5.14	BHT grafted MWCNT in ethanol (a) before and (b) after application of magnetic field to demonstrate the magnetic severability of the antioxidants	5.15

Abbreviations and symbols used

AM 1.5	Air-mass 1.5
BHT	Butylated hydroxytoluene
CNT	Carbon nanotube
CVD	Chemical vapour deposition
DD	Double distilled
DoF	Degrees of freedom
EDX	Energy-dispersive X-ray
FAME	Fatty acid methyl ester
fc-MWCNT	Functionalized cut-MWCNT
FF	Fill-factor
f-MWCNT	Finctionalized MWCNT
FTIR	Fourier transform infrared spectroscopy
FTO	fluorine doped tin oxide
ITO	indium tin oxide
MIM	Metal–insulator–metal
MWCNT	Multi-walled carbon nanotube
OPV	Organic photovoltaic
P3HT	Poly (3-hexathiophene)
P3OT	Poly (3-octylthiophene-2, 5-diyl)
PANI	Polyaniline
PCBM	[6,6]-Phenyl C ₆₁ butyric acid methyl ester
PPV	poly (p-phenylene vinylene)
PVD	Physical Vapour Deposition
q	Bragg's angle
qc	Chiral angle
QD	Quantum dot
RE	Renewable Energy
S/N ratio	signals-to-noise ratio

SAD	Selected area (electron) diffraction
SEM	Scanning electron microscope
SoS	Summing of the squares
SWCNT	Single-walled carbon nanotube
TEM	Transmission electron microscope
XRD	X-ray diffraction

Chapter 1

Introduction

Chapter 1 Introduction

The delicate balance in the energy-environment relationship needs close observation, perpetual consolidation and consistent efforts for improvement. This chapter presents a brief account of the energy-environment relationship and the role of renewable energy and materials in improving this. Initially some of the most viable renewable energy technologies (RETs) having largest impact on this relation have been identified. Carbonnanotube, one of the well-known potential materials with high prospect of influencing the future course of development of the identified renewable energy technologies, has been thoroughly explored. The rationale of the thesis was formed after reviewing the current literature on its synthesis and on discovering the possibility of use of green precursors for this. Subsequently on the basis of a detailed analysis of the possibility of specific applicability of these carbon nanomaterials in the identified renewable energy technologies the aims and objectives of the work have been set. Finally this chapter concludes with the outline of the thesis.

1.1. Impact of materials on energy, environment and sustainability

Materials have always played significant role for sustainability of development of civilizations through the ages. Progress made by civilizations has been associated with the discovery, development, and use of new materials. Very recently the functionalities of these materials have been redefined with the discovery of their nanoforms. These materials have been identified to be capable to address many of the present day global challenges related to energy and environment. The growing energy demand and the associated environmental problems converge towards global unsustainability. In addition to this the instabilities due to the geopolitical confinement of fossil fuel reserves poses a imminent threat to energy security and unconfined nature of environmental problems challenges the very existence of the most of the nations including India. Renewable energy (RE) technologies have great potential to achieve sustainability and can address both energy security and climate change issues.

Although most of the renewable energy technologies are quite mature but the constraints like efficiency and cost could not bring many of these to the level of commercialization. Use of nanomaterials in such RE systems has shown encouraging results in a number of RE technologies. In the current scenario, research, development and application of some of the important nanomaterials for the most potent RE technologies is the basic motivation behind the work presented in this thesis. For this availability of the potent RE resources needs to be assessed first, as discussed next.

1.2. Renewable energy resources and potential

Out of all the renewable resources, solar, wind, bio and hydro are the identified potential resources in India. Technologies available for harnessing wind and hydro are now mature and have reached a stage of full commercial exploitation. It may be noted that both are site and region-specific. Now solar and bio-energy resources are uniquely poised. Both are equitably distributed in the tropical regions and both are dependent on materials for their efficient conversion and storage. The conversion technologies for both are also reasonably developed and matured but due to a big role of material science and technology in these there is a vast scope of improvement in the performance of the systems. India being tropical country endowed with these resources naturally [1]. It is pertinent to look for materials with promising characteristics to enhance the performance of the related energy systems and processes. Figure 1.1 shows the potential renewable energy (RE) resources in the globe along with India. It can be seen that India has a major global share of solar and biomass energy resource.

Keeping the resource availability and technologies in mind the present work focuses on the use of carbon nanotubes for these RE technologies.

1.3. Carbon nanotube

A cylindrical tubular nanostructures made of carbon is termed as carbon nanotube (CNT). The tubular structure is made up of graphitic carbon sheets rolled over to form tubular hollow cylindrical structures, it may have single, double and multiple concentric graphitic sheets. Thus depending upon the number of concentric graphene layers CNTs are classified into single-walled carbon nanotube (SWCNT), double-walled carbon nanotube (DWCNT) and multi-walled carbon nanotube (MWCNT).

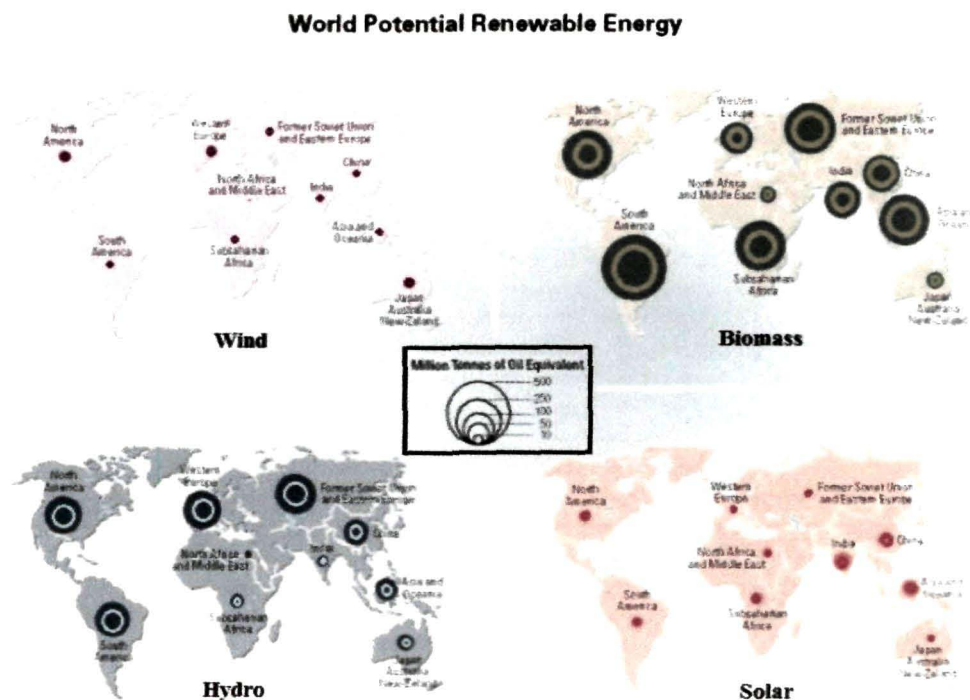


Figure 1.1: Global potential important RE resources, taken from Peter Milson's report on 'Overview of RE potential in India', (GENI, 2006) [2]

Carbon nanotube (CNT), discovered by Iijima in 199, is an allotrope of carbon just like graphite and diamond [3]. Unlike diamond, where a 3-dimensional cubic crystal structure of diamond is formed with each carbon atom having four nearest neighbours arranged in a tetrahedron, graphite is formed as a 2-dimensional sheet of carbon atoms in a hexagonal array arrangement. Here, each carbon atom has three nearest neighbouring carbon atoms. 'Rolling' sheets of graphite into cylinders forms carbon nanotubes. The atomic structure of nanotubes is described in terms of tube chirality, or helicity, which is defined by the chiral vector, C_h , and the chiral angle, θ . In figure 1.2, the rolling of the graphite sheet along different axis to form a tube of different chirality is shown. The chiral vector can be described by the following equation:

$$\vec{C}_h = n\vec{a}_1 + m\vec{a}_2 \quad (1.1)$$

where the integers n and m are the number of steps along the zig-zag carbon bonds of the hexagonal lattice and \vec{a}_1 and \vec{a}_2 are unit vectors, as shown in figure XX.

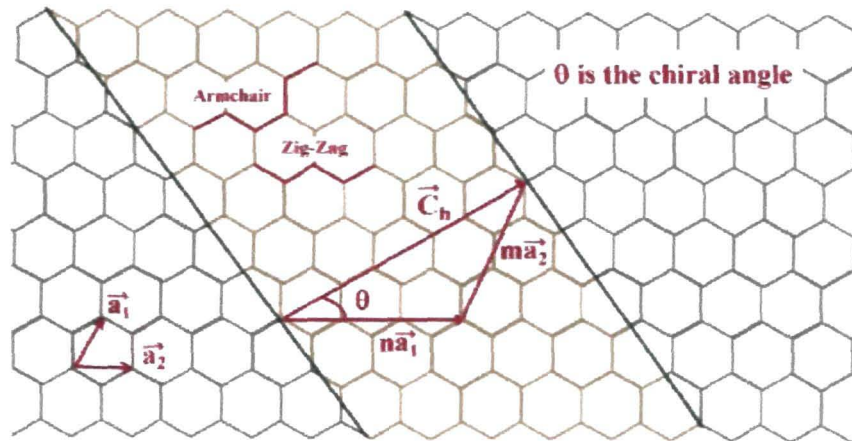


Figure 1.2: Schematic diagram explaining a hexagonal sheet of graphite ‘rolled’ to form a carbon nanotube

The chiral angle (θ) determines the amount of ‘twist’ in the tube. There are two limiting cases where the chiral angle is at 0° and 30° . These limiting cases are referred to as zig-zag (0°) and armchair (30°) based on the geometry of the carbon bonds around the circumference of the nanotube.

1.3.1. Properties of CNT

The CNT due to their distinctive structure and morphology possesses unique physical and chemical properties as tabulated in the Table 1.1. CNTs are considered to be one of the strongest materials known to mankind. The reason for the strength of CNTs is the sp^2 bonds within the rolled graphite sheets. The Young’s modulus of near perfect SWNTs in the axial direction has been estimated to be 1 TPa [4]. In another study of CVD produced MWNTs the tensile strength was measured to be lower than 100 GPa. Reasons for differences between such estimates and measurements may be due to point defects within the graphite planes and a mis-alignment of the graphitic planes with regard to the central axis. Nanoscale point defects should intuitively have a greater impact on nanotube sized features, versus their micro- and macro-sized fibers. Other more recent research, however has suggested that point and planar defects can act

to strengthen MWNTs as they are strained in the axial direction [5]. SWNTs can be either semiconducting or metallic depending on the chiral vector.

Table 1.1: Some of the important physical properties of CNTs [4-12]

Physical property	SWCNT	MWCNT
Tensile strength (Gpa)	50-200	11-63
Young's Modulus (GPa)	1000	270-950
Current density (A/cm ²)	10 ⁷ -10 ⁸	10 ⁹
Electrical conductivity (S/m)	1x10 ⁶	1/13

Besides these, high surface area [13], tunable electrical (both in semiconducting and metallic ranges) and high thermal conductivity [14], are some of the major attributes of CNT, which make them strategic material for some of the RE systems and applications. Thus because of these properties CNTs find applications in RE systems including organic photovoltaic (OPV) cells, fuel cells and supercapacitors. But, the synthesis of CNT has many challenges while still a number of new applications are being proposed. The synthesis and applications of CNTs is being discussed in detail in the following sections of this chapter.

1.3.2. Synthesis of carbon nanotubes

CNT synthesis is one of the focus areas of research for desired quality (such as orientation, diameter, wall thickness, length) and quantity (yield) to address different applications. Since its discovery, several techniques have been reported for their synthesis. Arc discharge [15-16] and laser ablation [17-18] and physical vapour deposition [19] belong to physical techniques whereas chemical vapour deposition (CVD) [20-23] technique is a simple chemical route for synthesis of CNTs. The CNT synthesis techniques differ according to the nature of carbon atomization, which may involve either physical or chemical techniques. Physical technique involves relatively high energy input to the carbon source (precursor) atomization in the form of arc-discharge or laser evaporation [24-26]. Thus, CVD technique is relatively advantageous compared to physical synthesis techniques due to two reasons: i) its ability to be easily modified and scaled-up in terms of quantity of output, and ii) its low energy intensity

processing. But the challenge of the CVD technique lies in the multitude of parameters involved because a small change in the parameters shows remarkable effects on the morphology of the CNTs synthesized [27]. The comparison of CNT synthesis techniques are tabulated in Table 1.2.

The synthesis of CNTs involves transition metal catalysts with high affinity to atomized carbon. Thus the use of metal nanoparticles as a catalyst source to the CVD process is of great interest. The use of nanoparticles and thin films of transition metals as catalyst substrate is a well documented method for the synthesis reaction [28-31]. The success of CVD as a reliable synthesis method for producing commercial quality CNTs requires a detailed, systematic study of all the growth parameters involved in a given synthesis setup.

Table 1.2: Comparison of CNT synthesis techniques [32].

Attributes	CVD	Laser Ablation	Arc Discharge
Process temperatures	500-1000° C	3000-4000° C	3000-4000° C
Carbon source	Solid, liquid and gas	Solid	Solid
Catalyst type	Particles or thinfilm	Particles	Particles
Growth surface or collector	High temperature compatible substrate	Copper collector	Carbon rod
Diameter control	Large distribution	Small distribution	Small distribution
CNT relative defectiveness	High	Low	Low
CNT arrangement	Yes, vertical alignment possible	No, randomly arranged	No, randomly arranged

Precursors for CNT synthesis using CVD: Though there is extensive study on yield and quality of CNT synthesized at various synthesis parameters using various precursors, there are some major issues to be addressed a priori, viz., origin and sustainability of

supply of precursors and specific energy intensity of production. The CNT industry currently depends on petroleum based precursors for the synthesis of CNTs. The non-renewable nature of these precursors puts questions on the sustainability of the technology for future production and use. Moreover, the consumption of petroleum based precursors for CNT synthesis is not a carbon neutral process. The CNT synthesis is a high energy intensive process whether it is through physical route (laser ablation or arc discharge) or chemical (such as CVD). As discussed the CVD technique is less energy intensive than the physical techniques and could be scaled up for large scale production, but the scope for improvement to lower the energy consumption needs to be explored.

1.4. Application of carbon nanotubes in selected RE technology

The remarkable properties of CNTs resulted in direct and indirect applicability in various RE technologies viz. fuel cell, super-capacitor, catalyst support and organic solar cells. Solar and bio-energy being the most prominent energy resource in India [2], the need, scope, and efforts directed to employ CNTs to enhance the efficiency of these systems is investigated in detail.

1.4.1. CNT in organic photovoltaic (OPV)

Sustained research interests have been shown in the development of photovoltaic cells over the past six decades for their high quality energy output, long life, modularity, reliability and applicability. But fulfilment of cost and efficiency criteria set for its commercialization is still elusive due to high cost and Shockley-Queisser limit (SQ limit) on the efficiency of silicon solar cells, hitherto dominating the solar cell technology. To reduce the processing energy intensity (and hence the cost) and to go beyond the SQ efficiency limit there is a need to look for new PV materials. It makes organic or polymeric material based PV cells a good candidate because of ease of blending of multiple materials and low processing cost. But in spite of the best efforts the efficiency of organic solar cell is still very low as compared to Si solar cells. However the other trade-offs of light weight, large area and flexible shape and form make it very attractive even now. For improvement in the cell characteristics the characteristics of the material employed for the photoactive region, charge separation and collection, and optimization of the device structural components is critical. Due to their unique physical and chemical properties the semiconducting single-walled or

multi-walled carbon nanotubes are attractive candidates for different functions in OPV solar cells.

The single-walled carbon nanotubes not only act as electron acceptor but also as an electrode in organic solar PV cell. The properties of CNT which are useful for solar cells are high carrier mobility, large surface area, enormous current carrying capacity, and tuneable conducting behaviour [33].

Efficiency of a solar PV cell is characterized by its open circuit voltage (V_{oc}), short circuit current (I_{sc}), and fill-factor (FF). Here V_{oc} of an OPV is dependent on the difference of the molecular energy levels of the dissociated charge carriers while I_{sc} depends on the active area of interface responsible for exciton dissociation. The presence of shunt and series resistances in a solar cell also affect these characteristic parameters. These resistances are determined by the polymeric materials used in the cell design.

As stated earlier the efficiency of organic photovoltaic cell is limited because of low electron mobility, and poor charge separation and transport. It has already been reported that CNTs along with photoactive conjugated polymers bring about drastic changes in the charge transportation and exciton dissociation in organic photovoltaic cell [34-35]. The formation of an interpenetrating blend of polymer as electron donors and carbon nanotubes as electron acceptor can solve some part of these problems. The charge separation in the mixture of donor and acceptor materials is achieved due to a band offset at the interface. The collection of charge carriers in the respective electrode is achieved because of the existence of a bi-continuous network along which electrons and holes can travel through the electron acceptor and the electron donor. The blend can be considered as a network of donor and acceptor heterojunctions that allows efficient exciton dissociation and balanced bipolar transport through its entire volume.

The carbon nanotubes can also be used as an electrode in organic solar cell. There are different criteria for selecting the electrodes in organic solar cell. It is based on the contact between electrode and the active layer (ohmic or not), the energy level alignment, the transparency of the electrode etc. For certain type of solar cells some of these factors are very specific. In bulk heterojunction solar cells the electrode should be carrier selective. The work function difference between two electrodes is not an important factor in organic solar cell. Because, the exciton dissociation is caused by the band-offset at donor – acceptor interface and the exciton binding energy is larger than the internal electric potential drop across the exciton. Currently, the material of choice

as transparent anode in organic photovoltaic cell is (indium tin oxide) ITO and (fluorine doped tin oxide) FTO coated glass.

In 1998 Curan *et al.* demonstrated the use of multiwalled carbon nanotubes (MWCNT) to increase the conductivity within poly (p-phenylene vinylene) (PPV) [36]. They made a blend of PPV with 15% of CNTs by mass and got improvements of five orders of magnitude of conductivity. The use of MWCNT in the organic photovoltaic cell was first investigated by Ago *et al.* [37]. They used a layer of CNT as a cathode in PPV/Al diode. The polymer-nanotube composite was prepared by spin coating, using high concentration of MWCNT. The external quantum efficiency of the device was larger than the device having ITO as the electrode. The first SWCNT-conjugated polymer photovoltaic device was reported by Kymakis and Amaratunga in 2002 [38]. They made a blend of P3OT with low SWCNT concentration sandwiched between ITO and Al electrode. The CNT-P3OT interfaces act as dissociation centre for excitons on polymer and electron transport via the nanotubes to the metal electrode. With this arrangement the power conversion efficiency increased in comparison to the undoped polymer film by three orders of magnitude. The device reported by Kymakis and Amaratunga's [38] showed an open circuit voltage (V_{oc}) of 0.75 V, which is larger than the theoretical limit calculated by the metal-insulator-metal (MIM) model. As stated earlier, V_{oc} measured is only very weakly dependent on the work function of the metal. From the analysis of the current-voltage characteristics and electron microscopy imaging of the composite structure, it is proposed that the photovoltaic response of these devices is based on the introduction of internal polymer/nanotube junctions within the polymer matrix, which due to a photoinduced electron transfer from the polymer to the nanotube contribute to enhanced charge separation and collection [39]. But due to bandgap problem the cell cannot absorb whole spectrum in the visible range. So photon losses will occur. Use of organic dye is a good solution to this problem. Because dye has the capability to absorb more light and also help in charge transport. Bhattacharyya and Kymakis [40] reported the photovoltaic properties of blend composite of dye, N-(1-pyrenyl) malenide, functionalized SWNT and conjugate polymer in OPVs. The device was fabricated by spin cast from the solution of composite onto ITO coated glass. Improved performance was achieved by functionalizing the SWNT with dye molecules with V_{oc} as 0.6 – 0.7 V and short circuit current was found to increase by more than an order than SWNT-polymer diode without dye. Length of the CNT is critical in actual device performance, because if the length is greater than the thickness of the active

layer then it may get shorted resulting in decrease in its efficiency. To increase the performance Nakhayama and Asakura [41] used cut-SWCNT (by acid treatment) - polymer composite films. Acid treatment by mixture of H_2SO_4 and HNO_3 cut the long CNT and improved dispersion into polymers as well. The film showed high electrical conductivity depending on the concentration of CNTs. They reported a cell of about three times higher short circuit current than the one not including nanotubes.

Challenges

The use of CNT in organic photovoltaic cell leads to solve some of the problems. But there are several other factors in using CNT, because of which the efficiency is limited. Firstly, the mismatch of optical absorption spectra of the polymer and CNT, because of which total absorption of the cell will not match with solar spectrum. Secondly, the wide range of electrical conductivity of CNT depending upon the morphology, the conductivity of CNT ranges from metallic to semiconducting. Thus, each type of CNTs has to be identified for different architectures. Thirdly, at low concentration of CNT the dissociation of exciton is incomplete and at high concentration the dissolving in polymer matrix decreases the efficiency of the cell. Finally, CNT is not soluble in some common solvents.

To overcome the barrier of limited efficiency researchers are trying to incorporate CNTs more efficiently. For efficient exciton dissociation the higher surface area is preferred. Najeeb and Hyeok [42] reported surface modification of CNT to enhance the surface area for efficient exciton dissociation. They purified SWCNT by acidic treatment, carboxylated by chemical oxidation and enhanced improved dispersibility in polymer matrix.

Recently, a new concept of hybrid solar cells with organic and inorganic composites is being studied. Photovoltaic devices based on SWCNT and n-Si heterojunction showed a conversion efficiency of 1.7% [43]. Somani reported a multifunctional device combining the PV action and pressure sensitivity based on n-Si and carbon nanotube using copper phthalocyanine surface modified electrode [44]. Chen and Pan reported a device based on P3HT and Si-MWCNT nanocomposite [45]. The power conversion efficiency of P3HT/Si and MWCNT hybrid film is two to three times better in comparison to simple P3HT/Si nanoparticles or P3HT/MWCNT. The improved performance is because of efficient charge generation by P3HT/Si nanoparticles bulk heterojunction and efficient charge collection.

The use of SWCNT in OPV generates better performance if they are placed vertically aligned. Bissett and Shapter showed better photocurrent response of vertically aligned SWCNT array in visible light [46]. The solubility of nanotubes also plays a major role in the efficiency of the cell. Nie and Guo reported that the water solubility of carbon nanotubes can be increased [47]. They used functionalized CNTs with polyethylene glycol synthesized by a cyclo-addition reaction. Functionalization affords a large increase in aqueous solubility of CNTs.

The use of quantum dot concept also leads to increase the power conversion efficiency of the cell. Shukla and Tymish reported enhanced efficiency by blending of IR sensitive quantum dots and CNTs [48]. The presence of CNTs in QDs shows quenching of the IR photoluminescence. They reported a device with PbSe QD: CNT/P3OT, which shows a better performance than PbSe: P3OT without CNTs.

The use of hybrid nanocomposites like SWCNT and polyaniline (PANI) increases the performance of solar cells. Yao and Chen reported a hybrid nanocomposite containing CNTs and polyaniline for enhanced thermoelectric performance [49]. The SWCNT/PANI nanocomposites show higher electrical conductivity and Seebeck co-efficient, which could be attributed to the enhanced carrier mobility in the ordered chain structure of PANI. The present work intends to take this route because of superior properties of hybrid nanocomposites, for OPV application. However demonstration of applicability of CNT prepared from plant based precursors is another challenge. The growing number of scientific publications contributing to OPVs is shown in the Figure 1.3 [50].

1.4.2. Bio-energy and biofuels

Bio-energy is a form of renewable energy derived from biological sources. Biomass is any organic material which stores sunlight in the form of chemical energy. Even though such biofuels are made from plant material and hence are a renewable source, they are not as 'green' as they seem. To produce biofuels, large amount of land is need to cultivate the crop, together with irrigation, use of fertilizers, transportation, conversion and refining processes. All these require energy input and emit carbon dioxide. There are a large and growing number of studies that suggest that the use of current biofuels would save very little greenhouse gas, destroy wildlife habitats, as well as affect indigenous and rural poor communities around the world. Biofuels are one of the forms of energy made from biomass. It is used as transport fuel and it may be

produced from a wide range of plant materials (biomass). Biodiesel and bio-ethanol are well known biofuels. Other forms of bio-energy, for example biogas, combustible biomass, generally have a higher overall efficiency. As the world is going to witness a transition between petroleum to renewable very soon, biofuels in general and biodiesel in particular would be the bridge between these. If managed sustainably, biofuel has its merits and is key to tackle global climate change

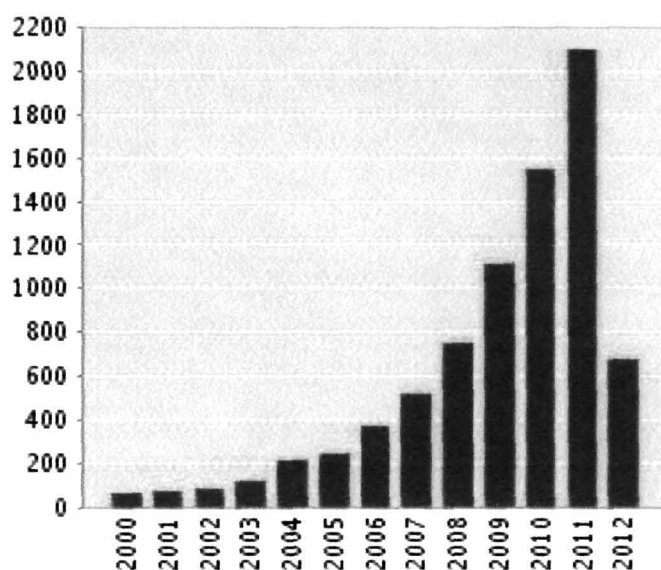


Figure 1.3: Number of papers published in scientific journals in the area of OPVs from January 2000 to March 2012 (Search done through ISI, Web of Science)

Biodiesel may be produced by the trans-esterification reaction. The process involves a reaction between a triglyceride and an alcohol to form esters and glycerol. A triglyceride is a glycerin molecule with three long fatty acid chains attached to it. The triglyceride reacts with the alcohol, either methanol or ethanol but most often methanol, in the presence of a catalyst such as sodium hydroxide or potassium hydroxide, to form mono-alkyl ester and crude glycerol. The combination of methanol and potassium hydroxide is preferred in fatty acid methyl ester (FAME) production because biodiesel produced in this way is less resistant to oxidation than typical fossil fuel untreated with additives [51]. The general mechanism of oxidation in biodiesel has been well documented. Fatty acids present in biodiesel, in general, are more susceptible to oxidation because they vary in level of unsaturation, meaning there are more carbon-

carbon double bonds and fewer hydrogen molecules on the fatty acid chains. When biodiesel made from unsaturated oil is exposed to oxygen, the oxygen attaches itself to the bis-allylic site directly adjacent to the two double bonds, which initiates an autoxidation chain reaction sequence. Oxidation stability is not related to the number of double bonds available but rather the number of bis-allylic sites [52]. The initiation step is the formation of a free radical that can react directly with oxygen. This leads to the formation of a peroxide or hydroperoxide molecule. The most reactive site for initial formation is the bis-allylic position. The radicals formed at the bis-allylic sites immediately isomerize to form a more stable conjugated structure, which reacts directly with oxygen to form peroxide. The existence of these molecules is an early indication of oxidation taking place, and it is measured in terms of peroxide value [53]. Later, aldehydes and ketones are formed. Finally, during the polymerization process, resins are produced making the fuel unusable [53]. Thus, the major problem with biodiesel is their susceptibility towards oxidation. The regulations put in place for biodiesel advancement resulted in the rapid development of standardization of specification of the test procedures. These testing specifications all include oxidation stability as a major test method requirement. The trend of scientific publications contributing to Biodiesel storage and their performance in IC engine is shown in the figure 1.4 [54]

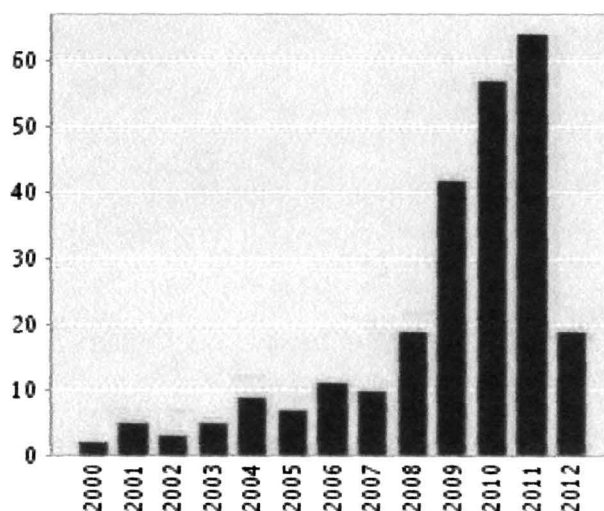


Figure 1.4: Number of papers published in scientific journals in the area of biodiesel storage from January 2000 to March 2012 [54]

Challenges

The production of biodiesel were studied by many researchers using various feed stock [55, 56]. But the major setback with biodiesels is their short shelf-life due to rapid oxidation. Karavalakis et al. have studied the stability and aging effect of biodiesel blends with different antioxidants [57]. Antioxidants like butylated hydroxytoluene (BHT), propyl gallate (PG), pyrogallol (PA) and butylated hydroxyanisol (BHA) displayed very low effectiveness in neat biodiesel. Hence, they designed a process to simulate the ageing of an automotive biofuel stored in the fuel tank of a vehicle. The results showed a sharp decrease in fuel stability over time [57]. Similar studies were conducted by Obadiah et al. [58] and Jain and Sharma [59-60] on biodiesels. Tung oil biodiesel characteristics were studied by Shang et al [61]. The results obtained show that B20 or lower blends could meet the specification of ASTM D7467 after storage for a month. Corn biodiesel was also found to be unstable for long hours of storage due to oxidation [62]. Along with natural antioxidants, researchers have also tried synthetic antioxidants to enhance the oxidation stability of the biodiesel. The potency of synthetic antioxidants for biodiesel storage was also studied by Focke et al. [63]. The use of antioxidants could not stop the oxidation completely but could enhance the shelf-life of biodiesels.

Another problem with biodiesel storage technology is related to emission characteristics and engine performance. The antioxidants, that are used, form homogeneous mixture with the biodiesel and it is not economically viable to separate them before they are fed to IC engine. The incorporation of antioxidants in biodiesel has adverse effects on the engine performance [64]. The use of antioxidants (viz. L-ascorbic acid, α tocopherol acetate, butylated hydroxytoluene, p-phenylenediamine and ethylenediamine) on biodiesel were found to control NO_x emission, however a substantial increase in unburned hydrocarbon and CO_x emissions could be seen [65]. Xue et al. have also found that addition of antioxidants affects the engine performance [66]. Thus, the use of existing homogeneous antioxidants poses another set of problems in the form of adverse effects of these antioxidants on engine performance and air pollution. The only route to address this problem is to look for higher performance antioxidants which may be separated out before use.

1.5. Origin of present work and Objectives

As discussed above, the fossil fuel based precursors for CNT synthesis are non-renewable, and the present technology may not sustain without exploring for renewable precursors for the synthesis of CNTs. This not only requires intense search for precursors but also for suitable catalyst and synthesis technique. North-eastern India is known for its floral biodiversity. Thus it calls for search for plant species rich in oil content (in seeds) which may be used for CNT synthesis. The oil extracted from plants may contain various fatty acid component. As discussed, CVD is considered for CNT synthesis because of its low energy intensity process as compared to other techniques. It can be scaled up of mass production as well. Thus, the next step includes development and/or modification of CVD setup for plant precursors.

The parameters for CNT synthesis from potential precursors needs to be optimized for acceptable quality and higher quantity. Due to existence of large number of parameters influencing these a resort is taken to statistical optimization technique. This would help researchers to synthesize different morphologies of CNTs for different applications.

The two active areas of research in energy technology and systems are solar OPV cells and biodiesel storage. CNT finds applications in these due to its unique characteristics. There are a number of problems in OPV which may be solved appropriately through the CNTs synthesized from plant precursors to get the desired result.

The problems with biodiesel, discussed earlier, suggests for the need of a heterogeneous antioxidant that can be removed before end use.

The present thesis attempts to sort out the above mentioned problems. The main aim of the thesis is to search plant based renewable precursors for CNT synthesis and to utilize the CNTs for application in OPVs and biodiesel storage. However, the specific objectives are:

- i. To search and screen renewable plant based precursors for CNT synthesis.
- ii. To optimize and evaluate the effect of each of the process parameters for acceptable quality and high quantity.
- iii. To suitably utilize the CNTs in OPV architecture and to study its impact on performance

- iv. To investigate and propose a heterogeneous antioxidant based on CNT for biodiesel storage.

1.6. Summary of the thesis

The thesis, consisting of six chapters and two appendices, dwells upon the above mentioned issues in detail as outlined here,

Chapter 1: It introduces the theme of the thesis including information about renewable energy resources in India, potential of solar and biofuels and application of CNTs in these areas. It also describes the need and importance of renewable plant based precursors for CNT synthesis. A detailed literature survey with regard to synthesis and applications of CNTs with a view to provide rationale of the work and to set the objectives are discussed.

Chapter 2: This chapter starts with the details of the process adopted to select plant precursors from different parts of North-east India which is one of the hot spots of the floral species and biomass resources found in the tropical regions of the globe. Few suitable plant varieties were screened for this purpose on the basis of availability, alternative commercial applications and oil content for carbon nanotube synthesis. In the next section of the chapter the synthesis of catalyst, and development & modification of the CVD setup for synthesis of CNT from plant precursors are discussed in detail.

The morphology and yield of CNTs synthesized from each precursor is carefully analyzed to sort them out based on suitability of each one of these for a particular application envisaged in the thesis.

Chapter 3: This chapter is dedicated to refinement of the process of synthesis by optimizing the process parameters like temperature of synthesis, flow rate of carrier gas, catalyst type and precursor type both for improving yield and quality of MWCNT. Taguchi robust technique has been used for the purpose. The six plant precursors, selected earlier, are divided on the basis of major fatty acid content. Three levels of catalyst types, flow rates, and synthesis temperature have used for optimization. The effect of each parameters on the synthesis is also important for acceptable quality and yield of CNTs. This is done to screen out some of them if they did not conform to the requirements. Taguchi robust technique is the best method to evaluate and optimize the process parameters. On the basis of preliminary analysis some of them appeared to be

potential candidates for organic solar cell application, for development of electrodes for fuel cells and to work as a substrate for heterogeneous antioxidants.

Chapter 4: The solar photovoltaic cells are developed from inorganic or organic photoactive materials. The technology for inorganic material based PV cells is proven and popular. However, the organic photovoltaic cells have many advantages over inorganic counterpart due to favourable economics, flexibility, form-factor independence and low energy intensity based fabrication technology. The major issue in organic photovoltaic cell is the efficiency and life time. Literature suggests that the use of carbon nanomaterials has improved the efficiency of the organic photovoltaic cells. CNTs have few problems like low dispersibility in organic solvents, the long tubular structure and the high workfunction of MWCNT. Some of these problems are addressed through suitable functionalization of the CNTs. The chapter also describes a method to cut MWCNTs using simple chemical route.

Finally, the chapter describes the application of the modified MWCNTs in OPVs. Three OPV devices, fabricated to understand the effect of pristine, functionalized-cut MWCNTs, have been investigated. The device architecture investigated are - Al/LiF/P3OT+PCBM/ITO (used as baseline device for the study), Al/LiF/P3OT+PCBM+MWCNTs/ITO and Al/LiF/P3OT+PCBM+fc-MWCNTs/ITO and Al/LiF/P3OT+PCBM+fc-MWCNTs/PANI+fcMWCNT/ITO. The device with functionalized-cut MWCNTs showed best performance.

Chapter 5: Biodiesel technology has attracted keen interest of the stakeholders in the past decade and is being projected as an alternative future fuel. But, one of the major limitations of biodiesel is its short shelf-life. This is due to the degradation of biodiesel through the process of oxidation. At present homogeneous antioxidants are used to enhance the shelf-life of the oils (both mineral and bio-oil). But these homogeneous antioxidants cannot be removed before use and are consumed during the end-use. Moreover, in the case of biodiesel the engine performance and exhaust emission is affected by the addition of antioxidants. This chapter discusses a new nanomaterial structure which is engineered to contain a magnetic nanoparticle and an antioxidant attached to a substrate. The idea has a potential to make the antioxidant removable without affecting the performance of the engine.

This chapter also dwells upon the basics of biodiesel storage issues and analyzes the results of experiments which were designed to investigate the efficacy of the antioxidant material system.

Chapter 6: This chapter concludes about the synthesis of MWCNTs from plant precursors and their application in organic solar cells and bio-diesel storage. It also discusses about the scope of improvements in OPV and bio-diesel storage systems.

Appendix I : A method to utilize solid waste products like Polypropylene (PP) and Polyethylene terephthalate (PET) for synthesis of MWCNT has been demonstrated.

Appendix II : The utility of MWCNTs (synthesized from plant based renewable precursors) in Alkaline Fuel Cell electrode is discussed.

Reference

1. Twidell, J., and Weir, T. *Renewable energy resources*, second edition, Taylor & Francis, London.
2. Meisen, P., and Quéneudec, E. *Report on - Overview of Renewable Energy Potential of India*, Global Energy Network Institute (GENI), 2006.
3. Iijima, S., Helical microtubules of graphitic carbon, *Nature* **354**, 56 – 58, 1991.
4. Treacy, M. M., et al. Exceptionally high Young's modulus observed for individual carbon nanotubes, *Nature* **381**, 678-680, 1996
5. A. Barber, R. Andrews, L. Schadler, and H. Wagner, "On the tensile strength distribution of multiwalled carbon nanotubes," *Applied physics Letters* **87**, 1-3, 2005
6. Thess, A., et al. Crystalline Ropes of Metallic Carbon Nanotubes, *Science* **273**, 483-487, 1996
7. Callister, W. D. J., *Materials Science and Engineering an Introduction, 6th ed.* Wiley, 2003.
8. Yu, M.-F. et al. Strength and Breaking Mechanism of Multiwalled Carbon Nanotubes Under Tensile Load, *Science* **287**, 637-640, 2000
9. Melechko, A. V., et al. Vertically aligned carbon nanofibers and related structures: Controlled synthesis and directed assembly, *Journal of Applied Physics* **97**, 041301-041339, 2005
10. P. Poncharal, C. Berge, Y. Yi, Z. L. Wang, and W. d. Heer, "Room temperature ballistic conduction in carbon nanotubes," *Journal of Physical Chemistry B* **106**, 12104-12118, 2002
11. Treacy, M. M., et al. Exceptionally high Young's modulus observed for individual carbon nanotubes, *Nature* **381**, 678-680, 1996.
12. Wong, W., et al. Nanobeam Mechanics: Elasticity, Strength, and Toughness of Nanorods and Nanotubes, *Science* **277**, 1971-1975, 1997.
13. Pint, C. L., et al. Synthesis of high aspect-ratio carbon nanotube "flying carpets" from nanostructured flake substrates, *Nano Lett.* **8(7)**, 1879-1883, 2008.
14. Small, J. P., et al. Mesoscopic thermal and thermoelectric measurements of individual carbon nanotubes, *Solid State Communications* **127**, 181-186, 2003.
15. Journet, C., et al. Large-scale production of single-walled carbon nanotubes by the electric-arc technique, *Nature.* **388**, 756-758, 1997.

16. Nakahira, T. S. and Uemura, S. Growth Conditions of Double-Walled Carbon Nanotubes in Arc Discharge, *Journal of Physical Chemistry B* **107**, 931-934, 2002.
17. Puretzky, A., et al. Timeresolved diagnostics of single wall carbon nanotube synthesis by laser vaporization, *Applied Surface Science* **197**, 552-562, 2002.
18. Thess, A., et al. Crystalline Ropes of Metallic Carbon Nanotubes, *Science* **273**, 483-487, 1996.
19. Sinnot, S.B., et al. Model of carbon nanotube growth through chemical vapor Deposition, *Chem. Phys. Lett* **315** (25), 1999.
20. Choi, S. K., et al. The Role of Ammonia Treatment in the Alignment of the Carbon Nanotubes Synthesized with Ni and Fe via Thermal Chemical Vapor Deposition, *Journal of Korean Physical Society* **39**, S7-S10, 2001.
21. Choi, C. Y., et al. Controlling the diameter, growth rate, and density of vertically aligned carbon nanotubes synthesized by microwave plasma-enhanced chemical vapor deposition, *Applied Physics Letters* **76**, 2367-2369, 2000.
22. Lee, J. C., et al. Synthesis of bamboo-shaped multiwalled carbon nanotubes using thermal chemical vapor deposition, *Chemical Physics Letters* **323**, 560-565, 2000.
23. Rohmund, F., et al. A simple method for the production of large arrays of aligned carbon nanotubes, *Chemical Physics Letters* **328**, 369-373, 2000.
24. Bethune, D.S., et al. Cobalt-catalyst growth of carbon nanotubes with single atomic layer walls, *Nature* **363**, 605-7, 1993.
25. Guo, T., et al. Catalytic growth of single-walled nanotubes by laser vaporization, *Chem. Phys. Lett* **243**, 49-54, 1995.
26. Kim, K.S., et al. Single-Walled Carbon Nanotubes Prepared by Large-Scale Induction Thermal Plasma Process: Synthesis, Characterization, and Purification, *J. Phys. D: Appl. Phys* **40**, 2375-87, 2007.
27. Nerushev, R. -E. M. O.A., et al. The temperature dependence of Fe-catalysed growth of carbon nanotubes on silicon substrates, *Physica B* **323**, 51-59, 2002.
28. Ago, H., et al. Growth of double-wall carbon nanotubes with diameter-controlled iron oxide nanoparticles supported on MgO, *Chemical Physics Letters* **391**, 308-313, 2004.
29. Hafner, H. J., et al. Catalytic growth of single-wall carbon nanotubes from metal particles, *Chemical Physics Letters* **296**, 195-202, 1998.

30. Sato, S., et al. Carbon nanotube growth from titanium-cobalt bimetallic particles as a catalyst, *Chemical Physics Letters* **402**, 149-154, 2005.
31. Zaretskiy, N. S., et al. Growth of carbon nanotubes from Co nanoparticles and C₂H₂ by thermal chemical vapor deposition, *Chemical Physics Letters* **372**, 300-305, 2003.
32. Sunden, E. O., Carbon nanotube synthesis for microsystem applications, M. S. Thesis 2006, Georgia Institute of Technology, USA.
33. Dresselhaus, M.S., et al. *Carbon nanotubes synthesis, structure, properties and applications*, Springer Verlag, Berlin and Heidelberg, 2001.
34. Guldi, D. M., et al. Carbon Nanotubes in Electron Donor–Acceptor Nanocomposites. *Acc. Chem. Res* **38**, 871, 2005.
35. Kyamakisi, E., et al. Post-fabrication annealing effects in polymer-nanotube photovoltaic cells, *J. Phys. D* **39**, 1058, 2006.
36. Curran, S. A., et al. A composite from poly(m-phenylenevinylene-co-2,5-dioctoxy-p-phenylenevinylene) and carbon nanotubes: a novel material for molecular optoelectronics, *Adv Mater* **10**, 1091, 1998.
37. Ago, H., et al. Composites of carbon nanotubes and conjugated polymers for photovoltaic devices, *Adv Mater* **11**, 1281, 1999.
38. Kymakis, E. and Amaratunga, G. A. J. Single-wall carbon nanotube/polymer photo-voltaic devices. *Appl Phys Lett* **80**, 112, 2002.
39. Kymakis, E., et al. High open-circuit voltages photovoltaic devices from carbon-nanotube-polymer composite, *J. Appl. Phys* **93**, 1764, 2003.
40. Bhattacharyya, S. and Kymakis, E. Photovoltaic properties of dye functionalized single wall carbon nanotube / conjugate polymer devices, *Chem. Mater* **16**, 23, 2004.
41. Nakayama, K. and Asakura, Y. Photovoltaic device using composite films of polymer and carbon nanotube cut by acid treatment, *Mol. Crystal. Liq. Crystal* **424**, 2004.
42. Najeeb, C. K. and Hyeok, L. J. The effect of surface modifications of carbon nanotubes on the electrical properties of inkjet printed SWNT/PEDOT:PSS composite line patterns, *Nanotechnology* **21**, 385302, 2010.
43. Ong, P. L. and Euler, W. B. Hybrid solar cells based on single walled carbon nanotubes/Si heterojunctions, *Nanotechnology* **21**, 105203, 2010.

44. Somani, P. R. Pressure sensitive multifunctional solar cells using carbon nanotubes, *Applied physics letters* **96**,173504, 2010.
45. Chen, L. and Pan, X. Hybrid solar cells based on P3HT and Si@MWNT nanocomposite, *Nanotechnology* **21**, 345201, 2010.
46. Bissett, M. A. and Shapter, J. G. Photocurrent response from vertically aligned single walled carbon nanotube arrays, *J. Physic. chem.c* **114**, 2010.
47. Nie, H., and Guo, Wei. PE Glylation of double walled carbon nanotubes for increasing their solubility in water, *Nano Res* **3**, 103-109, 2010.
48. Shukla, S. and Tymish, Y. O. Polymeric nanocomposites involving a physical blend of IR sensitive Quantum Dots and carbon nanotubes for photodetection, *J. phys. chem. C* **114**, 2010.
49. Yao, Q. and Chen, L. Enhanced thermoelectric performance of single walled carbon nanotubes/polyaniline hybrid nanocomposites, *ACS Nano* **4**, 2010.
50. http://apps.webofknowledge.com/CitationReport.do?product=WOS&search_mode=CitationReport&SID=Z2pLo61@aPfDOoaEKF6&page=1&cr_pqid=1&viewType=summary. ISI, Web of Science
51. Waynick, J. A. et al., Characterization of Biodiesel oxidation and oxidation products, Technical report, National Renewable Energy Laboratory, U.S. Department of Energy, 2005.
52. McCormick, R. L., et al. Several factors affecting the stability of biodiesel in standard accelerated tests, *Fuel Processing Technology* **88**, 2007.
53. Sendzikiene, E., et al. Oxidation Stability of Biodiesel Fuel Produced from Fatty Wastes, *Polish Journal of Environmental Studies* **14**, 2005.
54. http://apps.webofknowledge.com/CitationReport.do?product=WOS&search_mode=CitationReport&SID=Z2pLo61@aPfDOoaEKF6&page=1&cr_pqid=3&viewType=summary, ISI, Web of Science.
55. Morshed, M., et al. Rubber seed oil as a potential source for biodiesel production in Bangladesh, *Fuel* **90**(10), 2981-2986, 2011.
56. Endalew, A, K., et al. Inorganic heterogeneous catalysts for biodiesel production from vegetable oils, *Biomass and Bioenergy* **35**(9), 3787-3809, 2011.
57. Karavalakis, G., et al. Storage stability and ageing effect of biodiesel blends treated with different antioxidants, *Energy* **36**(1), 369-374, 2011.

58. Obadiah, A., et al. Studies on the effect of antioxidants on the long-term storage and oxidation stability of Pongamia pinnata (L.) Pierre biodiesel, *Fuel Processing Technology* **99**, 56-63, 2012.
59. Jain, S. and Sharma, M.P. Long term storage stability of Jatropha curcas biodiesel, *Energy* **36** (8), 5409-5415, 2011.
60. Jain, S. and Sharma, M.P. Oxidation stability of blends of Jatropha biodiesel with diesel Fuel, *ISRN Renewable Energy* **90**(10), 3014-3020, 2011.
61. Shang, Q., et al. Properties of Tung oil biodiesel and its blends with 0[#] diesel Bioresource Technology, *Bioresource Technology* **101**(2), 826-828, 2010.
62. Dantas, M.B., et al. Evaluation of the oxidative stability of corn biodiesel, *Fuel* **90** (2), 773-778, 2011.
63. Focke, W. W., et al. The effect of synthetic antioxidants on the oxidative stability of biodiesel, *Fuel* **94**, 227-233, 2012.
64. Ryu, K. The characteristics of performance and exhaust emissions of a diesel engine using a biodiesel with antioxidants, Original Research Article, *Bioresource Technology* **101**(1), S78-S82, 2010.
65. Varatharajan, K., et al. Mitigation of NO_x emissions from a Jatropha biodiesel fuelled DI diesel engine using antioxidant additives, *Fuel* **90** (8), 2721-2725, 2011.
66. Xue, J., et al. Effect of biodiesel on engine performances and emissions, Review Article *Renewable and Sustainable Energy Reviews* **15**(2), 1098-1116, 2011.

Chapter 2
*Synthesis of carbon nanotubes from renewable
plant precursors*

Chapter 2

Synthesis of carbon nanotubes from renewable plant precursors

This chapter includes the basic theory and details of the synthesis, and the results of characterization of the catalyst, and subsequently, of the carbon nanotubes (CNTs) using plant based precursors. A number of plant species from the bank of floral reserves in North-eastern part of India have been identified and screened on the basis of their suitability to provide precursors. It is followed by the details of i) synthesis and characterization of catalyst, ii) design and development of CVD set-up and controls for synthesizing CNTs, and iii) synthesis and characterization of the CNTs.

2.1. Introduction

The ongoing research in CNTs may be divided into three general areas based on the main activity being undertaken by different researchers. These are: (1) exploration of the probability of *synthesis* of CNTs from different precursors using different techniques, (2) *investigation of parametric conditions* and techniques for different types, yield and quality of CNTs from a given precursor, and (3) identification of potential *applications* of the nanofoms of CNTs in the development of different systems and devices.

The research on synthesis of CNT is focused on the use of a variety of different techniques, and molecular species and phase of precursors which basically have non-renewable origin. These precursors are commonly low molecular weight derivatives of petroleum based hydrocarbons and coal [1-5]. The type, yield and quality of CNTs synthesized from the existing precursors depend on various factors like precursor used, catalyst type, temperature of synthesis, carrier gas used and flow rate of the carrier gas. Thus, optimization of the control parameters for a desired form, yield (gravimetric), aspect ratio and structural quality of the CNTs is investigated by many researchers [6-10]. The unique properties of each nanofom,

dimension, and quality of a CNT determine its suitability for a given application. In fact many of these are still being explored for applications in a number of future technologies. The CNTs have already found applications in electrochemical systems [11], structural composites [12], sensors [13], actuators [14-15], biomaterial and biomedical system [16-18], solar cells [19-20], fuel cell electrodes [21-23] and hydrogen storage [24].

Till date mostly purified petroleum products such as methane, ethene, acetylene, benzene and xylene are popular choices for synthesizing CNTs. In view of the foreseen crisis of fossil fuels in near future, it is important to explore regenerative precursors for CNT synthesis. Moreover, non-renewable precursors have following limitations [25]:

- i. long term unavailability: the precursors will deplete one day or the other,
- ii. large carbon footprint: the overall process is not carbon neutral if we consider the exploration, extraction and purification of precursors to the synthesis of CNTs from them, and
- iii. unfavorable economics: the cost of the precursors is high if the whole chain of exploration, extraction, separation, purification, storage and transportation is included.

Renewable plant based precursors have the potential to address the above problems. The use of locally available plant sources may be one of the better options for the synthesis of CNTs. The processing and extraction of the plant precursors is a carbon neutral process. Use of the renewable plant based precursors makes the process green as it conforms to the principle of green chemistry and green technology [26]. But scanty literature is available on use of renewable plant precursors being used for synthesis of CNTs [25, 27-29]. Thus, it is very important to explore new renewable precursors for the synthesis of CNTs. The oil extracted from plants is generally a mixture of fatty acids and their compositions differ from plant to plant. The property of the oil mainly depends on the major fatty acid composition. The study of different plant precursors for CNT synthesis may give some insight about the use of renewable plant based precursors for CNT synthesis.

The CNT synthesis extensively depends on the material, morphology, and type of catalyst nanoparticles. The nature of catalyst affects the morphology of CNTs in terms of tubular structures, waviness, entanglement, lengths, and growth density, which are important issues for application developments [7, 30]. The use of iron, cobalt, nickel nanoparticles are commonly used for this purpose [30]. The synthesis of these metal catalysts is high energy intensive process which also adds to the cost of CNT. Recently, Felisberto *et al.* [31] has reported the use of iron oxide catalysts for CNT synthesis. Iron oxide is easy to synthesize through a low energy intensive process. Thus, study on the use of a metal oxide for CNT synthesis from different precursors appears to be useful for sustainability of CNT manufacturing industry.

The main aim of the chapter is to explore locally available renewable plant based precursors for CNT synthesis. To achieve the aim, following steps are identified: selection of plant, extraction of oil, synthesis of Fe₂O₃ nanoparticles - catalyst for CNT synthesis, modification of CVD setup for plant precursors and synthesis of CNT using CVD technique.

2.2. Materials and method

2.2.1. Chemicals and reagents used

For the extraction and purification of the oil precursors, petroleum ether (grade: pro analysi, 90%; B.P. 40°C - 60 °C, Merck, India) was used. For the synthesis of iron oxide nanoparticles, iron nitrate monohydrate (grade: purified, 98%) and urea (grade: extra pure, 99.5%) were procured from Merck, India. Oleic acid (grade: pure, 65-88%; Merck India) was used as surfactant during the synthesis of iron oxide nanoparticles. Hydrochloric acid (grade: GR) and sulfuric acid (grade: pure, 97-99%) used for purification of CNTs were procured from Merck (India). Nitrogen gas (grade: 99.9 %, Rass cryogenics, India) was used as carrier in CVD. All the chemicals and reagents were used as received without further purification.

2.2.2. Selection of plant for precursor of CNT

North-eastern part of India is one of the richest biodiversity regions of the world and is a reservoir of wide variety of flora and fauna. The plant precursors were selected on the basis of availability and oil content in the kernel of the seed. The seeds were collected during the seeding season of the year for each species.

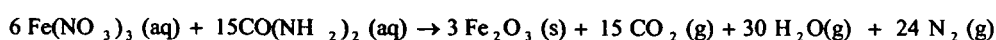
2.2.3. *Extraction of oil*

Chemical extraction also known as solvent extraction is used to extract oil from the seed or kernel. Solvent extraction is a process which involves extracting oil from oil-bearing materials by treating it with a low boiling point solvent as opposed to extracting the oils by mechanical pressing methods (such as expellers, hydraulic presses, etc.). The solvent extraction method recovers almost all the oils with a very less residual oil in the raw material, whereas, in the case of mechanical pressing the residual oil left in the oil cake is as high as 40-50% [32]. Thus, chemical extraction of oil from the seeds is employed in the reported work. It ensures a good quality of the oil and enables to assess the yield of oil from each species accurately.

The seeds of the six plants were collected, cleaned, dried, and finally grinded into fine powder. Soxhlet apparatus was used to extract oil from the grinded seeds using petroleum ether as a solvent. Oils extracted using Soxhlet process is a mixture of extracted oil from the seeds and petroleum ether. The mixture was purified using a rotary vacuum evaporator (Strike 202, Steoglass, Italy) to obtain pure oil. Each of the purified oil samples were sealed properly to prevent their tendency to oxidation in the presence of air during storage.

2.2.4. *Synthesis of Fe₂O₃ nanocatalyst for CNT synthesis*

The iron oxide nanoparticles were synthesized using solution combustion method following the method given by Suresh and Patil [33] with some modification. The synthesis process involved the combustion of redox mixture with iron nitrate as oxidizing reactant and urea as reducing fuel. The oxidizing valence of the oxidizer and the reducing valence of the fuel were taken into account for determining the composition of the solution. The theoretical equation assuming complete combustion can be written as follows:



Accordingly appropriate ratio of iron nitrate and urea was dissolved in water (50% w/v) in a quartz crucible. Few drops of oleic acid were added as surfactant.

Surfactant is used essentially to get nanoparticles of small size. Surfactants form micelle around the molecules in the solution inhibiting the growth in the number of molecules. The solution was ultrasonicated for 15 min. The crucible containing the solution was kept for aging at 80 °C for an hour. The samples, after aging, were directly put into a muffle furnace at 450 °C, 550 °C and 650 °C, respectively. The samples were named as S1, S2 and S3, respectively, and are, henceforth, referred accordingly.

2.2.5. CVD setup and its modification for plant precursors

As discussed in Chapter 1, CVD technique being the simplest and of low energy intensity, is commonly used for the CNT synthesis. Schematic of basic CVD setup commonly employed for batch mode synthesis is shown in figure 2.1. In general a CVD unit consists of two cylindrical furnaces: first furnace for evaporating the precursor kept in a quartz boat and the second furnace for depositing the precursor on the catalyst. A quartz tube (100 cm long and 2.5 cm ID) is used as reactor. An inert gas (viz. nitrogen, argon and helium) is used as the carrier gas for vaporized precursor inside the CVD reactor tube. It also helps to maintain inert atmosphere inside the reactor by employing bubblers both at the inlet and the outlet of the CVD setup. The flow rate of the gas is controlled using a regulator and a flowmeter. But it has a limitation on the quantity of the precursor used in each batch for synthesis of CNTs. So a need for modification in the CVD setup was felt to get high yield. To achieve this, the input of the plant precursor is to be copious. A continuous flow of plant precursor in each batch is needed to get desired yield.

The fabrication of CVD setup includes assembling a furnace, temperature controllers, flow controls, reactor tube and provision for gas connection. The fabricated furnace consists of Kanthal wire as the heating element. A ceramic tube was used to house the quartz tube (reactor tube). The heating element (Kanthal wire) was fixed over the ceramic tube. Furnace was covered using ceramic wool to reduce heat loss. A galvanized iron caging was used to house the furnace. Cromel-alumel thermocouple was used to monitor the temperature and was coupled with a PID controller for temperature control. Necessary provisions for gas inlet and outlet were employed using silicone tubes at both ends of the reactor. Gas flow controller was employed at the inlet side to control the flow of carrier gas. An attempt was made to

modify the existing CVD setup to be used for plant precursors so as to increase amount of precursor in a single batch and to redesign the furnace. These, modifications are expected to result in higher yield and lower the energy consumption in the synthesis process.

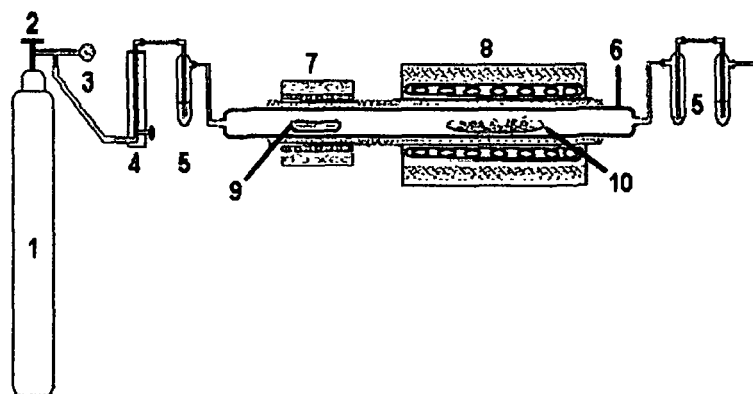


Figure 2.1: Schematic diagram of CVD unit (1-carrier gas cylinder, 2-gas regulator, 3-manometer, 4-flowmeter, 5- bubbler, 6-quartz tube, 7- 0.5 kW furnace, 8- 5 kW furnace, 9- precursor on quartz boat, 10- catalyst on quartz boat).

2.2.6. *Synthesis and purification of CNT*

The synthesis of CNT was carried out using precursor oil over iron oxide catalyst. A temperature range of 800° C – 900° C and flow rate 25-100 cc/min is reported for synthesis of CNT using plant based precursors viz., turpentine, camphor etc. [34-36]. Thus, renewable precursor oil was evaporated and pyrolyzed over 0.5 g of catalyst particles on semi-cylindrical quartz boat (ID 2 cm and length 10 cm) at a temperature of 850° C for 60 min. Nitrogen gas was used as the carrier gas during the synthesis at an optimized flow rate of 150 cc/min. The synthesized CNT samples were first added to 6M NaOH solution for 15 min. CNTs were collected by centrifugation and were washed several times with double distilled water. The process was repeated using 6M HCl for complete removal of catalyst particles.

2.2.7. *Characterization*

The surface morphology and size of the catalyst particles and CNTs were investigated using scanning electron microscopy (SEM), model no. JSM-6390LV

JEOL Japan. The samples were directly observed under SEM without platinum or gold coating. The transmission electron microscope (TEM), model no. JEM-100CX II (JEOL Japan) was used to study the internal structure and morphology. X-ray diffractometry (XRD) analysis was performed using Miniflex, Rigaku (Japan) to investigate the crystallinity of the nanoparticles.

2.3. Results and discussion

2.3.1. Selection of plant precursor and extraction of oil

Initially eight potential plant species of north-east, India origin were identified to be used as precursor for CNT synthesis. These plant species were selected on the basis of wide availability in the region. As oil content in the seed or kernel also plays an important role, the next stage of screening was based on the oil content in the seed or kernel of the plant species. The oil from the seeds or kernel was extracted using Soxhlet apparatus. Based on the oil content it was found that only six plant species are economically suitable for CNT synthesis, these are *Cocos nucifera*, *Brassica nigra*, *Sesamum indicum*, *Mesua ferrea*, *Ricinus communis*, *Azadirachta indica*, *Pongamia pinnata* and *Gossypium barbadense*.

The major fatty acid component, total oil content, ash content and viscosity were found out using standard techniques. The results summarizing total oil content, major fatty acid component, ash content and viscosity for the selected eight species are summarized in the Table 2.1. The analysis of the extracted oil shows that *Sesamum indicum*, *Mesua ferrea* and *Azadirachta indica* contain oleic acid as the major component in the oil, whereas *Cocos nucifera*, *Brassica nigra*, *Ricinus communis*, *Gossypium barbadense* and *Pongamia pinnata* have Lauric acid, Erucic acid, Ricinoleic acid, Linoleic acid and Behenic acid as the major fatty acid component in the oil.

This variation in the fatty acid composition of the oils may affect the morphology and yield of CNTs from these oils. The variation of morphology and yield for each precursor oil is studied in section 2.3.4 of this chapter. The oil extracted from each precursor was kept in an air sealed bottle to prevent oxidation.

2.3.2. Characterization of Fe_2O_3 nanocatalyst

X-ray diffraction pattern along with the scanning electron micrographs of the synthesized iron-oxide particles are shown in figure 2.2 and 2.3, respectively. As shown, with increase in calcination temperature the particle size decreases. S1, synthesized at 450°C shows size distribution ranging from 0.8 μm to 5 μm (Figure 2.3, S1). At temperature of 550 °C, particle size distribution of 0.8-1 μm is seen (Figure 2.3, S2). The iron oxide particles synthesized at 650°C (S3) shows very good particle size distribution having smaller particles as compared to S1 and S2. S3 had a particle size distribution of 0.25-0.5 μm (Figure 2.3, S3). The temperature variation not only has an impact on the size but also on the morphology of the particles. The sample S1 showed completely irregular shape of the particles synthesized. As the synthesis temperature increased the uniformity in the morphology of the particles also increased. In S2 the particles showed almost uniform shape, but from the SEM image it is clearly observed that the S3 particles have more uniform shape throughout with few agglomerates. It must be noted that small particle size of the catalysts is desirable to synthesize CNTs.

Table 2.1: Selected plant species along with their oil content, ash content, viscosity and the major fatty acid composition.

S.No	Precursor	Oil content (% w/w)	Ash content (% w/w)	Viscosity (mPa s)	Major fatty acid (%)
1	<i>Cocos nucifera</i>	63.4	1.1	6.5	Lauric acid (47-55)
2	<i>Brassica Nigra</i>	34.6	2.9	1.2	Erucic acid (40-55)
3	<i>Sesamum indicum</i>	49.2	3.9	33.7	Oleic acid (45-50)
4	<i>Mesua ferrea</i>	63.7	1.6	16.0	Oleic acid (55-65)
5	<i>Ricinus communis</i>	45.9	1.9	32.1	Ricinoleic acid (85-90)
6	<i>Azadirachta indica</i>	48.7	1.4	12.3	Oleic acid (25-50)
7	<i>Gossypium barbadense</i>	19.8	2.1	7.4	Linoleic acid (44-50)
8	<i>Pongamia pinnata</i>	29.2	0.5	5.0	Behenic acid(10-20)

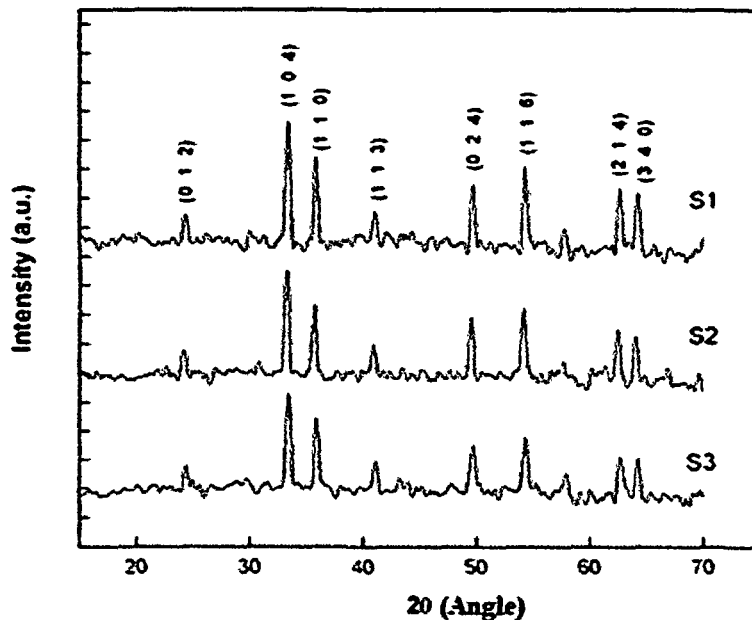


Figure 2.2: XRD analysis of the synthesized iron oxide particles prepared at different temperatures – S1 (450 °C), S2 (550 °C) and S3 (650 °C).

Presence of peaks at angles (2θ), 24.20°, 33.23°, 35.69°, 40.99°, 49.50°, 54.16°, 62.49° and 64.05° in the XRD pattern portrays the synthesized iron oxide particles to be hematite. The intensity of the peaks increased with temperature which indicates increase in crystallinity of the particles at higher temperature.

The sample S3 is found to have smallest iron oxide particles among the synthesized samples. But, the exact size cannot be estimated in SEM analysis. To reveal the exact size of the iron oxide nanoparticles TEM analysis was performed for the sample S3 (Figure 2.4). As seen in the TEM micrograph, the iron oxide nanoparticles range from 10 – 20 nm. The synthesis of CNT requires nano-sized catalyst particles. Thus the sample S3 may be used as catalyst for the synthesis of CNTs.

2.3.3. Modification of CVD setup for plant precursors

In the first stage of modification the batch mode was converted to continuous flow mode for plant precursors. It is done by attaching a tank (which contains

precursor oil) in the CVD setup instead of using a boat which can only contain limited amount precursor oil. The setup is shown in the figure 2.5.

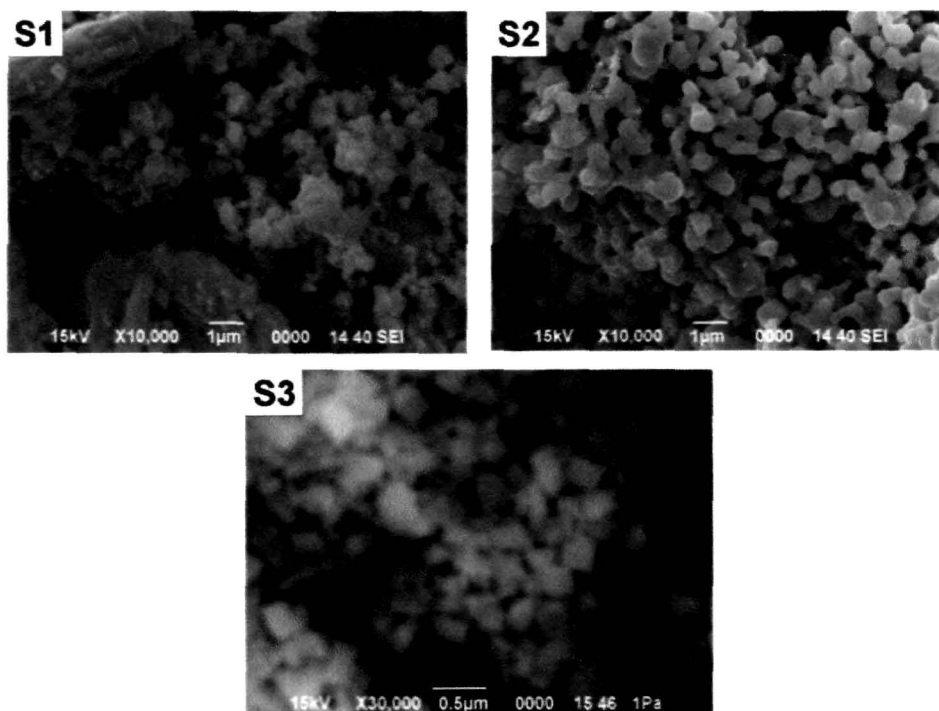


Figure 2.3: SEM analysis of the synthesized iron oxide particles prepared at different synthesis temperatures, S1 (450 °C), S2 (550 °C) and S3 (650 °C)

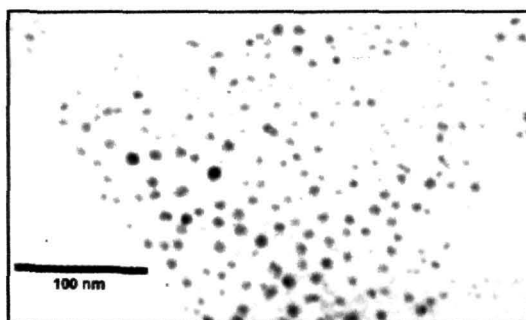
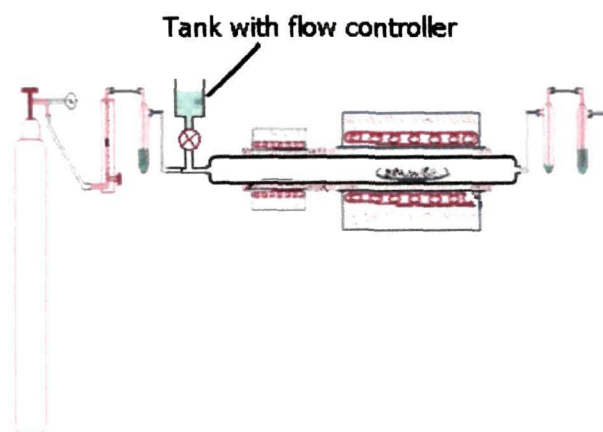


Figure 2.4: TEM image of the iron oxide nanoparticles (S3)

The modified CVD solved the problem of yield of CNTs in single batch. In the second stage, based on the experience, the basic setup was planned to be further improved in terms of energy intensity and energy efficiency. The CVD setup was modified to decrease the energy intensity in synthesis of CNTs from plant precursors. For this the 0.5 kW furnace was

removed and the quartz tube (along with the furnace) was tilted by at angle ' α ', as shown in the figure 2.6. It was expected to provide enough heat to the precursor to be evaporated and get suitably deposited on the catalyst.



(a)



(b)

Figure 2.5: Modified CVD setup (stage-1): a) schematic representation of the setup and b) indigenously modified set up

The angle ' α ' was optimized for proper flow of precursor into the furnace. Depending on the viscosity the angle is optimized by trial and error. It was found that for precursors *Sesamum indicum*, *Mesua ferrea*, *Ricinus communis* and *Azadirachta indica* an angle of 20° (α) is suitable whereas for precursors *Cocos nucifera*, and *Brassica nigra* it is 15° .

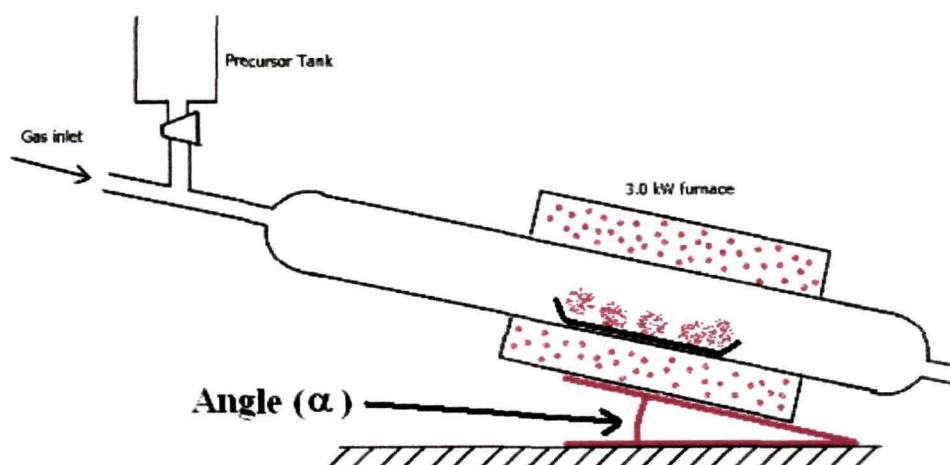


Figure 2.6: Modification of CVD setup (stage 2)

The modifications resulted in improved performance in terms of CNT output using the procedure outlined in section 2.2.6 employing a single furnace. The quality of CNT can be assessed based on characterization results discussed next.

2.3.4. Characterization of CNT synthesized

The scanning electron microscopy (SEM) micrograph of the CNTs is shown in Figure 2.7. The SEM micrograph enables us to have a clear view of the overall structure, growth and surface morphology of the CNTs synthesized from each precursor. The yield in the form of entangled noodle-like densely packed multi walled carbon nanotubes (MWCNTs) is evident in the case of *Cocos nucifera*, *Brassica Nigra* and *Ricinus communis*, with an average tube diameter of 90nm, 100 nm and 80 nm, respectively. The SEM micrograph of MWCNTs synthesized using these precursors further reveals that these MWCNTs are having very high aspect ratio. The length of the tubular structures were found to be in the range of 5-10 μm , 3-5 μm and 10-12 μm for *Cocos nucifera*, *Brassica nigra* and *Ricinus communis* precursors, respectively. Applications where higher aspect ratio is needed the CNTs synthesized using *Cocos nucifera*, *Brassica Nigra* and *Ricinus communis* precursors may be used. On the other hand, the precursors, *Azadirachta indica*, *Sesamum indicum* and *Sesamum indicum* yielded short length, straight CNTs. The diameters of the CNTs synthesized were in the range of 100-150 nm, 60-80 nm and 60-75 nm for

Sesamum indicum, *Mesua ferrea* and *Azadirachta indica* precursors, respectively. It is observed that the CNTs synthesized from precursors containing oleic acid as major fatty acid component yielded short length, straight CNTs with identical tubular diameter distribution. The Energy-dispersive X-ray (EDX) analysis of all the samples shown in Table 2.2, confirms the presence of carbon and iron in the samples. The presence of oxygen is also evident from the results. The yield of CNT from different precursors is given in the Table 2.2.

Table 2.2: Yield of CNT from different plant based precursors

Sl. No.	Precursor oil	Yield of CNT (g/25ml)	Atomic % (using EDX)			
			Carbon	Iron	Oxygen	Other elements
1	<i>Brassica Nigra</i>	3.9±0.2	58.46	0.04	40.70	0.80
2	<i>Cocos nucifera</i>	3.2±0.2	56.19	0.12	43.20	0.49
3	<i>Ricinus communis</i>	4.1±0.3	68.71	1.28	29.5	0.51
4	<i>Azadirachta indica</i>	3.1±0.1	75.47	16.18	7.73	0.62
5	<i>Sesamum indicum</i>	3.5±0.2	90.21	9.24	0.42	0.13
6	<i>Mesua ferrea</i>	3.6±0.1	78.07	18.12	2.62	0.10

The TEM micrographs of the synthesized nanomaterials are shown in figure 2.8. The presence of catalyst particles inside MWCNT can be clearly seen. The defects in the concentric graphitic layers is also evident in the case of CNTs synthesized from *Cocos nucifera*, *Brassica nigra* and *Ricinus communis*, respectively. The defects in the walls may be attributed to the presence of different types of fatty acids in the precursors and the resultant pentagons and heptagons in the graphitic structure of CNTs. As discussed, this type of CNTs may find application in fuel cells and batteries, because of their high aspect ratio. Whereas, the CNTs synthesized from *Sesamum indicum*, *Mesua ferrea* and *Azadirachta indica* precursors have straight tubular structures as also seen in SEM analysis. These CNTs have minimal structural defects which makes them an important candidate for solar cell applications. The result also confirms the multiwalled structure of the CNTs.

The effect of composition of precursor oil on the morphology of CNTs is evident from the morphological study. It can be inferred that the fatty acid

composition of the precursor widely determines the morphological properties of the CNTs. Thus, based on the end use of CNTs, the precursor for CNT synthesis can be chosen. As this is the primary work on synthesis of CNTs using these renewable plant based precursors, a direct comparison could not be made.

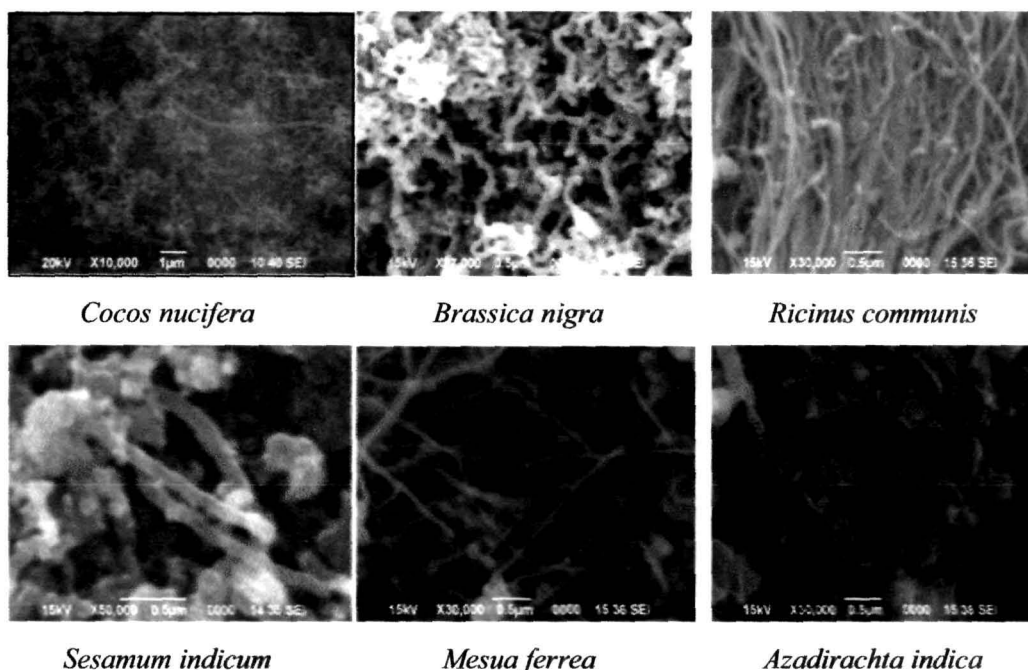


Figure 2.7: SEM micrographs of the CNTs synthesized from plant precursors

2.4 Conclusion

From the present study it can be concluded that the six screened renewable plant oils are potential precursors for MWCNT synthesis. Depending on the major fatty acid composition of the precursors the morphology and yield of the MWCNT varies. The best synthesis conditions for iron oxide nanoparticle synthesis using solution combustion method was found to be at 650 °C, with an aging time of 1.0 h at 80 °C. The modified CVD is found to be more effective design to be used for synthesis of MWCNTs using plant based precursors.

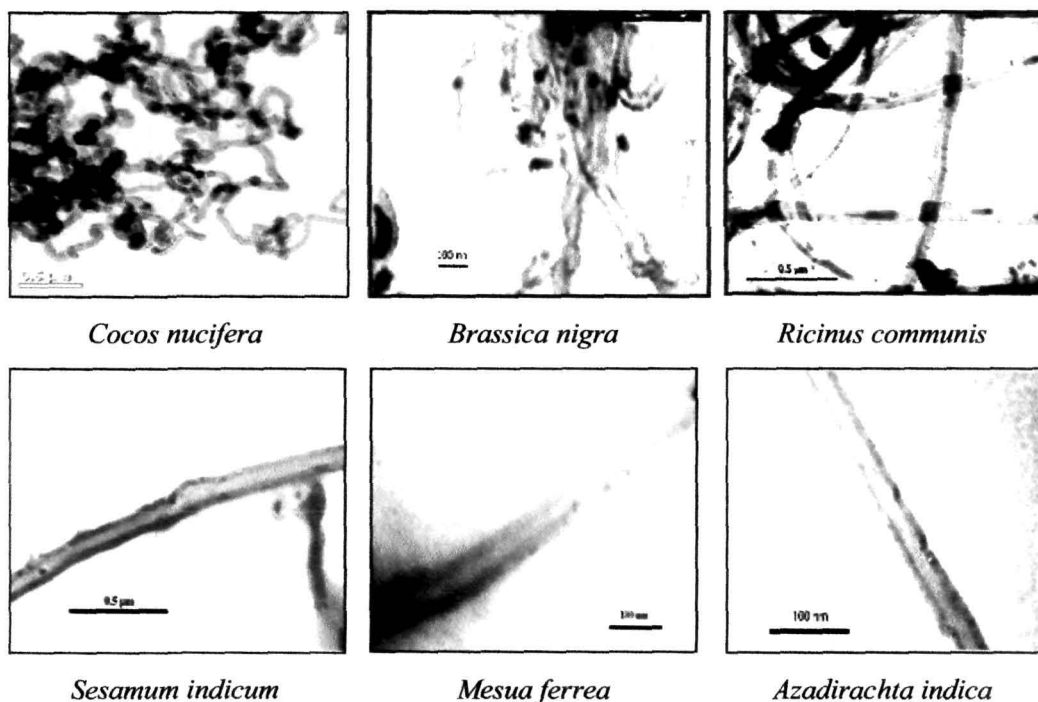


Figure 2.8: TEM micrographs of the CNTs synthesized using plant precursors

The structural features of carbon nanotubes prepared by CVD have delicate dependence on carbon precursor, catalyst, carrier gas, flowrate, reaction temperature and time. Since, this is the first report of MWNTs synthesis from plant based precursors, no data are available for direct comparison of the results. The use of natural renewable precursors gives reasonable yield and makes the process environment friendly as well. This method can be easily implemented and scaled up for mass production of MWNTs from renewable natural precursor. But, the optimization of the physical parameters for the synthesis of MWCNTs for a particular plant based precursor needs to be done. The yield and quality of MWCNTs depends to a great extent on the process parameters. Thus it becomes essential to study of the impact of each parameter along with optimization for better yield and quality of MWCNTs.

References

1. Ebbesen, T. W., and Ajayan, P. M. Large scale synthesis of carbon nanotubes, *Nature* **358**, 220, 1992.
2. Weiwei, F., et al. Synthesis of SWNTs from charcoal by arc-discharging, *Journal of Wuhan University of Technology- Materials Science Edition* **25**(2), 194-196, 2010.
3. Sadeghian, Z. Large-scale production of multi-walled carbon nanotubes by low-cost spray pyrolysis of hexane. *New Carbon Material* **24** (1), 33-338, 2009.
4. Edgar, K., and Spencer, J. L. The synthesis of carbon nanotubes from Muller clusters, *Current Applied Physics* **6**, 419–421, 2006.
5. Qiu, J., et al. Synthesis of double-walled carbon nanotubes from coal in hydrogen-free atmosphere, *Fuel* **86**, 282–286, 2007.
6. Samant, K. M., and Haram, S. K., Synthesis of carbon nanotubes by catalytic vapor decomposition (CVD) method: Optimization of various parameters for the maximum yield, *Pramana-journal of physics* **68**(1), 51–60, 2007.
7. See, C. H., and Harris A. T., A Review of Carbon Nanotube Synthesis via Fluidized-Bed Chemical Vapor Deposition, *Ind. Eng. Chem. Res.* **46**, 997-1012, 2007.
8. Akinwande, D., et al. Surface Science of Catalyst Dynamics for Aligned Carbon Nanotube Synthesis on a Full-Scale Quartz Wafer, *J. Phys. Chem. C* **113**, 8002-8008, 2009.
9. Luo, Z., et al. Effect of ion bombardment on the synthesis of vertically aligned single-walled carbon nanotubes by plasma-enhanced chemical vapor deposition, *Nanotechnology* **19**, 255607-255612, 2008.
10. Wang H., et al. Synthesis of Aligned Carbon Nanotubes on Double-Sided Metallic Substrate by Chemical Vapor Deposition, *J. Phys. Chem. C* **111**, 12617-12624, 2007.
11. Vinayan B.P., et al. Catalytic activity of platinum cobalt alloy nanoparticles decorated functionalized multiwalled carbon nanotubes for oxygen reduction reaction in PEMFC, *International Journal of Hydrogen Energy* **37**, 412-421, 2012.

12. Zhang, H., et al. Preparation and electrochemical performance of SnO₂ @ carbon nanotube core-shell structure composites as anode material for lithium-ion batteries, *Electrochimica Acta* **59**, 160–167, 2012.
13. Fabre, B., and Samori C., Immobilization of double functionalized carbon nanotubes on glassy carbon electrodes for the electrochemical sensing of the biotin-avidin affinity, *Journal of Electroanalytical Chemistry* **665**, 90–94, 2012.
14. Sugino, T., et al. Actuator properties of the complexes composed by carbon nanotube and ionic liquid: The effects of additives, *Sensors and Actuators B* **141**, 179–186, 2009.
15. Xi, B., et al. Electrochemical pneumatic actuators utilizing carbon nanotube electrodes, *Sensors and Actuators B* **138**, 48–54, 2009.
16. Klumpp, C., et al. Functionalized carbon nanotubes as emerging nanovectors for the delivery of therapeutics, *Biochimica et Biophysica Acta (BBA) – Biomembranes* **1758**, 404 – 412, 2006.
17. Feng, W., and Ji, P., Enzymes immobilized on carbon nanotubes, *Biotechnology Advances* **29**, 889–895, 2011.
18. Liu, X., et al. Optimization of surface chemistry on single-walled carbon nanotubes for in vivo photothermal ablation of tumors, *Biomaterials* **32**, 144–151, 2011.
19. Noureldine, D., et al. Investigation of carbon nanotube webs as counter electrodes in a new organic electrolyte based dye sensitized solar cell, *J. Mater. Chem.* **22**, 862–869, 2012.
20. Nam, J. G., et al. Enhancement of the efficiency of dye-sensitized solar cell by utilizing carbon nanotube counter electrode, *Scripta Materialia* **62** (3), 148–150, 2010.
21. Soin, N., et al. Sputter deposition of highly dispersed platinum nanoparticles on carbon nanotube arrays for fuel cell electrode material, *Diamond and Related Materials* **19** (5-6), 595–598, 2010.
22. Prehn, K., et al. Towards nitrogen-containing CNTs for fuel cell electrodes, *Composites Science and Technology* **69** (10), 1570–1579, 2009.

23. Shu, Q., et al. Hybrid Heterojunction and Photoelectrochemistry Solar Cell Based on Silicon Nanowires and Double-Walled Carbon Nanotubes, *Nano Lett.*, **9** (12), 4338–4342, 2009.
24. Skripnyuk, V. M., et al. Hydrogen storage properties of as-synthesized and severely deformed magnesium – multiwall carbon nanotubes, *International Journal of Hydrogen Energy* **35** (11), 5471-5478, 2010.
25. Ghosh, P., et al. Symplified synthesis of single-walled carbon nanotubes from botanical hydrocarbon : Turpentine oil, *Journal of alloys and compounds* **462** (1-2), 289-293,2008.
26. Kumar M., and Ando, Y., Gigas Growth of Carbon Nanotubes, *Defence Science Journal* **58** (4), 496-503, 2008.
27. Kumar M., and Ando, Y., A simple method of producing aligned carbon nanotubes from an unconventional precursor – Camphor, *Chemical Physics Letters* **374** (5-6), 521–526, 2003.
28. Afre, R. A., et al. Carbon nanotubes by spray pyrolysis of turpentine oil at different temperatures and their studies, *Microporous and Mesoporous Materials* **96** (1-3), 184-190, 2006.
29. Andrews, R. J. and Smith, C. F. Mechanism of carbon nanotube growth from camphor and camphor analogs by chemical vapor deposition, *Carbon* **44**(2), 341-347, 2006.
30. Li, Z., et al. Micro-Raman spectroscopy analysis of catalyst morphology for carbon nanotubes synthesis, *Chemical Physicse* **353** (1–3), 25-31, 2008.
31. Felisberto, M., et al. The growth of carbon nanotubes on large areas of silicon substrate using commercial iron oxide nanoparticles as a catalyst, *Materials Letters* **64** (20), 2188-2190, 2010.
32. Luque-de-Castro, M. D., and García-Ayuso, L. E., Soxhlet extraction of solid materials: an outdated technique with a promising innovative future, *Analytica Chimica Acta* **369** (1–2), 1–10, 1998.
33. Suresh, K., and Patil K. C., Combustion synthesis and properties of fine particle Li-Zn ferrites. *Journal of Alloys and Compounds*, **209**(1-2), 203-206, 1994.
34. Chuang, K. H., et al. Influence of Catalysts on the Preparation of Carbon Nanotubes for Toluene Oxidation, *Ind. Eng. Chem. Res.* **48** (9), 4202–4209, 2009.

35. Liao, X. Z., et al. Effect of catalyst composition on carbon nanotube growth, *Applied Physics Letters* **82** (16), 2694-2696, 2003.
36. Triantafyllidis, K. S., et al. Formation of carbon nanotubes on iron/cobalt oxides supported on zeolite-Y: Effect of zeolite textural properties and particle morphology, *Microporous and Mesoporous Materials* **110** (1), 128-140, 2008.
37. Jagadale, P., et al. Carbon Thin Films from Plant-Derived Precursors, *Synthesis and Reactivity in Inorganic, Metal-Organic, and Nano-Metal Chemistry* **37**,467–471, 2007.
38. Sharon, M., and Sharon, M., Carbon Nanomaterials and their Synthesis from Plant-Derived Precursors, *Synthesis and Reactivity in Inorganic, Metal-Organic and Nano-Metal Chemistry* **36**, 265–279, 2006.

Chapter 3

Optimization of process parameters for synthesis of MWCNTs from renewable plant based precursors using Taguchi robust method

Chapter 3

Optimization of process parameters for synthesis of MWCNTs from renewable plant based green precursors using Taguchi robust method

The pre-requisite for process optimization is to set an objective parameter. For the synthesis of MWCNTs it is necessary to optimize the process for the objective parameter such as better yield or quality. This needs to be done for each precursor type. To achieve the twin objective of physical optimization of the process parameters for better yield and acceptable quality for each precursor type poses almost an impossible task because of time and cost involved. However, a statistical technique such as Taguchi robust technique is expected to be an efficient and effective tool to do this. The process needs to be optimized for each of the precursors selected for MWCNT synthesis for higher yield and acceptable relative quality conforming to requirement of applications. In this chapter, a few parameters that influence the yield and quality of CNT have been identified. Taguchi robust technique is employed which not only helps to optimize the parameters but also analyse the extent of effect of each parameter on the synthesis.

3.1. Introduction

In the earlier chapter, the potency of six plant based precursors for CNT synthesis was outlined with details of synthesis and characterization of CNTs which were multiwalled in nature. The yield and quality of those MWCNTs depend on various process parameters like temperature of synthesis, flow rate of carrier gas, catalyst type and characteristics. Thus, it becomes very important to explore the optimum conditions for better yield and acceptable quality for synthesis of MWCNTs from the six screened plant precursors. The work in this chapter is an attempt to use Taguchi robust technique for determining the optimum conditions for MWCNT synthesis from plant based precursors.

Statistically a process to be optimized has control factors (several process parameters for CNT synthesis) which directly decide the target or desired value of the output (the objective parameter high yield). The optimization then involves determining the best control factor levels so that the output is at the target value [1-2]. Such a problem is called as a "static problem". This is best explained using a P-diagram which is shown in figure 3.1(a). Noise is shown to be present in the process but should have no effect on the output. In any technique which minimizes variations in output even though noise is present in the process is said to have become robust. In the present study, noise may be in the form of minor molecules in the precursor, impurity of the carrier gas and impurity of the catalyst. Thus, the present work has all the conditions which make it a static problem. If on the other hand the product to be optimized has a signal input that directly decides the output, the optimization involves determining the best control factor levels so that the "input signal / output" ratio is closest to the desired relationship. Such a problem is called as a "dynamic problem". This is also explained by a P-diagram which is shown in figure 3.1(b). In the present work it is not possible to provide any input once the process has started. Hence, conditions of dynamic problem are not satisfied making it a static problem.

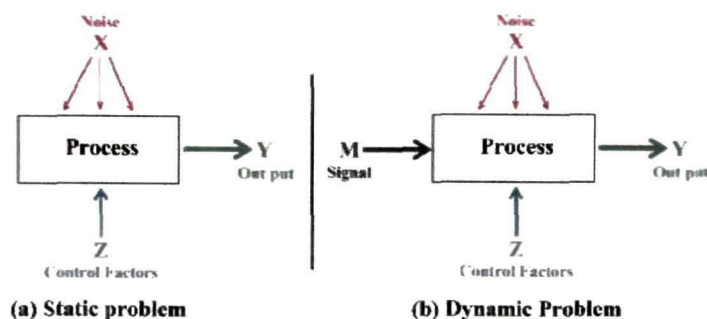


Figure 3.1: Schematic representation of static and dynamic problems by using P-diagram.

Taguchi robust method was, hitherto, used by researchers to optimize the process parameters for wastewater treatment, CVD method for film deposition, carbon nanotube growth [8-11]. Taguchi robust method may be employed to optimize the process parameters and also to evaluate the effect of these parameters on the synthesis of MWCNTs from renewable plant precursors [12]. The present

chapter aims to do so with the twin objectives identified as: Optimization of the process parameters and to study the level of influence of each parameter on the quality (morphology) and yield of MWCNT. It may be noted that quality of MWCNT may be judged qualitatively and quantitatively by SEM & TEM, SAD studies while quantitatively it may done by Raman. The present work reports the quality on the basis of SEM, TEM and SAD studies only.

3.2. Materials and method

3.2.1. Taguchi robust method

Taguchi method is a robust optimization method based on “Orthogonal Array” experiments [3-4]. This method gives much reduced “variance” in the results. The Orthogonal Arrays (OA) provide a set of well balanced (minimum) experiments and have a set of combination of parameters’ levels [5]. For each experiment (which is a particular combination of the parameters) the signal-to-noise ratio (S/N), which is the logarithmic function of desired output; serves as objective function for optimization [6]. Taguchi technique can not only be used to optimize the parameters but also provides the effect of each parameter [7]. There are 3 types of signals-to-noise ratios (S/N ratio) for optimization as used by researchers for optimizing the process parameters [2, 7]:

i) *Smaller-the-better*

$$\eta = -10 \log [\text{mean of sum of squares of measured data}] \quad (3.1)$$

This is usually the chosen S/N ratio for all undesirable characteristics like “defects” etc. for which the ideal value is zero. Also, when an ideal value is finite and its maximum or minimum value is defined, then the difference between measured data and ideal value is expected to be as small as possible. The generic form of S/N ratio then becomes,

$$\eta = -10 \log [\text{mean of sum of squares of \{measured - ideal\}}] \quad (3.2)$$

$$\eta = -10 \log - \sum (y_i) \quad (3.3)$$

Where y_i is the signal (reaction rate) and n is the number of repetitions in each experiment. If “defect” in the CNT is taken as the parameter then this S/N ratio may be used. But it is not the case in the present work.

ii) Larger-the-better

$$\eta = -10 \log[\text{mean of sum squares of reciprocal of measured data}] \quad (3.4)$$

$$\eta = -\log - \sum (1/y) \quad (3.5)$$

This case may be obtained considering *smaller-the better* and taking reciprocals of measured data and followed by calculation of S/N ratio as in the *smaller-the-better* case. As both quality and yield of CNT have to be higher under optimum condition, this S/N ratio is used in the present chapter.

iii) Nominal-the-best

$$\eta = 10 \log \left[\frac{\text{Desired Value}^2}{\text{Sum of Squares}} \right] \quad (3.4)$$

This case arises when a specified value is desired, meaning that neither a smaller nor a larger value is desirable.

Taguchi method can be used to obtain effect of parameter level (deviation it causes from overall mean of the signal). To determine the effect of each parameter level (m_i), average value of S/N ratios are calculated using analysis of mean (ANOM). For this calculation, the S/N ratios of experiments with corresponding parameter levels are employed [15]. The parameters effects (or factor effect), i.e. the contribution of each experimental parameter to the reaction rate are calculated by the analysis of variance (ANOVA). This is done by summing the squares (SoS) of variance of all levels of a given parameters which then is normalized with respect to the degrees of freedom (DoF) of the corresponding parameters (DoF = number of parameter levels - 1).

$$= -\sum \quad (3.5)$$

where, N_i is the number of experiments conducted with the same parameter levels. Sum of squares (SoS) of variances for all levels for a given parameter are obtained using equation (3.6). This term is divided by degree of freedom (DoF) of corresponding parameter to obtain factor effects of various experimental parameters given by expression 3.7.

$$\left(\right) = \sum \left(\left(- < \right) \right) \quad (3.6)$$

Where $\langle m_i \rangle$ is the average of m_i 's for a given parameter and the coefficient N_i represents the number of times the experiment is conducted with the same factor level.

$$\text{Factor effect} = \frac{\quad}{\Sigma} \quad (3.7)$$

Finally, it is used in data analysis and prediction of optimum results [1-5]. Again, the primary aim of the Taguchi experiments - to minimize variations in output even though noise is present in the process- is achieved by getting improved linearity in the input/output relationship.

3.2.2. Processes parameters to be optimized

As discussed by many researchers the quality and quantity of CNT synthesized mostly depend on the synthesis conditions for the conventional non-renewable precursors. The physical parameter during CNT synthesis for a particular precursor depends mostly on temperature of synthesis, catalyst type and flow rate of carrier gas. Thus, these physical parameters are to be optimized for better quality and higher yield. It was envisaged to investigate the influence of temperature, catalyst type and flow rate and different precursors for the synthesis of CNT using an L9 orthogonal array, where the inputs could be tested at three levels. It was further assumed that no interaction exists between the factors considered in the experiments. The precursors were divided on the basis of fatty acid composition in the oil, the first group of precursors containing Oleic acid as the major component and the second group which does not have Oleic acid. The parameters for the synthesis shown in Table 3.1.

Table 3.1: Different parameters to be optimized for optimum yield

Parameter	Level 1	Level 2	Level 3
Temperature (°C)	750	875	1000
Catalyst	Iron oxide	Cobalt oxide	Nickel oxide
Flow rate (cc/min)	150	175	200

3.2.3. Design of L9 experiments

As stated, the plant based precursors screened for CNT synthesis are categorized in terms of major fatty acid constituent. Thus the precursors, as planned, are grouped into two: first one is having oleic acid as its major fatty acid constituent and the second one without oleic acid as its major constituent. Thus, two L9 tables

were designed for optimization. The first L9 table (experiment L₁1-L₁9) was designed using the precursors which contain oleic acid as the major compound whereas the second L9 table (experiment L₂1-L₂9) consists of the precursors which do not have oleic acid in the oil are shown in Table 3.2 and Table 3.3 respectively, with the parameter levels.

Larger-the-better type of objective function for getting maximum yield of MWCNTs from the plant precursors is used hence the relation (3.5) was used for calculating S/N ratio.

Table 3.2: L9 table for precursors with oleic acid as the major fatty acid constituent

Experiment No.	Parameter Levels			
	Precursor oil (Level 1)	Temperature (°C) (Level 2)	Catalyst type (Level 3)	Flow rate of gas (cc/min) (Level 4)
L ₁ 1	<i>Azadirachta indica</i>	750	Iron oxide	150
L ₁ 2	<i>Azadirachta indica</i>	875	Cobalt oxide	175
L ₁ 3	<i>Azadirachta indica</i>	1000	Nickel oxide	200
L ₁ 4	<i>Sesamum indicum</i>	750	Cobalt oxide	200
L ₁ 5	<i>Sesamum indicum</i>	875	Nickel oxide	150
L ₁ 6	<i>Sesamum indicum</i>	1000	Iron oxide	175
L ₁ 7	<i>Mesua ferrea</i>	750	Nickel oxide	175
L ₁ 8	<i>Mesua ferrea</i>	875	Iron oxide	200
L ₁ 9	<i>Mesua ferrea</i>	1000	Cobalt oxide	150

3.2.4. Synthesis of catalysts

Three metal oxides (viz. iron, cobalt and nickel oxides) were synthesized using solution combustion method [16] with some modification as described in chapter 2 section 2.3.2. For synthesis each metal nitrates were mixed with urea in the ratio 1:3 w/w. The samples were synthesized at 650° C.

3.2.5. Synthesis of CNT using CVD technique

The MWCNTs were synthesized using the modified CVD setup. The synthesis of the MWCNTs was done as discussed in Chapter 2, nitrogen gas was used as carrier as well as to make inert atmosphere inside the furnace. The other process parameters were set as per the orthogonal table.

Table 3.3: L9 table for precursors without oleic acid as the major fatty acid constituent

Experiment No.	Parameter Levels			
	Precursor oil (Level 1)	Temperature (°C) (Level 2)	Catalyst type (Level 3)	Flow rate of gas (cc/min) (Level 4)
L ₂ 1	<i>Brassica nigra</i>	750	Iron oxide	150
L ₂ 2	<i>Brassica nigra</i>	875	Cobalt oxide	175
L ₂ 3	<i>Brassica nigra</i>	1000	Nickel oxide	200
L ₂ 4	<i>Cocos nucifera</i>	750	Cobalt oxide	200
L ₂ 5	<i>Cocos nucifera</i>	875	Nickel oxide	150
L ₂ 6	<i>Cocos nucifera</i>	1000	Iron oxide	175
L ₂ 7	<i>Ricinus communis</i>	750	Nickel oxide	175
L ₂ 8	<i>Ricinus communis</i>	875	Iron oxide	200
L ₂ 9	<i>Ricinus communis</i>	1000	Cobalt oxide	150

3.3. Results and discussion

3.3.1. L9 experiments

The eighteen experiments for the two Taguchi L9 tables were performed. The parameters were varied and controlled as suggested by L9 table. The synthesis of MWCNTs was carried out using 25 ml of plant based precursor. As discussed in chapter 2 the flow of carrier gas was controlled using a gas flowmeter whereas the temperature was regulated using a PID controller attached to the CVD unit. The catalyst (0.5 g) was loaded on a quartz boat placed inside the reactor chamber of

CVD. After synthesis of CNT they were heated to 400 °C for an hour to remove amorphous carbon and weighed. The weight of catalyst was deducted to get the weight of CNT synthesized. The synthesized MWCNTs were characterized using transmission electron microscopy as shown in the figure 3.2 and figure 3.3 corresponding to first and second Taguchi experiments, respectively.

In the figure 3.2, L₁1-L₁3 shows the TEM micrograph of MWCNTs synthesized from *Azadirachta indica*. The MWCNTs are found to have a diameter distribution of 50-60 nm, 100-120 nm and 90-100 nm at the synthesis conditions L₁1, L₁2 and L₁3, respectively. The MWCNTs synthesized using *Sesamum indicum* oil is shown in L₁4-L₁6, and has a diameter distribution of 100-120 nm, 90-100 nm and 80-90 nm for L₁4, L₁5 and L₁6, respectively. The L₁7-L₁9 shows the TEM micrographs of MWCNT from *Mesua ferrea*. The diameter distribution for the MWCNTs synthesized at different conditions are 80-110 nm, 80-90 nm and 70-90 nm for L₁7, L₁8 and L₁9, respectively.

L₂1-L₂3, L₂4-L₂6 and L₂7-L₂9 shown in figure 3.3 shows the MWCNTs synthesized using *Brassica nigra*, *Cocos nucifera* and *Ricinus communis* oil. As discussed in Chapter 2, the MWCNTs synthesized using these precursors yield longer, entangled MWCNTs with more defects in the walls than the precursors having oleic acid. The figure 3.2 and 3.3 show the yield and quality of the MWCNTs in different condition of synthesis as per the orthogonal table described by Taguchi. The results have been analyzed statistically for yield and quality of MWCNTs.

The selected area diffraction (SAD) pattern obtained by TEM is shown in figure 3.4 and figure 3.5 for the first and second Taguchi experiments, respectively. The diffuse halos in the SAD micrograph are due to the amorphous carbon film on the copper grid. The prominent sharp rings are due to the concentric graphitic planes of MWCNTs. The variation of crystallinity due to the variation of the process parameters could be seen. The results show that the best quality MWCNT samples were obtained under the condition L₁5 and L₂8 for the first and second Taguchi experiment respectively. Thus, it is evident that *Sesamum indicum* and *Ricinus communis* produce acceptable quality MWCNTs.

3.3.2. S/N calculations

S/N ratios, which determines the success of an experiment for each experimental yield, was obtained using equation (3.5). Table 3.4 and 3.5 displays the experimental parameter matrix and corresponding S/N ratios of CNT synthesis.

3.3.3. Effect of each parameters

According to the Taguchi method, the parameter levels leading to the maximum yield can be found by using the results given in Table 3.4 and Table 3.5. Justification of this argument lies in the properties of L9 and can be found in [15]. SoS, DoF and Factor effects were obtained employing corresponding equations (3.2), (3.3) and (3.4). The influence of each parameters for optimum yield was obtained by ANOVA using equation 3.5. The contribution of each parameter level towards the S/N ratio (η) as obtained from ANOM is displayed along with it.

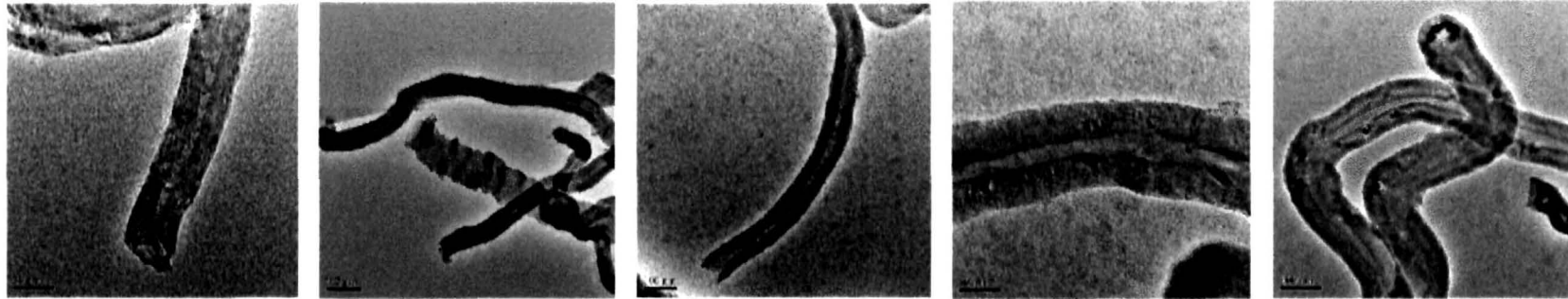
The effect of each parameter on yield was obtained using equation (3.7). The effect of the parameters for both the Taguchi L9 experiments is summarized in the Table 3.6 and Table 3.7. The results of first Taguchi experiment with precursors containing Oleic acid as the major fatty acid component in the oil reveals that the best temperature of synthesis to be 875 °C.

Iron oxide was found to be the most effective catalyst out of the catalysts chosen, whereas, a flow rate of 150 cc/min gave best results. Out of the precursors in the first group *Sesamum indicum* oil gave the best yield. In the second group the best conditions viz. precursor, synthesis temperature, catalyst type and flow rate for optimum yield was found out to be *Ricinus communis* oil, 875 °C, iron oxide and 150 cc/min, respectively.

From the Taguchi analysis of both the precursor type, it was found that the temperature of synthesis, catalyst type and flow rate affects the yield of MWCNTs. Out of these four parameters optimized, temperature of synthesis and flow rate were found to have greater impact on the yield. The descending order of the effect of parameters for yield is found out to be Temperature>Flow rate>Catalyst>Precursor. MWCNTs synthesized were found to have acceptable quality as is evident from SAD analysis.

Table 3.4: S/N ratio for first Taguchi L9 experiment

Exp. No.	Parameter Levels				Yield of CNT (g/25ml)	S/N (η)
	Precursor oil (Level 1)	Temperature ($^{\circ}$ C) (Level 2)	Catalyst type (Level 3)	Flow rate of gas (cc/min) (Level 4)		
L ₁ 1	<i>Azadirachta indica</i>	750	Iron oxide	150	3.2	1.01
L ₁ 2	<i>Azadirachta indica</i>	875	Cobalt oxide	175	3.0	0.95
L ₁ 3	<i>Azadirachta indica</i>	1000	Nickel oxide	200	1.8	0.51
L ₁ 4	<i>Sesamum indicum</i>	750	Cobalt oxide	200	2.2	0.68
L ₁ 5	<i>Sesamum indicum</i>	875	Nickel oxide	150	4.2	1.24
L ₁ 6	<i>Sesamum indicum</i>	1000	Iron oxide	175	2.6	0.82
L ₁ 7	<i>Mesua ferrea</i>	750	Nickel oxide	175	2.2	0.68
L ₁ 8	<i>Mesua ferrea</i>	875	Iron oxide	200	3.4	1.06
L ₁ 9	<i>Mesua ferrea</i>	1000	Cobalt oxide	150	3.2	1.01



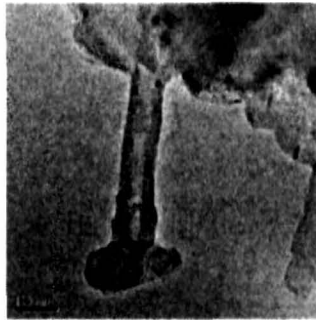
L₁₁

L₁₂

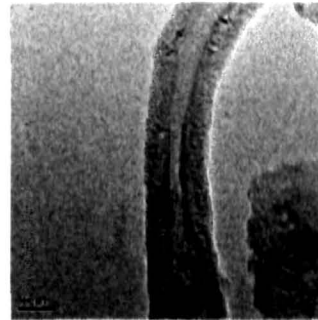
L₁₃

L₁₄

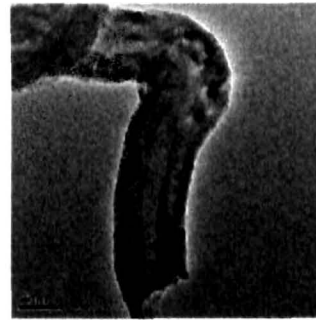
L₁₅



L₁₆



L₁₇

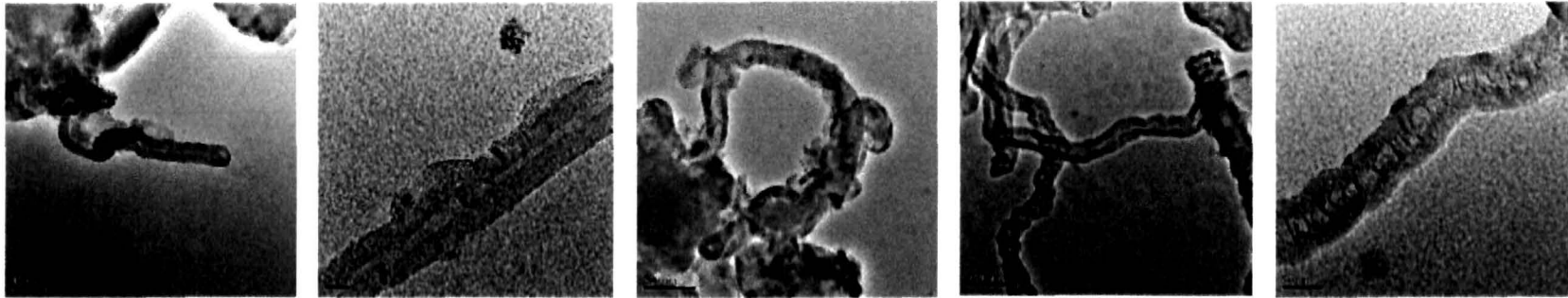


L₁₈



L₁₉

Figure 3.2: TEM micrographs for first Taguchi L9 experiments



L₂₁

L₂₂

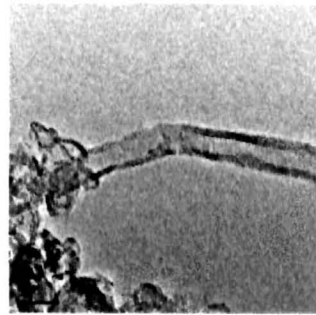
L₂₃

L₂₄

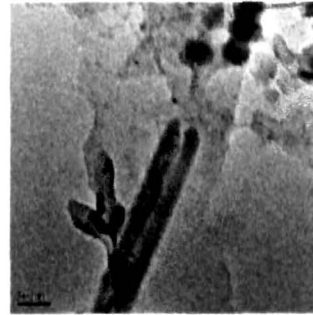
L₂₅



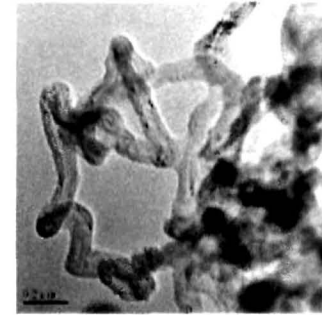
L₂₆



L₂₇



L₂₈



L₂₉

Figure 3.3: TEM micrographs for second Taguchi L9 experiments

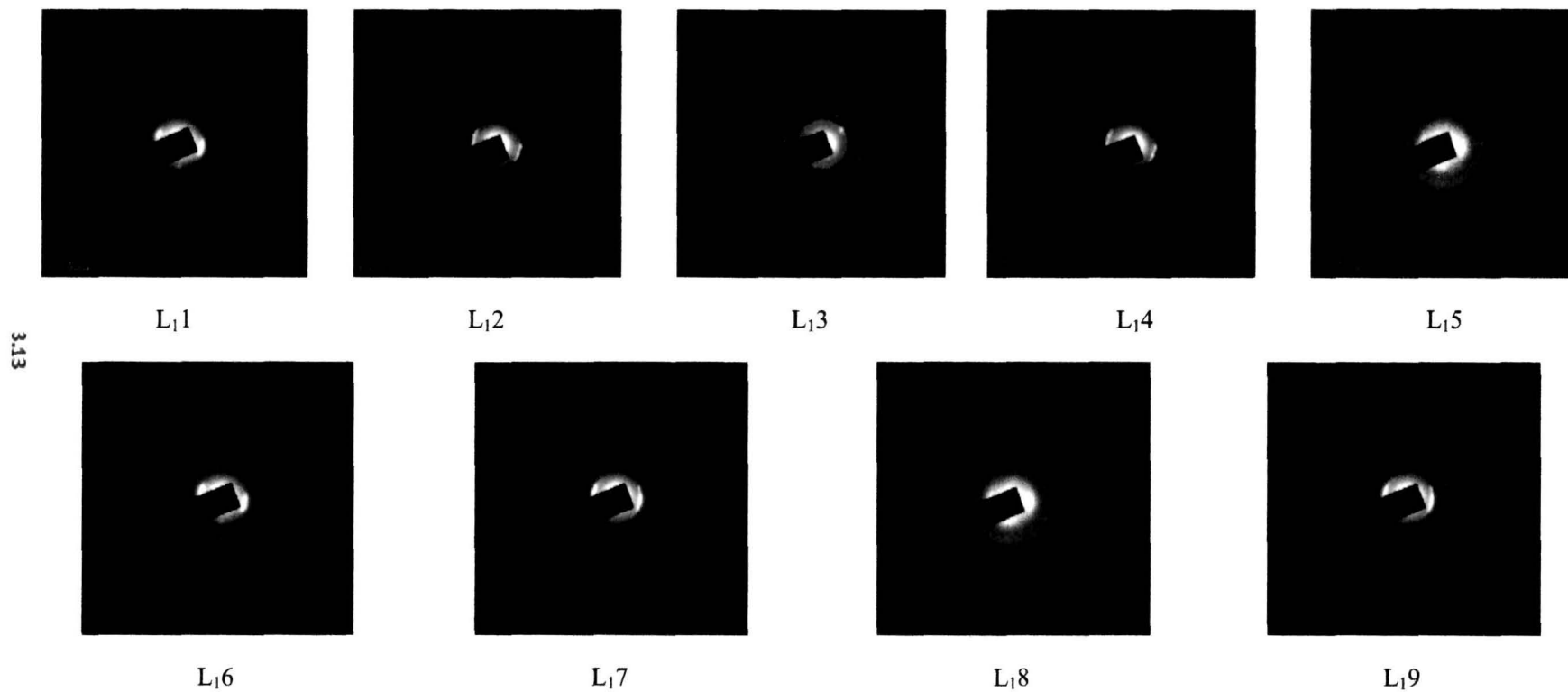


Figure 3.4: SAD pattern of synthesized MWCNTs corresponding to first Taguchi experiment for precursors containing oleic acid as major fatty acid composition.

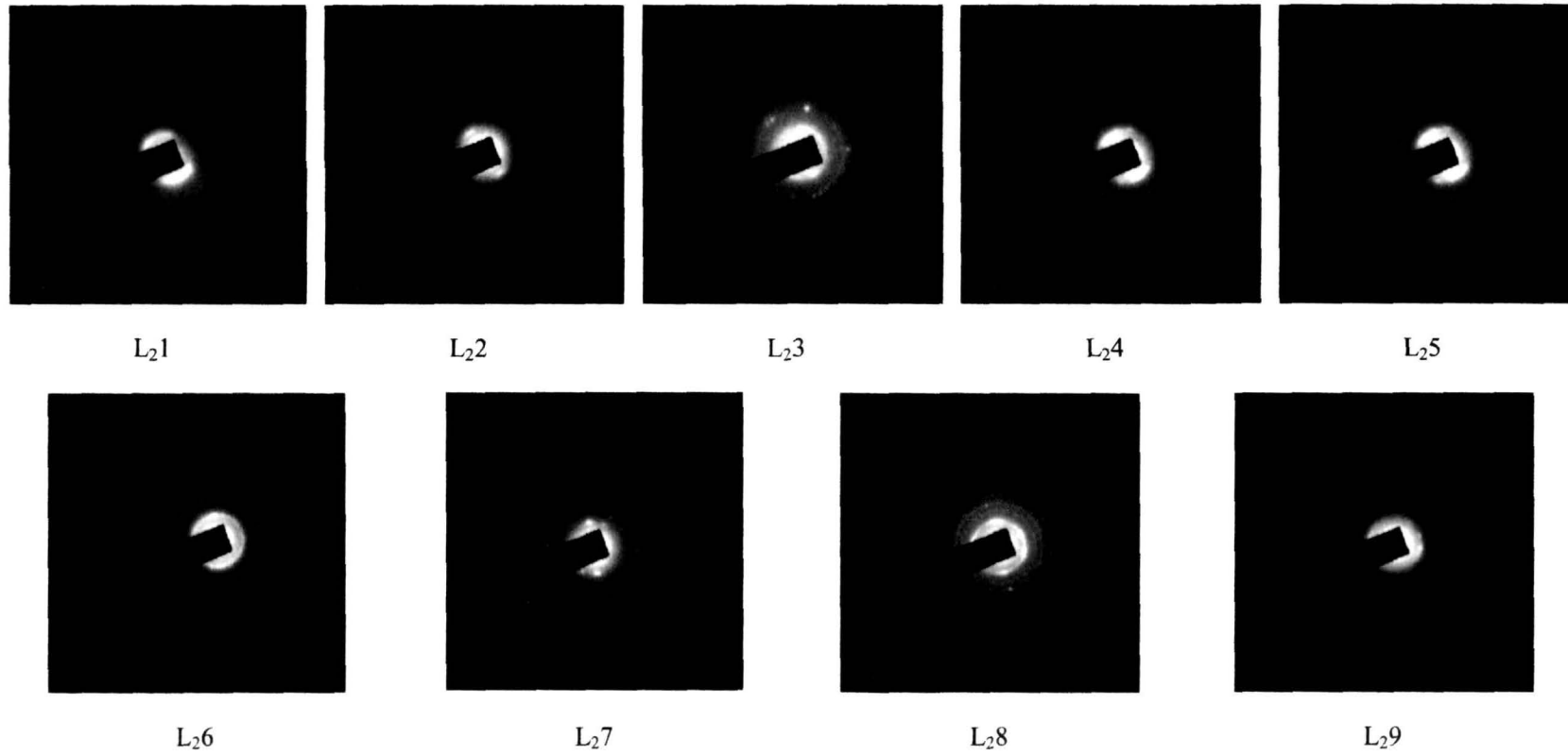


Figure 3.5: SAD pattern of synthesized MWCNTs corresponding to second Taguchi experiment for precursors without oleic acid as their major composition

Table 3.5: S/N ratio for second Taguchi L9 experiment

Exp. No.	Parameter Levels				Yield of CNT (g/25ml)	S/N (η)
	Precursor oil (Level 1)	Temperature ($^{\circ}$ C) (Level 2)	Catalyst type (Level 3)	Flow rate of gas (cc/min) (Level 4)		
L ₂₁	<i>Brassica nigra</i>	750	Iron oxide	150	3.3	1.03
L ₂₂	<i>Brassica nigra</i>	875	Cobalt oxide	175	2.9	0.92
L ₂₃	<i>Brassica nigra</i>	1000	Nickel oxide	200	2.4	0.76
L ₂₄	<i>Cocos nucifera</i>	750	Cobalt oxide	200	2.1	0.64
L ₂₅	<i>Cocos nucifera</i>	875	Nickel oxide	150	4.0	1.20
L ₂₆	<i>Cocos nucifera</i>	1000	Iron oxide	175	2.4	0.76
L ₂₇	<i>Ricinus communis</i>	750	Nickel oxide	175	2.6	0.83
L ₂₈	<i>Ricinus communis</i>	875	Iron oxide	200	3.6	1.11
L ₂₉	<i>Ricinus communis</i>	1000	Cobalt oxide	150	3.5	1.08

Table 3.6: Effect of parameters of synthesis of CNT for first Taguchi L9 experiment

Parameter	Level 1	Level 2	Level 3
Oil	0.825	0.920	0.919
Temperature ($^{\circ}$ C)	0.841	1.087	0.784
Catalyst	0.968	0.883	0.814
Flow rate	1.089	0.823	0.753

3.3.4 Yield at best conditions

In earlier section 3.3.3, the precursor and the conditions for optimum yield was screened out. The MWCNTs were synthesized at the optimized conditions with the precursor found to be most suitable for higher yield in each case. It is found that for *Sesamum indicum* oil 4.8 g/20 ml could be achieved. Whereas, in case of *Ricinus communis* oil the yield of MWCNT was found out to be 4.3 g/20 ml. Tables 3.8 and 3.9 presents the results for the yield of MWCNTs at best conditions.

Table 3.7: Effect of parameters of synthesis of CNT for second Taguchi L9 experiment

Parameter	Level 1	Level 2	Level 3
Oil	0.907	0.869	1.010
Temperature (C°)	0.813	1.080	0.869
Catalyst	0.970	0.886	0.931
Flow rate	1.109	0.883	0.839

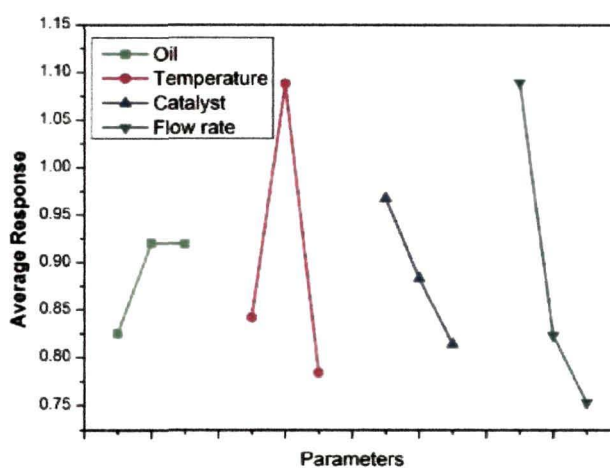


Figure 3.6 Graphical representation of average response for each parameter obtained from first L9 experiment

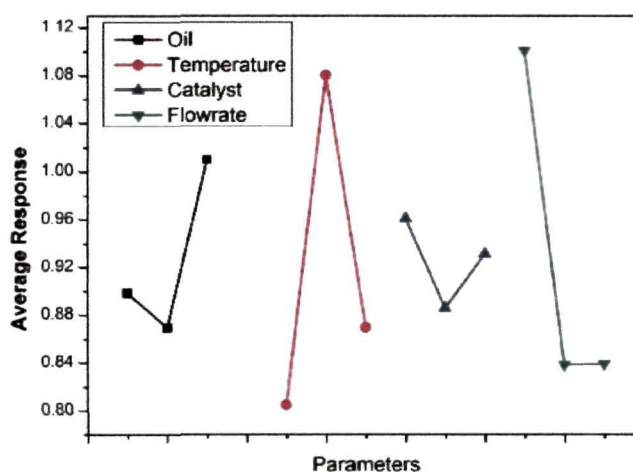


Figure 3.7 Graphical representation of average response for each parameters obtained from second L9 experiment

Table 3.8: Yield of CNT at best conditions for first Taguchi L9 experiment

Synthesis of CNT at best conditions-first L9 experiment		
Parameters	Best Level	Yield (in g/20 ml of precursor)
Oil	Level 2 (<i>Sesamum indicum</i>)	4.8
Temperature	Level 2 (875°C)	
Catalyst	Level 1 (Iron oxide)	
Flow rate	Level 1 (150 cc/min)	

Table 3.9: Yield of CNT at best conditions for second Taguchi L9 experiment

Synthesis of CNT at best conditions – 2 nd L9 Experiment		
Parameters	Best Level	Yield (in g/20 ml of precursor)
Oil	Level 3 (<i>Ricinus communis</i>)	4.3
Temperature	Level 2 (875°C)	
Catalyst	Level 1 (Iron oxide)	
Flow rate	Level 1 (150 cc/min)	

3.4 Conclusion

This chapter presents the Taguchi optimization of the process parameter for synthesis of MWCNTs using two different types of plant based precursors. Relative effects of four experimental parameters in determining the output of the experiments and their optimum factor levels are quantitatively obtained. All parameters are found to be contributing to the yield of MWCNTs, while temperature of synthesis, flow rate of carrier gas and catalyst type are found to be dominant parameters. Our experiment also proved that the precursor type and catalyst have low impact on the yield as compared to temperature of synthesis and flow rate. The effectiveness of the Taguchi method to optimize the process for CNT synthesis has been demonstrated in this study. It has been observed that the precursors having oleic acid yield shorter length CNT as

compared to those precursors which don't have oleic acid. The quality of CNT tubular structure is found to have minor defects when synthesized with oleic acid bearing precursors. Thus these precursors appear to be suitable for thin film fabrication devices like organic solar cells. Those precursors which does not contain oleic acid, give entangled noodle like structures.

From the TEM analysis it is clear that *Sesamum indicum* oil produces MWCNTs of short length but have good quality tubular structures. These MWCNTs may find application in organic solar cells. *Ricinus communis* oil on the other hand, may be used to develop Fuel cell electrodes and as substrate to hold catalysts.

References

1. Wadsworth, H. M. *Handbook of statistical methods for engineers and scientists* (2nd ed.). McGraw-Hill Professional, New York, 1997.
2. Taguchi, G. *Introduction to Quality Engineering*, Asian Productivity Organization, Tokyo, Japan 1990.
3. Ross, P.J. and Taguchi, G., *Techniques for Quality Engineering*, McGraw- Hill, New York, 1988.
4. G. Taguchi, *Introduction to Quality Engineering*, Asian Productivity Organization, 1986.
5. Li, Y., et al. Orthogonal Robust Design Method for Product Quality, IEEE conference proceedings- International Conference on Innovation Management (ICIM '09), Wuhan, China, 120 – 123.
6. Sharma, P., et al. Process parameter selection for strontium ferrite sintered magnets using Taguchi L9 orthogonal design, *Journal of Materials Processing Technology* **168**, 147-151, 2005.
7. Kalita, G., et al. Taguchi optimization of device parameters for fullerene and Poly (3-octylthiophene) based heterojunction photovoltaic devices, *Diamonds and Related Materials* **17** (4-5), 799-803, 2008
8. Madaeni, S. S., and Koocheki, S. Application of Taguchi method in the optimization of wastewater treatment using spiral wound reverse osmosis element, *Chemical Engineering Journal* **119**, 37–44 2006.
9. Kim, K. D., et al. Applying the Taguchi method to the optimization for the synthesis of TiO₂ nanoparticles by hydrolysis of TEOT in micelles, *Colloids and Surfaces A: Physicochem. Eng. Aspects* **254**, 99–105. 2005.
10. Ali, N., et al. Optimization of the new time modulated CVD process using the Taguchi method, *Thin Solid Films*, **469** (12), 154–160, 2004.
11. Porro, S., et al. Optimization of a thermal CVD system for carbon nano-tube growth, *Physica E* **37**, 16–20, 2007.
12. Jagadale, P., et al. Carbon Thin Films from Plant-Derived Precursors, *Synthesis and Reactivity in Inorganic, Metal-Organic, and Nano-Metal Chemistry* **37**, 467–471, 2007.
13. Sharon, M., et al. Application of the Taguchi Analytical Method for Optimization of Effective Parameters of the Chemical Vapor Deposition Process

- Controlling the Production of Nanotubes/Nanobeads, *J. Nanosci. Nanotechnol.* **5** (3), 289-296, 2005.
14. Bhardwaj, S., et al. Taguchi optimization of the carbon anode for Li-ion battery from natural Precursors, *Curr. App. Phys.* **8** (1), 71-77, 2008.
 15. Phadke, M. S. *Quality Engineering Using Robust Design*, Prentice-Hall, USA 1989.
 16. Suresh, K., and Patil, K.C. Combustion synthesis and properties of $\text{Ln}_3\text{Fe}_5\text{O}_{12}$ and yttrium aluminium garnets, *Journal of Alloys and Compounds* **209** (1-2), 203-206, 1994.

Chapter 4
*Application of functionalized and cut-
MWCNTs in organic photovoltaic cells*

Chapter 4

Application of functionalized and cut-MWCNTs in organic photovoltaic cells

Solar energy is one of the most promising sources out of renewable energy resources in a tropical country like India. The most effective conversion technique is direct conversion of solar energy into electrical energy. But, due to the problems with conventional photovoltaic (PV) technology, the PV technology could not be popularized, as discussed in Chapter 1. Recent fall in PV price are in positive direction but can only be sustained if we look for other options of solar PV cells with low processing energy intensity. Organic photovoltaic (OPV) cells overcome all the problems in conventional Si based PV cells. The only constraint is very low conversion efficiency of OPVs. Application of CNTs has shown to enhance the efficiency of some of the OPV architectures. This chapter reports the application of MWCNTs synthesized from plant based renewable precursors in OPVs.

4.1. Introduction

An organic photovoltaic (OPV) cell is a photovoltaic device that utilizes organic electronics for light absorption, charge generation and charge transport. It incorporates with conductive organic polymers or small organic molecules [1]. At present, organic solar cells are being studied extensively worldwide in order to improve their power conversion efficiency (PEC). Organic semiconductors are usually soluble in an organic solvent, which makes it possible to produce liquid solutions termed as ink. Ink can be deposited on any flexible and transparent substrates. In presence of radiation these organic semiconductors generate excitons (electron – hole pair, bound to each other due to electrostatic force) known as donors. These excitons are broken by another set of organic molecules which have the affinity towards either electron or hole. Due to this process the electrons and holes are separated and are taken to respective electrodes [2].

Organic photovoltaic (OPV) cells can further be classified into three groups based on architecture: single layer, having one single layer in between the electrodes,

figure 4.1(a); Bi-layer cells, in which two different layers of donor and acceptor are fabricated, figure 4.1(b) and bulk hetero junction cells, in which the donor and acceptor are blended in a single photoactive layer (figure 4.1.c). These types of cells differ not only in structure, but also in materials and manufacturing processes to inorganic solar cells. An organic solar cell is characterized by its current–voltage curve, which is measured under standard AM 1.5 illuminations [3].

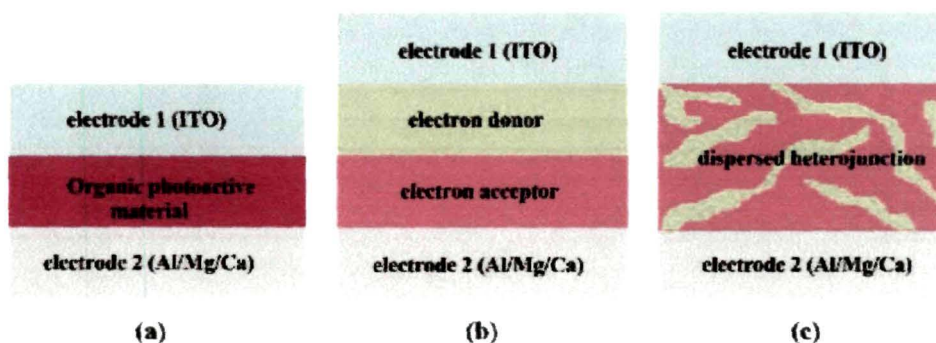


Figure 4.1: Different architecture of OPV device: a) single active layer, b) bi-layer consisting of donor and acceptor molecules and c) dispersed heterojunction of donor and acceptor molecules

Organic materials used in OPV cells have low cost but their efficiency is low [4-6]. OPVs are broadly classified into three types based on photoactive materials used in their architecture: polymer solar cells, dye sensitized solar cells and hybrid solar cells. The polymer solar cells use photoactive organic polymers for generation of excitons. Such organic photovoltaic cells fabricated with conjugated polymers and fullerene based compounds are promising alternative to energy intensive and expensive inorganic cells for solar photovoltaic conversion [7-9]. The dye sensitized solar cell uses an organic dye for generation of excitons and the hybrid solar cell incorporates both organic and inorganic photoactive material for power generation. Out of these, organic polymer solar cell is easy to fabricate and has better form factor flexibility. Organic polymer solar cells have higher shelf-life as they do not contain electrolyte as in case of dye sensitized solar cells. These facts make organic polymer solar cells to be better compared to other OPV types. But, the power conversion efficiency of polymer solar cells is very low due to short migration length of excitons, problems with exciton dissociation, low conductivity and recombination. As discussed in chapter 1,

nanomaterials like CNTs were incorporated to overcome these constraints. The use of CNT in the organic photovoltaic cell was first investigated by Ago et al. [10]. They used a layer of CNT as a cathode electrode. The polymer-nanotube composite was prepared by spin coating, using high concentration of MWCNT.

The efficiency of bulk heterojunction solar cells is the highest among all other OPV configurations. The various organic photoactive materials used in OPVs reported along with the current-voltage characteristics are summarized in Table 4.1 [11].

Table 4.1: Different photoactive materials used in OPVs along with reported I-V characteristics and fill factor of the fabricated device [11].

<i>OPV type</i>	<i>Photoactive Materials</i>	<i>Short circuit current</i>	<i>Open circuit voltage</i>	<i>Fill factor</i>
Polymer-polymer	F8TBT:P3HT	4 mA/cm ² at 100mW/cm ²	1250mV	45%
Polymer-hybrid	P3HT: CdSe nanorods	8.79 mA/cm ² at 92mW/cm ²	620mV	50%
Polymer-nanotube	P3OT:SWCNT	0.5 mA/cm ² at 100mW/cm ²	750mV	60%

The Basic energy level diagram of the OPVs is shown in figure 4.2(a) for heterojunction OPV cell. P3OT being commonly used photoactive polymer, the energy band diagram corresponding to P3OT is shown in figure 4.2(b). The relative position of the highest occupied molecular orbital (HOMO), lowest unoccupied molecular orbital (LUMO) levels of the photoactive material and the selection of the electrode materials with suitable work functions are basic requirements to make a solar cell work successfully. The HOMO level of the donor should be higher in energy than the HOMO of the acceptor. The LUMO level of the acceptor should be below the energy level of the LUMO of donor. Typically an organic acceptor possesses a reduction potential which determines the LUMO level, lower than its oxidation potential which determines the HOMO level. If the energy difference between the LUMO of donor and the LUMO of acceptor is relatively high the photoinduced electron transfer occurs within picoseconds so that no back transfer can take place. However if the required value of

$LUMO_{donor} - LUMO_{acceptor}$ difference is still uncertain then it depends on the material combination applied. In this case the difference should be as high as necessary to just achieve a directed donor-acceptor charge transfer since the $LUMO_{acceptor} - HOMO_{donor}$ difference determines the open circuit voltage of the device [12]. The problem with the OPV is difference of workfunction, improper charge dissociation and charge transport. These constraints may be overcome by using nanomaterials like multiwalled carbon nanotube (MWCNT) in different layers of OPV cell architecture as discussed in section 3.1.

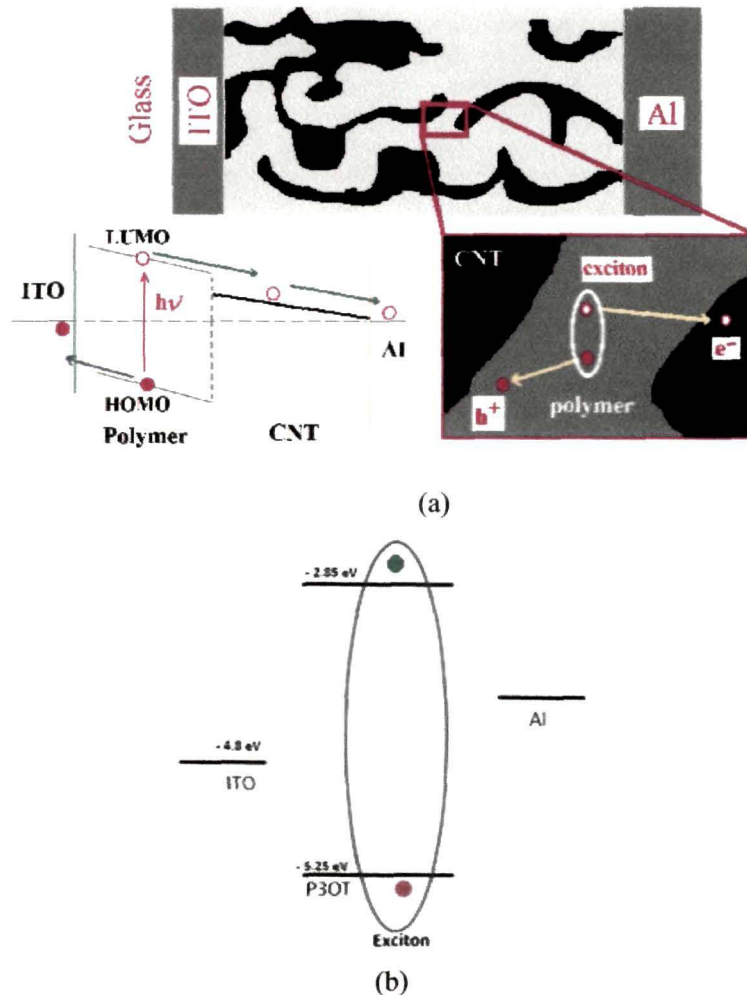


Figure 4.2: Mechanism of CNT-Polymer blend solar cell : a) Schematic of bulk heterojunction along with energy band diagram, and b) Energy band diagram of P3OT based OPV cell [4]

MWCNTs are known for their hole transport properties [13] and thus have been used in the photoactive layer of OPV by many researchers [14-16]. They provide improved exciton dissociation and charge transportation in OPVs [4, 17]. Carbon nanotubes blended with photoactive polymer provides high interfacial area, which can lead to an extended exciton dissociation region [13, 18-19]. These properties of CNTs with conjugated photoactive polymers have generated a great interest in developing other components/layers of photovoltaic cells/devices as well. But, there are two major limitations in the use of CNTs in OPVs; First, the CNTs with an average length of few micrometers limit the performance of OPV cells because a normal OPV cell has a film thickness of few nanometers [20]. Kalita *et al.* have proposed and successfully demonstrated the improvement in performance of OPV cells by cutting of CNTs to nanometer length using a physical route [20]. But the oxygen plasma technique used by them is highly energy intensive and complex and thus may not be feasible for large scale industrial purpose. Thus, a chemical route for cutting of the MWCNT must be designed. Second, the workfunction of CNTs did not match with all the available photoactive materials used in OPVs. Chemically functionalized-CNTs with the resultant reduced work function were used to enhance transport properties in OPV [21]. The carbon nanotubes can be functionalized by many functional groups (=O, -N, -COOH, -SO₃H etc.) using different techniques (like plasma deposition and chemical techniques). It is well known that MWCNTs are p-type in nature and thus exhibit enhanced hole transport properties [22]. Thus this property of functionalized MWCNT (f-MWCNT) may be used in active as well as hole collecting buffer layer to explore the possibility of enhancement in the cell performance. Recently, Kanai *et al.* have proposed and demonstrated cutting of SWCNTs using nitric acid [23]. They proposed a mechanism in which NO₃ radical get chemisorbed on the CNT wall. In chemisorbed state, the distance between the binding NO₃ oxygen atom and the SWCNT becomes shorter (1.60 Å), which results in the carbon atom binding to the NO₃ projects outward by 0.43 Å. This strain causes to form epoxy group formation with a C-O-C angle of 67° with the liberation of NO₂ resulting in breaking of weakened bond. Thus, this chapter proposes a chemical route for functionalization as well as for cutting the MWCNTs synthesized from renewable plant based precursors incorporating modifications to the process described by Kanai *et al.*

PANI nanoparticles have also been used as hole collecting and transport layer between ITO and photoactive layer (P3OT/PCBM). Incorporation of PANI nanoparticles has been reported to increase the short circuit current which is attributed to the resultant increase in the hole mobility. Polyaniline (PANI) nanoparticles were recently demonstrated to show enhancement in efficiency of OPVs [24]. In this chapter it is also proposed to incorporate PANI nanoparticles along with functionalized and cut MWCNT (fc-MWCNT) for enhanced charge transportation. Based on the assumptions as discussed, cells with four different architectures have been fabricated: i) a cell having P3OT-PCBM as active layer and no buffer layer. The performance of this cell is taken as the baseline for the present work, ii) a cell with pristine MWCNT added to the active layer of the cell, iii) a cell having fc-MWCNT in place of pristine MWCNT to see the effect of functionalization on the cell performance, and iv) a cell with an additional buffer layer of PANI+fc-MWCNT for efficient hole transport. It is expected that incorporation of such a buffer layer may further enhance the performance of the cell.

4.2. Materials and method

4.2.1. Chemicals and reagents used

The functionalization and cutting of MWCNTs were carried out by acid treatment using sulphuric (grade: Pure, 97-99%) and nitric acid (grade: Pure, 70%) procured from Merck, India. Aniline (grade: for syntheses, 99%) was polymerized using ammonium peroxodisulfate, (APS; grade: pro analysis, 98%) and hydrochloric acid (grade: GR) in presence of ethanol (grade: absolute for analysis, 99.9%) procured from Merck India. Poly (3-octylthiophene-2, 5-diyl) commonly known as P3OT was used as photoactive molecule (electronic grade, 99.995%; Sigma Aldrich). [6,6]-Phenyl C₆₁ butyric acid methyl ester (PCBM) was used as electron acceptor was procured from Sigma Aldrich (99% pure). Indium tin oxide (ITO) coated glass from Sigma Aldrich (30-60 Ohm/sq, transmittance 85% at 550 nm; size 2.5cm x 2.5cm) was used as substrate. A buffer layer of lithium fluoride (grade: precipitated, 99.995%; Sigma Aldrich) on ITO for better charge transfer to the electrode is employed All the chemicals and reagents were used as received without further purification and processing. Chlorobenzene (grade: GR; Merck India) was used as solvent for composite preparation. Double distilled (DD) water was used whenever needed.

4.2.2. *Synthesis of MWCNTs*

The MWCNTs synthesized from plant based precursor *Sesamum indicum* oil were used in OPV. These MWCNTs were prepared using chemical vapour deposition (CVD) at 850°C with Fe₂O₃ nanoparticles as catalyst for CNTs synthesis. The purification of synthesized MWCNTs was carried out by heating the MWCNTs at 450°C for 45 min in open atmospheric to remove the amorphous carbon. These MWCNTs were further treated with 6M NaOH and 6M HCl and washed with copious amount of water. Finally CNTs were again heated at 400 °C for 30 min.

4.2.3. *Functionalization and cutting of MWCNTs*

The chemical functionalization of CNT enhances its solubility in organic polar solvents. Moreover, the process improves the preparation of CNT/organic polymer composite. The first step of functionalization of CNT involves reaction of CNT with oxidants through acidic treatment [19]. It results in the opening and shortening of CNTs with insertion of functional groups such as carboxyl, hydroxyl, sulphonic groups, etc. [25]. Accordingly the functionalization of MWCNTs was carried out by dispersing MWCNTs in concentrated sulphuric acid-nitric acid mixture (3:1 v/v). For cutting the MWCNTs the process of Kanai et al. was followed with some modification [23] The process was accelerated by carrying out the reaction at elevated temperature (at 60 °C). The resultant dispersion was divided into three parts and each one of these was subjected to ultrasonication for 1.0 h, 2.0h and 3.0 h, respectively. The acid-treated MWCNTs were collected using centrifugation and washed initially with dilute aqueous solution (0.5M) of sodium hydroxide (NaOH) and then with DD water. Finally, the fc-MWCNTs were collected by centrifugation and dried in open air. The process of cutting and functionalization of MWCNTs is illustrated in figure 4.3 and figure 4.4, respectively.

4.2.4. *Synthesis of PANI nanoparticles*

PANI nanoparticles were synthesized using interfacial polymerization technique as described by Benerjee et al. [26] with some modifications. The synthesis involved preparing two solutions first the monomer solution (Aniline) and the second the oxidizer (APS). Aniline (1.0 M) was dissolved in ethanol (10 ml). APS (0.25 M) and

HCl (3.0 M) were dissolved in 10 ml double distilled water. Both the monomer and oxidizer solutions were slowly mixed to make a biphasic solution in a glass vial. The temperature was maintained at 0-1 °C using ice bath. The glass vial was kept undisturbed for 24 hours. After that, PANI nanoparticles were collected by filtration, washed with double distilled water, and dried at 105° C in open air.

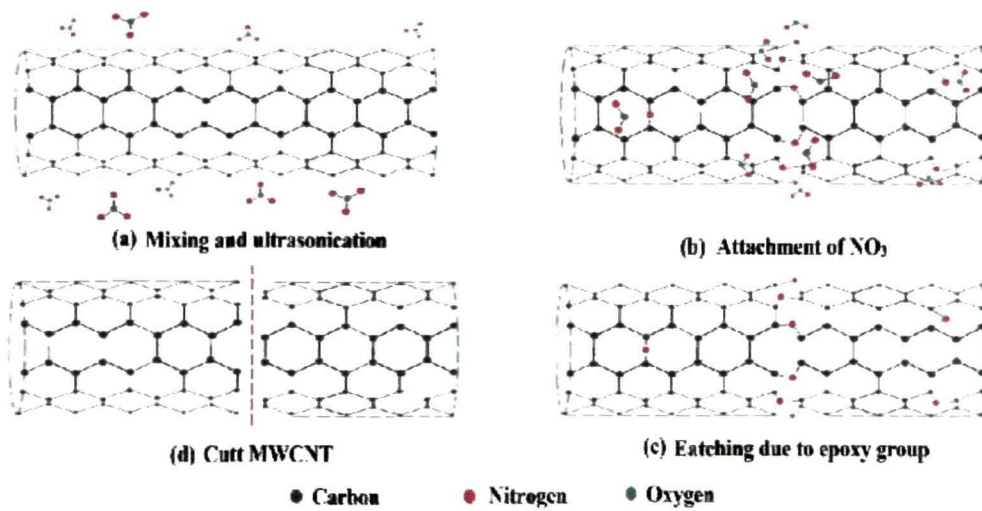


Figure 4.3: Schematic diagram showing cutting of MWCNTs using HNO₃

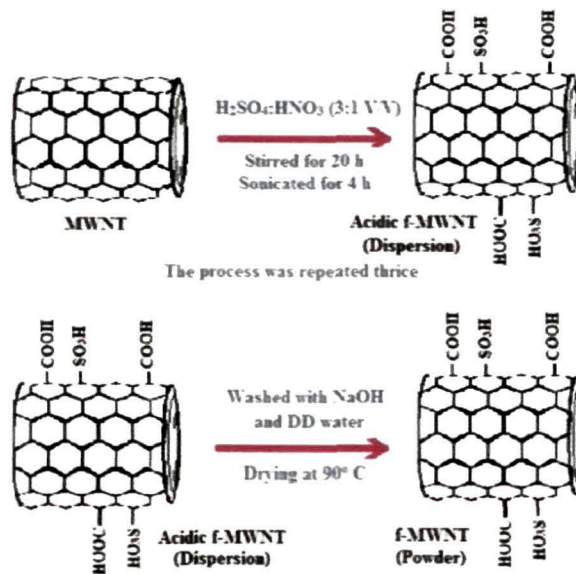


Figure 4.4: Schematic diagram showing functionalization of MWCNTs using H₂SO₄

4.2.5. Composite Preparation

The following composites were prepared for fabricating the cell:

Composite I (P3OT and PCBM): P3OT and PCBM (1:1 w/w) were mixed in chlorobenzene with 5 mg/ml concentration and the resultant mixture was ultrasonicated for 30 minutes to get the composite.

Composite II (MWCNTs+P3OT-PCBM): The MWCNTs were dispersed in chlorobenzene (0.5 mg/ml). Also P3OT-PCBM (1:1 w/w) was mixed in chlorobenzene at 5 mg/ml. The above two dispersions were mixed in equal proportions and ultrasonicated for 30 minutes to get a homogeneous composite.

Composite III (fc-MWCNTs+P3OT-PCBM): The same procedure as above was followed using f-MWCNT in place of MWCNT to prepare the composite.

Composite IV (PANI+fc-MWCNT): PANI and MWCNTs (1:1 w/w) were dispersed in chlorobenzene (0.1 mg/ml) using a sonicator.

4.2.6. Device Fabrication

Cleaning of ITO glass: Indium doped tin oxide (ITO) coated glass substrates were cleaned with acetone followed by ethanol and DD water. Then they were dried at 150 °C in nitrogen atmosphere.

Device Fabrication: The layers of the materials used in the device architecture are given below:

Device A	Al/LiF/P3OT+PCBM/ITO
Device B	Al/LiF/P3OT+PCBM+MWCNTs/ITO
Device C	Al/LiF/P3OT+PCBM+fc-MWCNTs/ITO
Device D	Al/LiF/P3OT+PCBM+fc-MWCNTs/PANI+fc-MWCNT/ITO

The fabrication started with the coating of the layers on ITO glass. The active layers of the devices A, B and C were coated on ITO glass by spin coating (SCU2007, Apex Instruments Co., India) of the composites prepared (see section 4.2.5,) at 2000 rpm for 5 min followed by drying at 120°C. Aluminium contacts were deposited using Physical Vapour Deposition (PVD) technique. For the fabrication of device D, the PANI+fc-MWCNT buffer layer composite was spin coated over ITO glass first (at 1000 rpm for 5 minutes) followed by drying of the substrate at 150°C. In the second step the active layer was spin coated (at 2000 rpm for 5 mins) and again dried at 120°C. Hung et

al. reported that a thin film of LiF between aluminium electrode and polymer layer enhances the charge collection [27]. Thus, a thinfilm of LiF was deposited on the composites using PVD technique. The Al layer was similarly deposited using PVD. Figure 4.5 shows the schematic representation of the fabricated devices.

4.2.7. Characterization

The morphology and size of the particles (MWCNT and PANI) were investigated using Scanning Electron Microscopy (SEM model no. JSM-6390LV of JEOL, Japan). Energy Dispersive X-ray analysis was done by EDX (Oxford Instrumentation Ltd, UK) attached to the SEM. TEM analysis was done using a 200 kV system of JEOL JEM 2100, Japan.

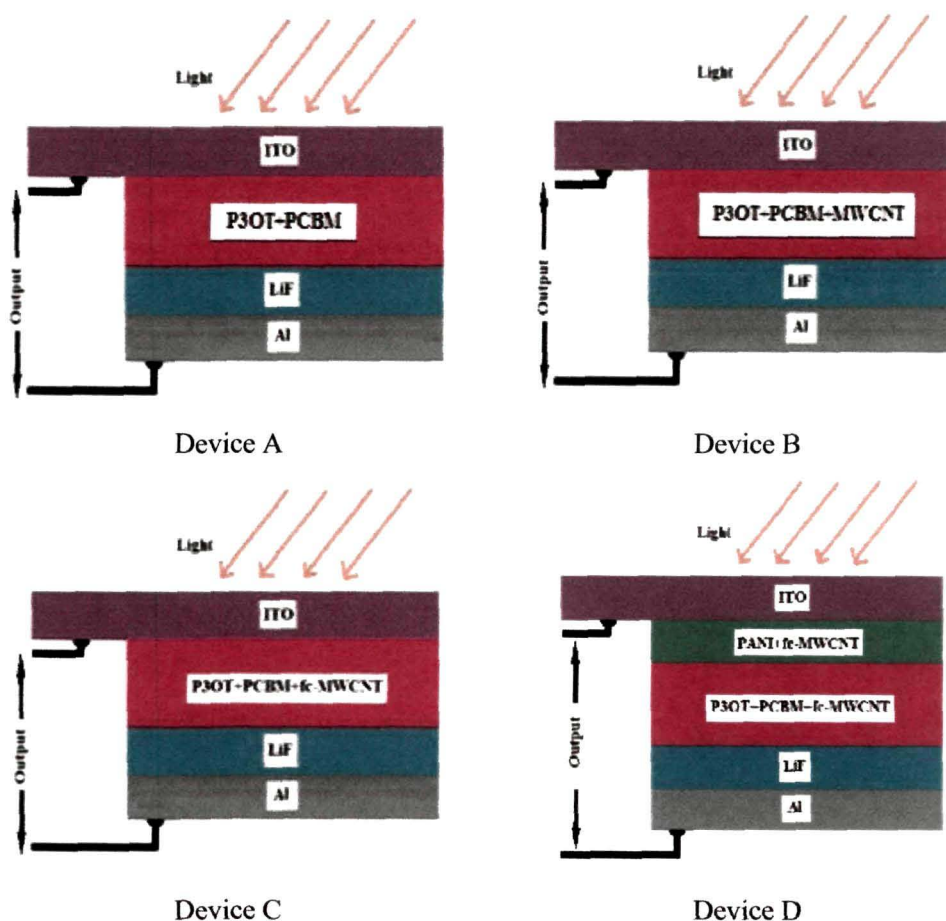


Figure 4.5: Schematic representation of the fabricated OPV devices.

4.2.8. *Characteristics of fabricated solar cell devices*

An organic solar cell is characterized by its current–voltage curve, which is measured under standard AM 1.5* illuminations [3, 28]. The current-voltage characterization of the fabricated devices was performed using a Potentiostat/Galvanostat (AUTOLAB Metrohm, Holland). The photograph of the setup is shown in figure 4.6. The electrodes were connected to ITO and Al electrodes and the analysis was performed at 1.5 AM at 1000W/m².



Figure 4.6: Potentiostat/galvanostat along with PC control for IV characteristics of fabricated OPV devices.

* "AM 1.5", is 1.5 atmosphere thickness, corresponds to a solar zenith angle of $z=48.2^\circ$. While the summertime AM number for mid-latitudes during the middle parts of the day is less than 1.5, higher figures apply in the morning and evening and at other times of the year. Therefore AM 1.5 is useful to represent the overall yearly average for mid-latitudes. Consequently, the solar industry uses AM 1.5 for all standardized testing of terrestrial solar panels as per ASTM standard [3]

4.3. Results and discussion

4.3.1. Characterization of nanoparticles

4.3.1.1. Characterization of MWCNTs synthesized

The Scanning Electron Microscopy (SEM) along with the Energy Dispersive X-ray (EDX) analysis micrograph (in inset), depicting the surface morphology and atomic percentage of constituents respectively of the MWCNTs, are shown in figure 4.7(a). The SEM micrograph enables us to have a clear view of the overall structure and growth of the CNTs synthesized. The yield in the form of entangled noodle-like densely packed CNTs of length 3 – 4 μm and diameter 80-90 nm is evident. The CNTs are found to be well distributed throughout the stub used for SEM analysis. The EDX analysis of the samples shows peaks at 0.278 keV ($K\alpha$ line corresponding to carbon) and 0.704 (L α line corresponding to iron). This confirms the presence of carbon and some amount of iron in the sample.

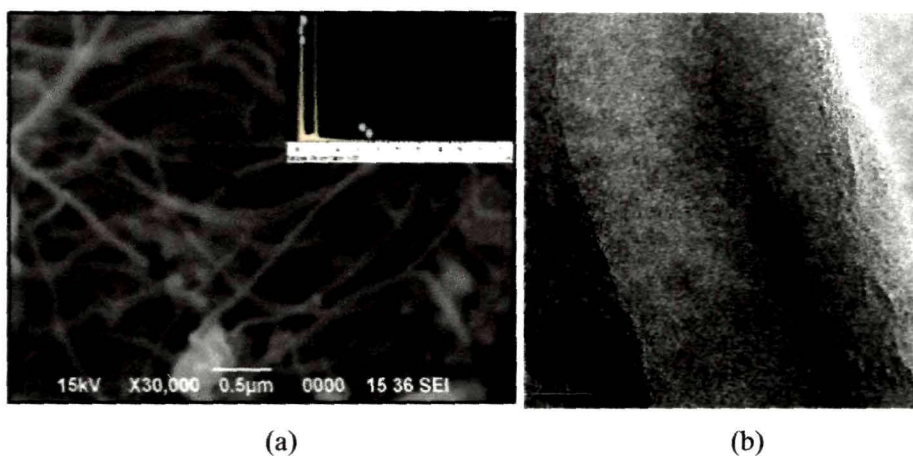


Figure 4.7: Characterization of MWCNTs synthesized using *Sesamum indicum* oil (a) SEM micrograph with EDX analysis (inset), (b) TEM micrograph

The TEM micrograph of CNTs from *Sesamum indicum* oil, figure 4.7(b) reveals them to be hollow tubes of approximate diameter ranging from 80–100 nm. The thick walls of the CNTs are due to multiple layers of concentric graphene sheets. This reveals that the synthesized nanotubes are MWCNTs. However, the MWCNTs are not aligned to a particular direction. Undesirable structures like amorphous carbon are negligible. It

confirms that the synthesized MWCNTs are reasonably pure (amorphous carbon free) albeit with some structural defects.

4.3.1.2. Characterization of *fc*-MWCNTs

The acid treated MWCNT was subjected to ultrasonication for three different time duration, viz 1.0 h, 2.0 h and 3.0 h. The effect of ultrasonication on the MWCNTs may be seen in the TEM micrographs shown in figure 4.8. The TEM micrograph reveals that as the time of ultrasonication increases the MWCNT walls are etched out. The epoxy group involved in etching the tubes eventually cut them down into pieces. Due to constant ultrasonication it is seen that the tubes were cut down into pieces of equal length (20-30 nm). The homogeneity in the tubular structure in terms of diameter and length makes them suitable for use in OPVs.

The XRD spectrum of MWCNT and *fc*-MWCNT was recorded with 2θ between 10° to 70° at a step size of 0.05° . Figure 4.9 shows the XRD diffraction pattern of MWCNT having three peaks at 26.2° , 35.4° and 44.6° . Some minor peaks at 42.9° , 53.6° , 57.0° , 62.6° and 65.0° are also identifiable. At a synthesis temperature of about 875°C (low temperature synthesis) the XRD pattern of MWCNT was reported to show mainly graphitic reflections at 26.2° , 42.3° , 77.4° and 83.5° corresponding to (002), (100), (110) and (112), respectively [29]. In figure 4.9 only two peaks at 26.2° and 42.3° corresponding to (002) and (100) respectively are prominent. The peaks at 59.6° , 61.7° , 62.6° and 64.9° suggest the presence of Fe_3O_4 indicating complete reduction of Fe_2O_3 . The peaks at 35.4° and 44.9° (2θ) portray the presence of Fe_5C_2 and Fe_3C , respectively in the sample. These metal carbides act as active catalysts in the formation of tubular structure of graphitic carbon.

The extent of graphitization of carbon in the sample has been estimated using the formula proposed by Maire and Mering as reported by Ermakova *et al.* [30]. According to this formula, the lattice spacing corresponding to the major diffraction peak is given by,

$$d = 3.354 + 0.086(1 - C_g) \quad (1)$$

where C_g is the graphitization percentage. The value of $d_{(002)}$ corresponding to the highest diffraction peak of carbon at 26.2° is 3.37 \AA . Hence the graphitization percentage using equation (1) for the sample comes out to be 81.39%. Debye-Scherrer formula gives the graphite crystallite size to be 9.13 nm . The analysis of the curve for

fc-MWCNTs shows peaks for carbon at 26.2° and 42.3° . The intensity of the peaks at 35.4° and 44.9° (2θ) is found to be reduced slightly. It suggests the presence of Fe_5C_2 and Fe_3C in the functionalized sample too. The reduced peaks corresponding to iron oxide suggest that the catalyst particles were dissolved during the functionalization by acids. The crystallite size of fc-MWCNTs was calculated to be 9.05 nm.

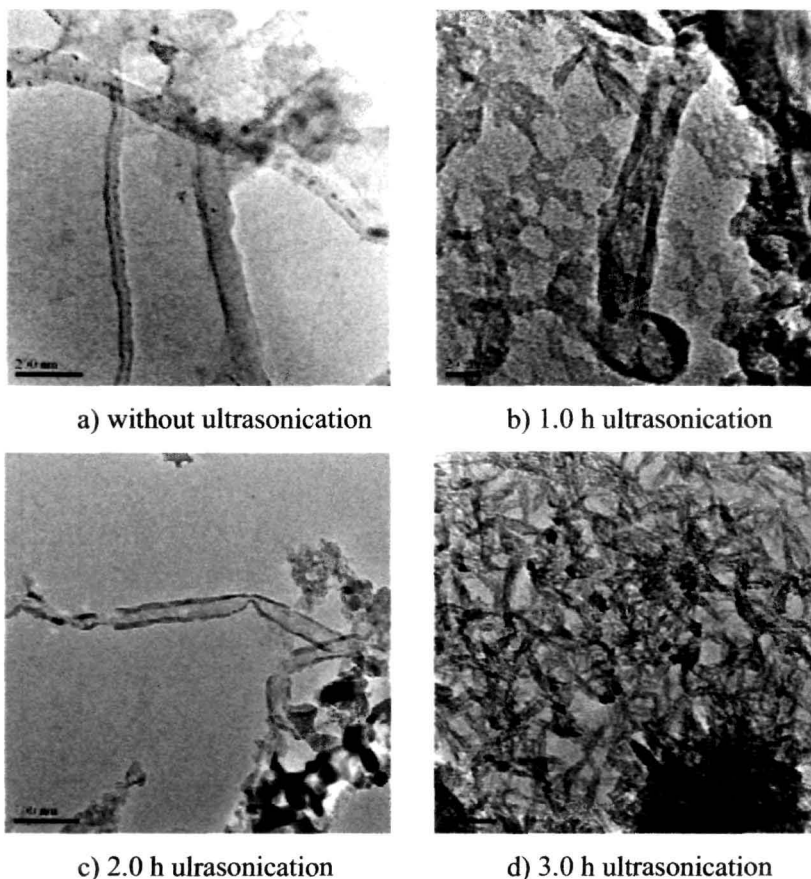


Figure 4.8: Effect of ultrasonication in chemically cutting of MWCNT

Analysis of the walls of the MWCNT at higher resolution shows presence of highly arranged graphitic crystalline planes (Figure 3b). It confirms the results obtained using XRD. As the MWCNTs are functionalized, the defects in the graphitic crystal planes start to become more prominent as seen in from the TEM image, figure 4(b). The tubular structures of fc-MWCNTs lose the uniformity in the diameter as the walls were damaged due to functionalization. The TEM micrograph confirms the reduced crystallinity as well as graphitization found in XRD analysis. The fc-MWCNT

disintegrated into pieces as if the tubes were cut. Apparently the acid treatment followed by ultrasonication at elevated temperature (60 °C) on MWCNTs incorporated defects in the walls of the tube as well.

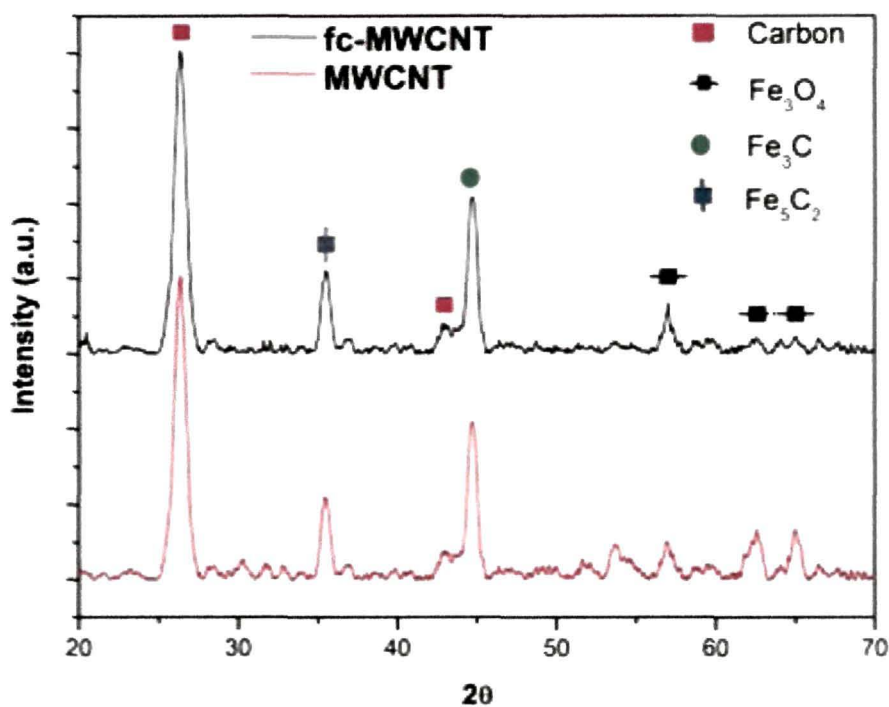


Figure 4.9: XRD analysis of MWCNT and fc-MWCNT

Fourier transform infrared spectroscopy (FTIR) of pristine and functionalized cut-MWCNTs was done to study the functional groups attached on the surface walls of the tubes, shown in the figure 4.10. FTIR spectrum from the pristine MWCNTs shows peak at 3467 cm^{-1} , which refers to the O-H stretch of the hydroxyl group, which is ascribed to the oscillation of carboxyl groups. Carboxyl groups on the surface of pristine CNTs could be due to the partial oxidation of the surfaces of MWCNTs during purification. After the acid treatment the peak intensifies as seen in the FTIR spectra of functionalized cut-CNT. The peak at 3730 cm^{-1} is attributed to free hydroxyl groups. The peak at 3455 cm^{-1} can be assigned to the O-H stretch from carboxyl groups (O=C-OH and C-OH). The peaks at 1640 and 1177 cm^{-1} are due to C=C and C-C of MWCNT. It is evident from the FTIR spectrum that the fc-MWCNTs were also

functionalized by carboxylic group during the process of cutting them. This is evident that SO_3H group is absent and hence are not attached in the walls of MWCNT.

The SAD micrographs of pristine MWCNTs and fc-MWCNTs are shown in the figure 4.11. The micrograph for pristine MWCNT shows hollow electron diffraction rings. The ring structures are due to graphitic carbon layers in the MWCNT walls. The intensity and sharpness of the rings reduces after functionalization. It is clear that the crystallinity of the MWCNT tubular structures have reduced due to the functionalization.

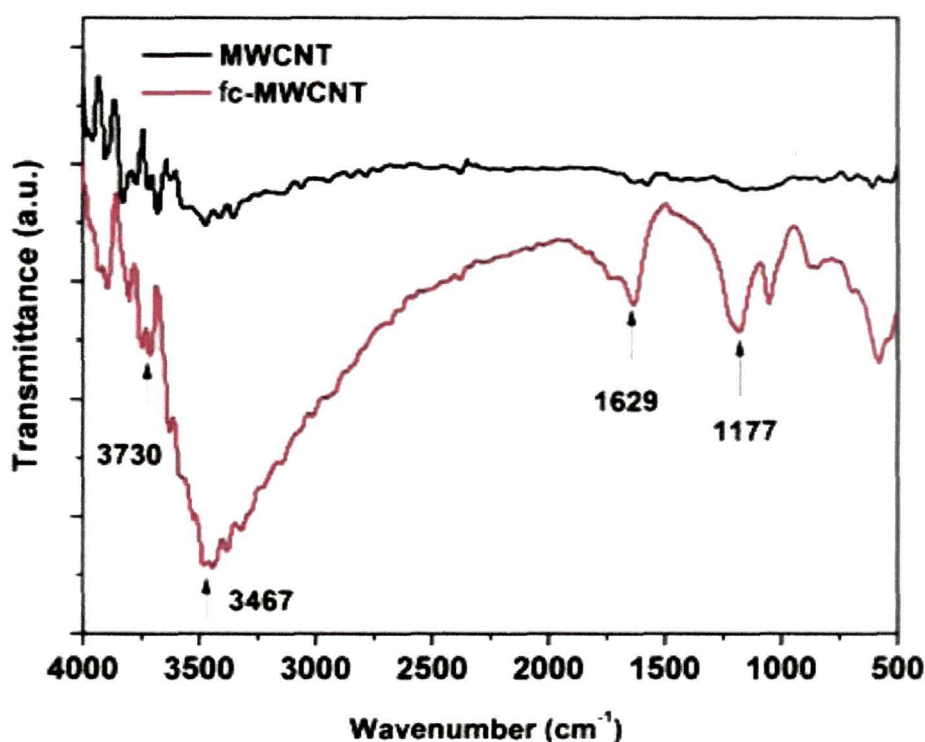


Figure 4.10: FTIR study of fc-MWCNTs and pristine MWCNTs

4.3.1.3. Characterization of PANI

The XRD spectrum was recorded at a step size of $0.05^\circ 2\theta$ and scanned between 10° to 70° . Figure 4.12 shows the XRD diffraction pattern having four peaks at 18.35° , 24° , 26.75° and 30.85° . This confirms the synthesized particles to be PANI. The XRD peaks obtained were similar to the results of other workers [26, 31].

The SEM micrograph portrays (figure 4.13) the external surface morphology of the synthesized PANI. The micrograph reveals that the synthesized particles are agglomerated. The size of the agglomerates is in the range of 100-120 nm. For a better analysis TEM was used to characterize the particles. The TEM micrograph (figure 4.14) shows uniform distribution of the nanoparticles of size ranging from 45 – 60 nm in size having high-quality crystalline structures.

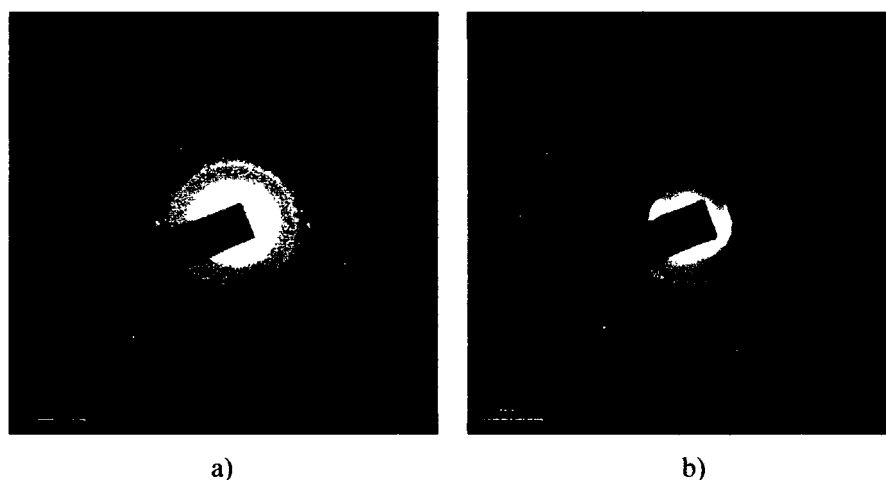


Figure 4.11: SAD pattern of a) pristine MWCNTs, and b) fc-MWCNTs

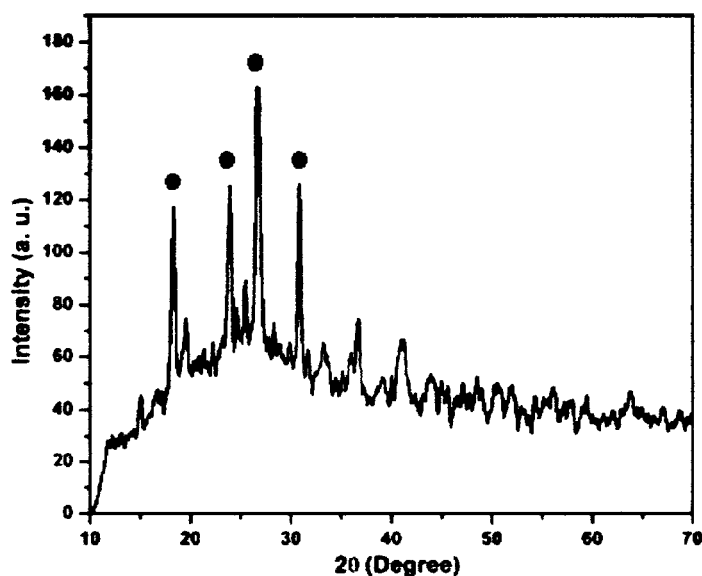


Figure 4.12: XRD analysis of PANI synthesized using solvent ethanol.

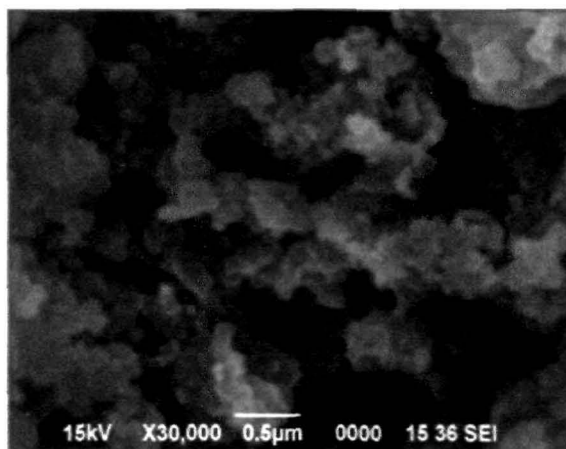


Figure 4.13: SEM micrograph of synthesized PANI nanoparticles

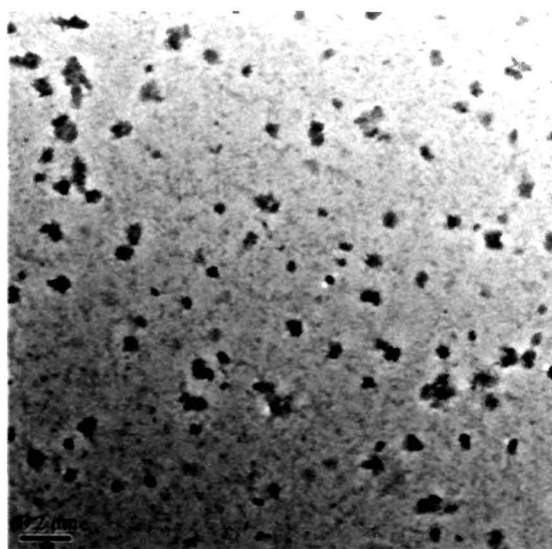


Figure 4.14: TEM micrograph of synthesized PANI nanoparticles

4.3.2. Current-voltage Characteristics of fabricated OPV cell

The current-voltage characterization of OPV devices was carried out under dark and white light illumination (1000 W/m^2 at 1.5 AM). The results are shown in figure 4.15. The fabricated device without MWCNTs (Device A) shows short circuit current density (J_{sc}), open circuit voltage (V_{oc}), fill factor FF and power conversion efficiency (PCE) of 4.056 A/m^2 , 0.2279 V , 29.21% , and 0.027% , respectively. In Device A the dissociation of the exciton can occur only at P3OT/PCBM interface. The hole transport in it is limited as the P3OT has low carrier mobility. PCBM is used to

provide necessary exciton dissociation by accepting the electrons from the LUMO level of the P3OT as the LUMO levels of PCBM and P3OT are close. The thin film of aluminum deposited over the active layer works as a competent and efficient electron carrier as its work function is very close to the conduction band of the photoactive polymer (P3OT). This architecture has a poor efficiency due to the fact that after dissociation the holes from P3OT (photoactive polymer), the holes cannot migrate to longer distances to reach the ITO electrode due to their poor mobility. To overcome this problem MWCNTs were incorporated in the active layer by many researchers as discussed in earlier sections. The device B was similarly fabricated incorporating pristine MWCNTs. It showed J_{sc} , V_{oc} , FF, and PCE of 4.8108 A/m^2 , 0.2313 V , 30.09% , and 0.033% , respectively. The addition of the MWCNTs, is done to enhance the collection and transportation of holes from the P3OT after exciton dissociation. The work function of the MWCNT is in the range of $4.6\text{--}5.1 \text{ eV}$ which is lower than the HOMO level of P3OT and PCBM. It suggests large probability of hole transfer from the P3OT to MWCNTs. In addition to that MWCNTs have hole mobility which is orders of magnitude larger than that of P3OT and PCBM. Addition of MWCNTs (0.5 mg/ml) creates numerous hole collection and transport sites in the active layer of the OPV architecture. Due to the favorable potential gradients at MWCNT terminals an efficient charge separation is possible. Hence, device B shows a noticeable increase in the value of J_{sc} as compared to device A. The incorporation of MWCNTs in the active layer blend enhances the performance of the device B by 22.22% with respect to the device A basically due to increase in J_{sc} . The MWCNTs were chemically treated to attach functional group on their surface, as explained in earlier section, to enable homogeneous dispersion of MWCNT in polymer matrix and better charge transport. The light characteristics of device fabricated with fc-MWCNT (Device C) gave J_{sc} , V_{oc} , FF and PCE of 5.0304 A/m^2 , 0.24602 V , 30.56% and 0.0380% respectively. It was observed that the incorporation of fc-MWCNTs further improved PCE of device C compared to the device A by 40.00% . It is mainly due to increase in J_{sc} attributable to efficient hole collection and transportation in the presence of uniformly dispersed fc-MWCNT and the resultant reduction in the recombination of the excitons. It is expected that after functionalization the surface chemical groups attached to MWCNTs increase the value of its work function [20]. This brings the fc-MWCNT energy level more closer to the HOMO energy level of P3OT consequently providing more efficient hole

collection and transportation. At present, we are unaware of the exact value of work function of fc-MWCNTs. A 4.6% increase in V_{oc} is evident from the graph. Increase in V_{oc} may be due to increase in shunt resistance.

Table 4.2 shows short circuit current density (J_{sc}), open circuit voltage (V_{oc}), fill factor (FF), power conversion efficiency (PCE) and percentage gain (with respect to Device A) of the fabricated devices for general comparison. The overall increase in the efficiency of the device D using fc-MWCNT and PANI over the one without nanomaterials (device A) is 40.07 %. This increase in the efficiency is mainly due to the increase in short circuit current attributed to the enhancement in the dispersibility of the fc-MWCNTs in the solvents leading to improved transport properties of the holes from the active layer to the electrode. The resultant decrease in the series resistance of the device and increase in hole conduction by layer of fc-MWCNT+PANI nanoparticles. This is clearly visible in the form of increased J_{sc} . The improvement in FF is also evident from the results shown in Table 4.2.

The energy band diagram of the fabricated device is shown in figure 4.16. The process of functionalization changes the workfunction of MWCNTs more closer to HOMO of P3OT [10, 20], this enhances the chances of exciton dissociation and hole transport to electrode. The work function of PANI is just higher than ITO and thus the holes collected by MWCNTs is transferred to PANI nanoparticles and finally to the electrode.

Table 4.2: Power conversion efficiency, fill factor and gain w.r.t device A.

Sl/No	Device	V_{oc} (V)	J_{sc} (A/m^2)	V_m (V)	J_m (A/m^2)	FF (%)	PCE (%)	Gain w.r.t Device A (%)
1	A	0.2279	4.0560	0.1206	2.2392	29.21	0.027%	-
2	B	0.2313	4.8108	0.1019	3.2856	30.09	0.033%	22.22%
4	C	0.2460	5.0304	0.1115	3.3912	30.56	0.03780%	40.00%
3	D	0.2425	5.0280	0.1115	3.3910	31.01	0.03782%	40.07%

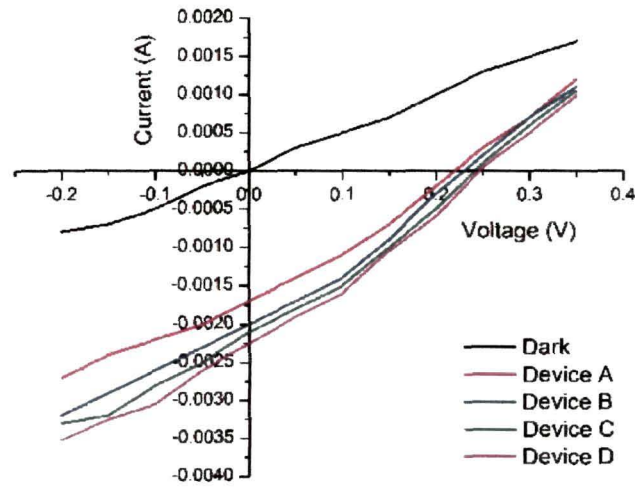


Figure 4.15: Current-voltage characteristics of the device A, B, C and D

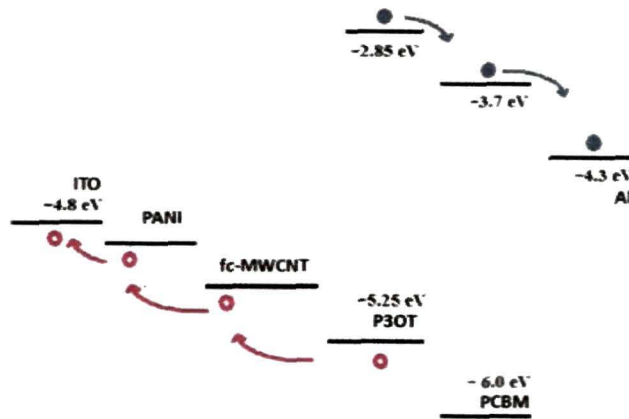


Figure 4.16: The energy band diagram of the fabricated device D

4.4. Conclusion

The potency of using *Sesamum indicum* oil as a precursor for MWCNT synthesis is demonstrated. The MWCNTs were successfully utilized in OPV cells showing an increase of 22.22 % in the PEC. The results also show that functionalized cut-MWCNTs synthesized from renewable precursor further increase PEC by 40.00%. This increase is attributable to increase in J_{sc} due to enhanced hole collection and transport along and increase in V_{oc} due to enhancement in shunt resistance. Thus the MWCNTs synthesized from renewable precursors can be successfully used in the active

layer of the OPV cell. The functionalization process discussed not only incorporated desirable defects to the MWCNTs but also cut the MWCNTs. The cutting of the MWCNTs reduced the probability of shorting the electrodes.

The enhancement in the performance of the OPV cell by incorporating f-MWCNT using MWCNT synthesized from a renewable precursor has been demonstrated for the first time. Further incorporation of PANI hole injection layer further enhances the PEC to 40.07% compared to Device A. The introduction of PANI+fc-MWCNT was successfully demonstrated to enhance the PEC of OPVs. The functionalizing and cutting of MWCNTs were successfully done. The results were better than the earlier results and may be because of uniform cutting of functionalized MWCNTs.

References

1. Pope, M., and Swenberg C. E., *Electronic Processes in Organic Crystals and Polymers*, 2 ed. Oxford University Press, 1999.
2. Tang, C. W., Two-layer organic photovoltaic cell, *Applied Physics Letters* **48** (2), 183–185, 1986.
3. Reference Solar Spectral Irradiance: Air Mass 1.5 NREL retrieved 1 May 2011, <http://rredc.nrel.gov/solar/spectra/am1.5/>
4. Song, Y. J., and Lee, J. U., Multiwalled carbon nanotubes covalently attached with poly(3-hexylthiophene) for enhancement of field effect mobility of poly(3-hexylthiophene)/multi-walled carbon nanotube composit. *Carbon* **48**, 389-395, 2010.
5. Valentini, L., and Cardinali, M. Selective deposition of semiconducting single walled carbon nanotubes onto amino-silane modified indium tin-oxide surface for the developement of poly(3-hexylthiophene)/carbon-nanotbe photovoltaic heterojunctions. *Carbon* **48**, 861-867 ,2010.
6. Cai, W., and Gong, X. Polymer solar cells: recent development and possible routes for improvement in the performance. *Sol. Energy Mater. Sol. Cells.* **94**, 114-127, 2010.
7. Kymakis, E., et al. High open-circuit voltage photovoltaic devices from carbon-nanotube-polymer composites, *Appl. Phys. Lett.* **93** 11764–11768, 2003.
8. Woo, H.S. et al. Hole blocking in carbon nanotube–polymer composite organic light-emitting diodes based on poly (*m*-phenylene vinylene-co-2, 5-dioctoxy-*p*-phenylene vinylene), *Appl. Phys. Lett.* **77**, 1393, 2000.
9. Kymakis, E. and Amaratunga, G. A. J., Carbon Nanotubes as Electron Acceptors in Polymeric Photovoltaics, *Rev. Adv. Mater. Sci.* **10**, 300–305, 2005.
10. Ago, H., et al. Composites of carbon nanotubes and conjugated polymers for photovoltaic devices. *Adv. Mater.* **11**,1281, 1999.
11. Hoppe, H., and Sariciftci, N. S., Polymer Solar Cells. *Adv. Polym. Sci.* **214**, 1–86, 2008.
12. Brabec, C. J., et al. Origin of the open circuit voltage of plastic solar cells. *Adv. Funct. Mater.* **11**(5), 374-380, 2001.
13. Pradhan, B., and Batabyal, S. K., Functionalized carbon nanotubes in donor/acceptor-type photovoltaic devices. *Appl. Phys. Lett.* **88**, 093106, 2006.

14. Kymakis, E. and Amaratunga, G. A. J., Single-wall carbon nanotube/conjugated polymer photovoltaic devices. *Appl. Phys. Lett.* **80**, 112, 2002.
15. Shaheen, S. E. *et al.* Fabrication of bulk heterojunction plastic solar cells by screen printing *Appl. Phys. Lett.* **78**, 841, 2001.
16. Reyes-Reyes, M., *et al.* Bulk heterojunction organic photovoltaic based on polythiophene–polyelectrolyte carbon nanotube composites. *Sol. Energy Mat. & Solar Cell* **91**,1478, 2007.
17. Liu, Z. *et al.* Improving photovoltaic properties by incorporating both SPFGraphene and functionalized multiwalled carbon nanotubes. *Solar Energy Materials and Solar Cells* **94** (12), 2148-2153, 2010.
18. Guldi, D. M., *et al.* Carbon nanotubes in electron donor-acceptor nanocomposites. *Acc. Chem. Res.* **38**, 871-878, 2005.
19. Patyk, R. L., *et al.* Carbon nanotube–polybithiophene photovoltaic devices with high open-circuit voltage, *Physics status solidi* **1**, R43-R45, 2007.
20. Kalita, G., *et al.* Cutting of carbon nanotubes for solar cell application, *Appl. Phys. Lett.* **92**, 123508, 2008.
21. Singh, R. K., *et al.* Poly(3-hexylthiophene): Functionalized single-walled carbon nanotubes: (6,6)-phenyl-C₆₁-butyric acid methyl ester composites for photovoltaic cell at ambient condition. *Solar Energy Materials & Solar Cells* **94**, 2386–2394, 2010.
22. Kalita, G., *et al.* Fullerene(C60) decoration in oxygen plasma treated multiwalled carbon nanotubes for photovoltaic application. *App. Phy. Lett.* **92**, 063508, 2008.
23. Kanai, Y., Atomistic Oxidation Mechanism of a Carbon Nanotube in Nitric Acid, *Physical review letters* **104**, 066401, 2010.
24. Bejbouji, H., *et al.* Polyaniline as a hole injection layer on organic photovoltaic cells, *Solar Energy Materials & Solar Cells* **94**, 176–181, 2010.
25. Kumar, J., Self-assembly of SWCNT in P3HT matrix, *Diamond Relat. Mater.* **16**, 446–453, 2007.
26. Banerjee, S., *et al.*, Photoluminescence studies in HCl-doped polyaniline nanofibers. *Jr. of Opt.* **38** (2), 124–130, 2009.
27. Hung, L. S., and Tang, C. W., Enhanced electron injection in organic electroluminescence devices using an Al/LiF electrode. *Appl. Phys. Lett.* **70** (2), 152-154, 1997.

28. <http://rredc.nrel.gov/solar/spectra/am1.5/>, Reference Solar Spectral Irradiance: Air Mass 1.5 NREL retrieved 1 May 2011.
29. Emmenegger, C., et al. Synthesis of carbon nanotubes over Fe catalyst on aluminium and suggested growth mechanism. *Carbon* **41**, 539-547, 2003.
30. Ermakova, M. A., et al. Decomposition of Methane over Iron Catalysts at the Range of moderate Temperatures: The Influence of Structure of the Catalytic Systems and the Reaction Conditions on the Yield of Carbon and Morphology of Carbon Filaments. *Jr. of Cat.* **201**,183–197, 2001.
31. Chaudhari, H. K. and Kelkar, D. S., X-ray Diffraction Study of Doped Polyaniline. *Jr. of App. Polymer Sc.* **62**, 15-18, 1996.

Chapter 5
***Application of antioxidant grafted MWCNTs
in biodiesel storage***

Chapter 5

Application of antioxidant grafted MWCNTs in biodiesel storage

As discussed in chapter 2 and chapter 3, plant derived oils can be used for synthesizing different forms of carbon nanomaterials, which are physically and chemically highly stable. However, the precursors themselves are not very stable and tend to get oxidized in air. This problem was faced during CNT synthesis and the related problem of biodiesel storage extracted from the literature resulted in the work being presented in this chapter. Biodiesel technology that has evolved in past decade has enormous potential and hence considered to be the future fuel which will power next generation vehicles. Though the technology is reasonably matured, its commercialization is still not possible due to its low shelf life. Biodiesels are chemically synthesized from plant based oils and hence start getting oxidized (degraded) within six hours. The antioxidants hitherto used are homogeneous in nature. The addition of such antioxidants can check the oxidation but at the cost of engine performance. This inhibits their widespread use due to recurring consumption cost as well as contribution to enhancement in emission. This chapter is an attempt to engineer magnetically separable heterogenous antioxidants for biodiesel storage.

5.1. Introduction

The use of antioxidants for long term storage is not new [1-3]. They are used for storage of organic compounds like oils derived from plants, strategic materials like rubber and paints as well as beneficial effect in the living body [4-6]. Most of these antioxidants are organic compounds which may be classified into synthetic and natural antioxidants. One of the important uses of these antioxidants is in storage of plant derived oils. Essential oils extracted from plant sources consist of mono fatty acid methyl esters and high molecular weight glycerin. Essential oils find applications in every sphere of life, from edible oils for cooking to raw material for biodiesel production. The main problem with these oils is their susceptibility to

oxidation. The oxidation of oils may be due to its thermal oxidative disintegration in the presence of air and/or moisture. Most of the antioxidants form a homogeneous mixture with these oils when added for storage [7-9] and cannot be separated before end-use thus affecting the overall property of the oils [10]. It is, therefore, necessary to search for new antioxidants which can be removed before end-use and which show enhanced antioxidant activity. This may be possible with the use of heterogeneous inorganic antioxidants. Preliminary research of metal nanoparticle antioxidant property was already reported by workers [11-12]. But these antioxidants like silver and gold are costly and hence can not be used in large quantities for storage of oils. Thus cost becomes another criterion in addition to possibility of removal before end-use.

Assessing the antioxidant potency of heterogeneous antioxidant pose a new challenge due to existence of multiple phases and diversely dispersed conditions. A method for antioxidant potency estimation of insoluble solids was proposed by Serpen et al. [13]. The method was designed for insoluble macroparticles and the thus the validity of the method for nanoparticles may be questioned. It is necessary to design a protocol for antioxidant potency assay which suits nanoparticles for correct estimation of their potency in scavenging free radicals.

The chapter aims to design and propose a new protocol for antioxidant potency estimation for nanoparticles, test the antioxidant potency of iron, cobalt and nickel oxide nanoparticles, design and develop a heterogeneous antioxidant using nanoparticles which can be removed after end use, and finally test the designed nanoparticle antioxidant in storage of oil.

5.2. Materials and method

5.2.1. Chemicals and reagents used

Iron nitrate nonahydrate (grade: purified, 98%), cobalt nitrate hexahydrate (Purified, 97%), nickel nitrate hexahydrate (grade: GR, 97%), urea (grade: extra pure, 99.5%) and oleic acid (grade: pure, 98%) were procured from Merck, India for the synthesis of metal oxide. Nitrogen gas (99.9 %) supplied by Rass cryogenics, India was used for synthesis of MWCNTs. Butylated hydroxytoluene (Merck, India, grade: AR), Ethanol (grade: absolute for synthesis, 99.9% Merck, India), and 1'-1'

diphenylpicryl-hydrazyle (DPPH°, grade: AR, Merck, India) were used for antioxidant potency estimation.

5.2.2. *Synthesis of metal oxide nanoparticles*

Metal oxide nanoparticles of iron, nickel and cobalt were synthesized using solution combustion method using similar technique as described in Chapter 2.

5.2.3. *Synthesis of MWCNTs*

The MWCNTs were synthesized using the modified CVD as described in Chapter 2. *Ricinus communis* oil was used as precursor. The synthesis of CNTs was carried out at 850°C. Fe₂O₃ nanoparticles were used as catalyst for CNTs synthesis. The purification of synthesized MWCNTs was carried out by heating at 450°C for 45 min in open atmospheric condition to remove the amorphous carbon. These MWCNTs were not treated further to remove the catalyst particles.

5.2.4. *Proposed design of the heterogenous magnetically separable nanomaterial antioxidant*

The proposed design of the nanomaterial antioxidant has three major components: i) a magnetic component, to ease the separation before end use, ii) an antioxidant component, to scavenge the free radicals, and iii) a substrate, to hold both the antioxidant and magnetic component. A schematic of the proposed design is shown the figure 5.1.

The catalyst particles (metal oxide nanoparticles) used for the synthesis of MWCNTs remains trapped inside the MWCNT structure. The oxides of iron, cobalt and nickel in nanorange show magnetic properties [14-16]. Thus unpurified MWCNTs (in terms of catalyst nanoparticles) may act as the substrate for a commercial antioxidant to be attached and may be separated using a magnetic field due to the presence of metal oxide nanoparticles inside the nanotubs.

In chapter 2 and chapter 3 it was discussed that the precursors not containing oleic acid as major fatty acid component in the oil produced MWCNTs with defective graphitic structures in the walls. Moreover in chapter 3, *Ricinus communis* oil was found to be the best precursor in terms of yield of MWCNTs using plant precursors not containing oleic acid. The defects on the walls may be used as

locations for grafting the antioxidants, because they have affinity towards such molecules. Butylated hydroxytoluene (BHT) is a commonly used antioxidant which may be used to in this case. BHT is also used as reference in the study of antioxidant potency of other compounds and materials by researchers [17-18]. For this reason, BHT was selected for the proposed antioxidant nanocomposite.

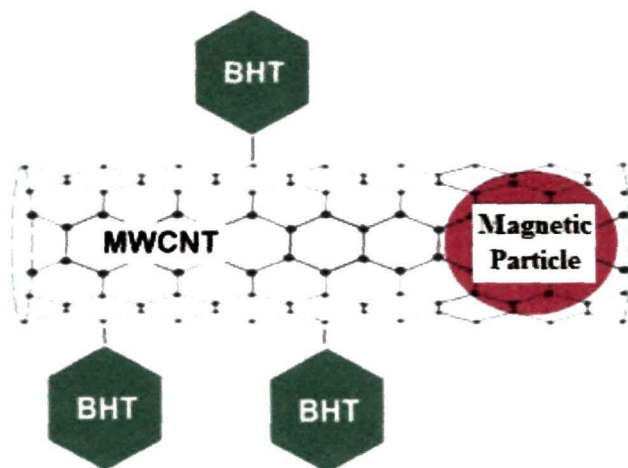


Figure 5.1: Proposed antioxidant nanocomposite

5.2.5. Grafting of BHT in MWCNT

BHT is a well known homogenous antioxidant which is used for storage of biodiesels. The process of grafting BHT on the defect sites of MWCNTs was done using ultrasonication. A concentrated 1.0 ml solution of BHT in ethanol was prepared at 40 °C. MWCNT synthesized using *Ricinus communis* oil was added to the BHT solution (0.1 g). The mixture was ultrasonicated for 30 minutes at 50 °C. It was centrifuged to collect MWCNTs which were then washed once in DD water and oven dried.

5.2.6. Proposed method for antioxidant potency determination for nanoparticles

To get the actual antioxidant potency of the engineered nanomaterial, it is desirable to evaluate the antioxidant potency of each nanomaterial individually. Serpen et al. [13] method for estimation of antioxidant potency of non-soluble particles holds for macroscopic particles. Thus, a modified method is proposed for

antioxidant potency assay of the nanoparticles. In the proposed method, nanomaterials/nanoparticles were washed with distilled water to get neutral pH supernatant. 10 mg of the each powdered samples were transferred to separate reaction vial. 1'-1'-Diphenylpicryl-hydrazyle (DPPH^o) reagent (1.7 mL) was added to start the reaction. The mixture was ultrasonicated for 45 min to ease the surface reaction between the nanoparticles and the DPPH^o reagent. The mixture was centrifuged at 9200 g for 10 min; finally, the absorbance of the supernatant was measured at 517 nm using UV-vis spectrophotometer. The antioxidant potency assays for the metal oxide nanoparticles, MWCNTs and the BHT grafted MWCNTs were investigated using this modified DPPH method for insoluble nanomaterials. All the measurements were carried out after ultrasonication of the insoluble nanoparticles with the DPPH reagent. The scavenging percentage was calculated using the formulae:

$$(\%) = \frac{(A_C - A_S)}{A_C} \times 100$$

where, A_C and A_S are absorbance of blank DPPH^o and the DPPH^o remaining after the test at 517 nm respectively.

5.2.7. Oxidation stability analysis of biodiesel

Oxidation stability analysis was performed by Rancimat apparatus (Biodiesel Rancimat 873, Metrom, Switzerland). In Rancimat method air is allowed to pass through a reaction tube containing the oil sample, held at a specified temperature (110 °C) in a thermostated aluminum block. The effluent air from the oil sample is then bubbled through a vessel containing deionized water, called the conductivity measurement cell. The conductivity of the water is continuously monitored and stored in an attached PC. During the degradation process (oxidation of oils) volatile organic acids, predominantly formic acid is blown out of the reaction tube which is allowed to pass through the cell and get absorbed in the water. At that time the conductivity of the water in the conductivity measurement cell begins to increase rapidly. Thus more stable oils will result in less conductivity in the conductivity measurement cell in a specific period of time and at a specific temperature and vice versa. In other words more the oil oxidizes more is the conductivity in the

conductivity measuring cell. Figure 5.2 and figure 5.3 show the schematic diagram and photograph, respectively of the Rancimat apparatus.

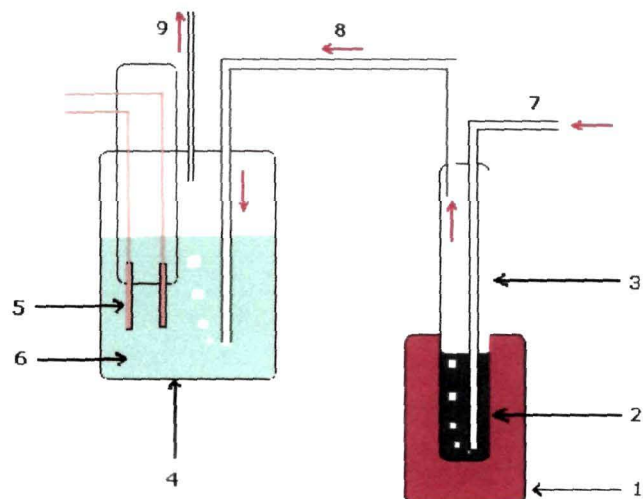


Figure 5.2: Schematic diagram of Rancimat apparatus. (1) heating block, (2) oil sample, (3) reaction tube, (4) conductivity measuring cell, (5) electrodes to measure conductivity, (6) deionized water, (7) air input, (8) tube carrying air and volatile organic acids from degraded oil in reaction tube and (9) air output.

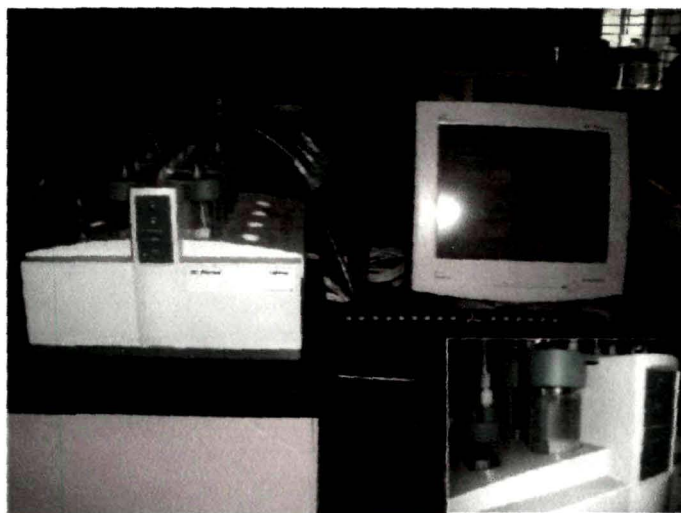


Figure 5.3: Photograph of Rancimat apparatus

Mesua ferrea biodiesel was taken in separate test tubes (3ml each). Nanoparticles were added to test tube (3.0 mg each). The test tubes were sonicated for 15 min to ensure proper dispersion of iron oxide and BHT grafted MWCNTs in the oil. Two test samples of biodiesel nanoparticle mixtures were transferred to reaction tubes in Rancimat apparatus. Oxidation stability measurements of oils were performed by Rancimat method at 110 °C with a gas flow of 10 ltr/hr. The time dependent conductivity for all the oils were recorded. For the study *Mesua ferrea* biodiesel without antioxidant was taken as control.

5.3. Results and discussion

5.3.1. Characterization of nanomaterials

5.3.1.1. Characterization of iron oxide nanoparticles

The figure 5.4 shows the TEM micrograph of the iron oxide nanoparticles. The size of the nanoparticles is found out to be 8–40 nm. X-ray diffraction pattern of the samples is shown in the Figure 5.5. Presence of peaks at angles (2θ), 24.20°, 33.23°, 35.69°, 40.99°, 49.50°, 54.16°, 62.49° and 64.05° portrays the synthesized iron oxide particles to be hematite.

5.3.1.2. Characterization of nickel oxide nanoparticles

TEM image of the synthesized nickel-oxide particles are shown in figure 5.6. The particle size ranges from 12 to 23 nm. The micrograph reveals that the synthesized particles show almost uniform shape and size. The X-ray diffraction pattern confirms the synthesized particles to be nickel oxide (figure 5.7). The presence of peaks at 2θ 44.85 and 52.15 confirms the presence of Ni₂O₃ (hexagonal). The peaks at 37.60, 43.65 and 63.20 are due to the presence of NiO (cubic)

5.3.1.3. Characterization of cobalt oxide nanoparticles

TEM micrograph of the synthesized cobalt oxide nanoparticles shows (figure 5.8) the particles are of three different sizes, ranging from 12 to 20 nm, 30-35 nm and 40-50 nm. The X-ray diffraction pattern confirms the synthesized particles to be cobalt oxide (figure 5.9). The presence of peaks at 2θ 42.61 and 57.81 confirms the presence of Co₃O₄ whereas the peaks at 40.36 and 22.06 are due to the presence of Co₂O₃.

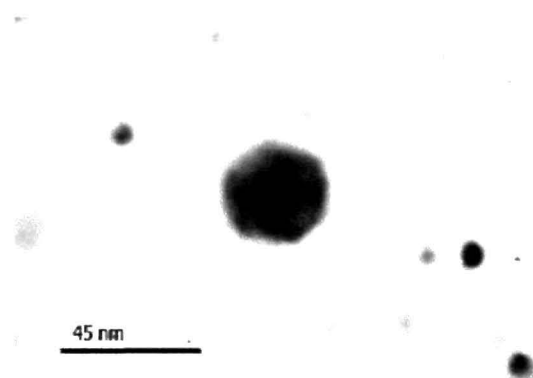


Figure 5.4: TEM micrograph of iron oxide nanoparticles synthesized at 650 °C

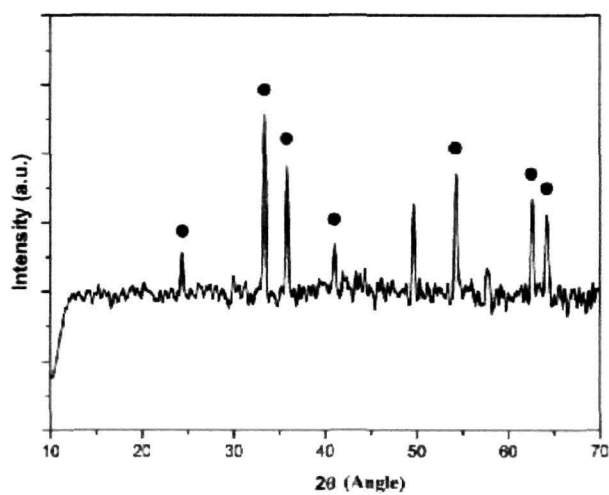


Figure 5.5: XRD analysis of iron oxide nanoparticles

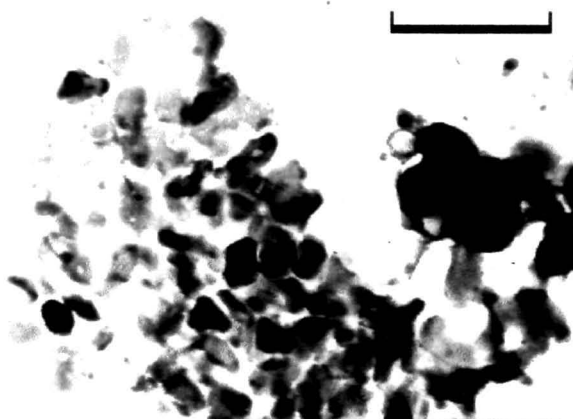


Figure 5.6: TEM micrograph of nickel oxide nanoparticles synthesized at 650 °C
(Scale inset = 100 nm)

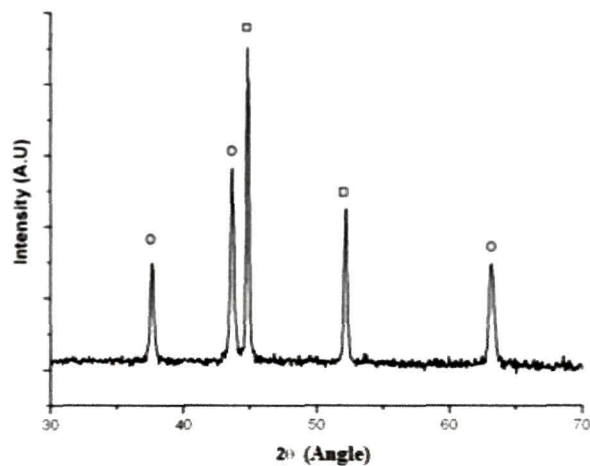


Figure 5.7: XRD analysis of nickel oxide nanoparticles

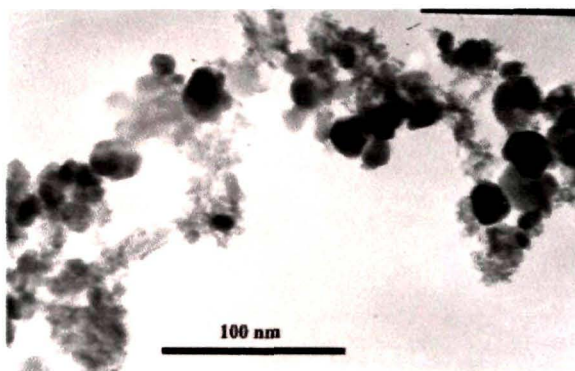


Figure 5.8: TEM micrograph of cobalt oxide nanoparticles synthesized at 650 °C.

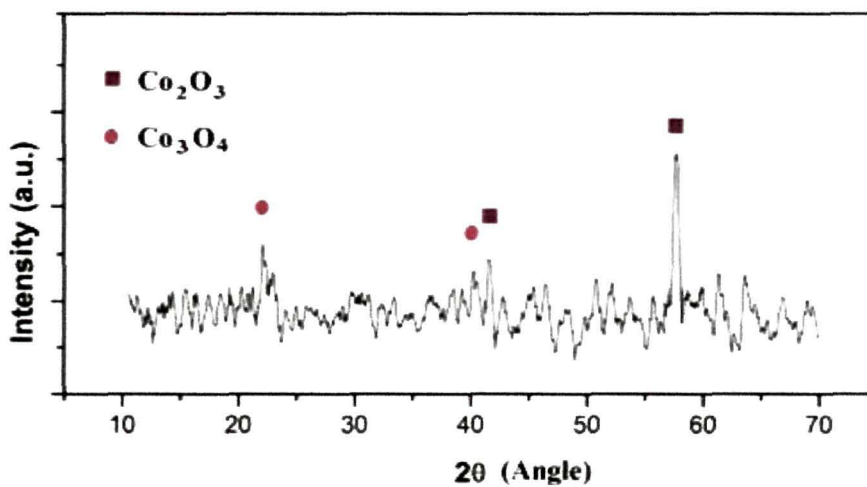
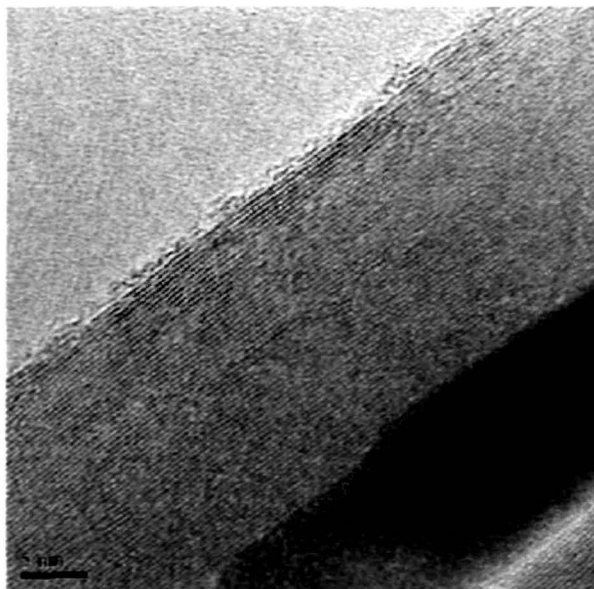


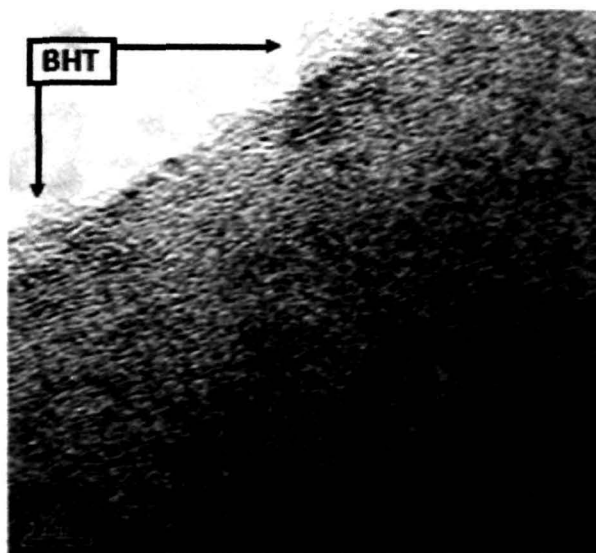
Figure 5.9: XRD analysis of cobalt oxide nanoparticles

5.3.1.4. Characterization of BHT grafted MWCNTs

The TEM micrograph of the pristine MWCNTs and the BHT grafted MWCNTs are shown the figure 5.10 (a) and (b) respectively. The presence of BHT may be seen on the walls of the nanotube. This suggests that BHT has been attached on the surface of the MWCNT walls successfully.



(a) Pristine MWCNT



(b) BHT grafted MWCNT

Figure 5.10: TEM image of (a) pristine and (b) BHT grafted MWCNTs

Fourier Transform Infrared Spectroscopy (FTIR) results of BHT, pristine MWCNT and BHT grafted MWCNTs are shown in the figure 5.11. All the samples contains moisture as evident from the peak at 3630 cm^{-1} . FTIR spectrum of pristine MWCNTs shows peaks at 1640 cm^{-1} and 1177 cm^{-1} are due to C=C and C-C of graphitic layers of the tubes. BHT shows peaks at 3069 cm^{-1} , $2956 - 2844\text{ cm}^{-1}$ and 1436 cm^{-1} corresponds to '=C-H' stretching, 'C-CH₃' stretching and 'CH₃' bending. The BHT grafted MWCNT show peaks at 1640 cm^{-1} and 1177 cm^{-1} corresponding to C=C and C-C. of graphitic structure of tubes. The peaks at $2956 - 2844\text{ cm}^{-1}$ and 1436 cm^{-1} may be due to BHT grafted on the walls of the nanotube structure. The 'C-O' stretching is evident in BHT at 1756 cm^{-1} is absent in BHT grafted MWCNT sample. This may be due to removal of oxygen from BHT molecule while it is attached to the MWCNT wall. The grafting of BHT in MWCNT showed reduced peak intensities w.r.t transmittance obtained for BHT. The FTIR confirms the attachment of BHT in MWCNT walls.

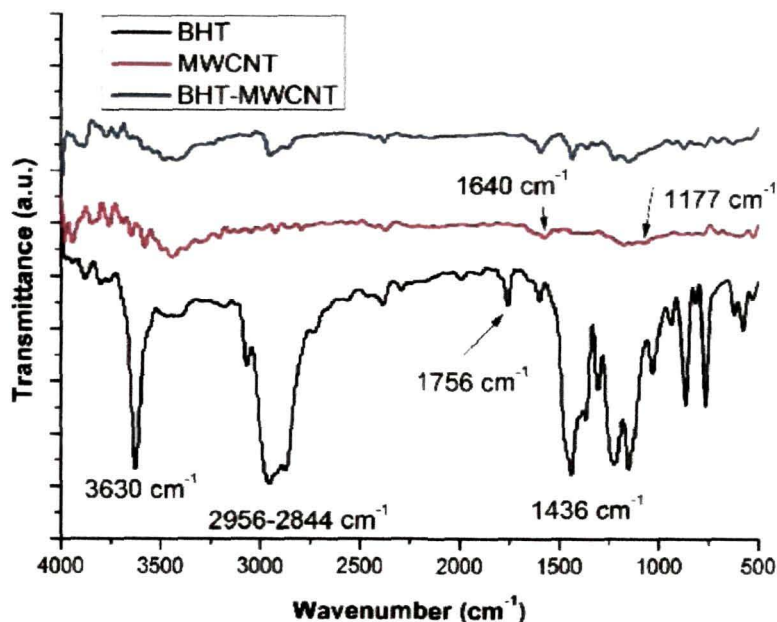


Figure 5.11: FTIR of BHT, pristine MWCNT and BHT grafted MWCNT

5.3.2. Antioxidant potency assay

The antioxidant potency estimation of individual metal oxide nanoparticles has also been carried out. It is expected to help in designing the proposed antioxidant. The method discussed in section 5.2.6 is followed to explore the antioxidant potency of the nanoparticles. The nanoparticles quenched the DPPH^o free radicals in a time-dependant manner (Figure 5.12). The DPPH^o scavenging activities for iron-oxide nanoparticles is higher as compared to cobalt and nickel oxide nanoparticles. For direct comparison SC 50 values are calculated from the absorbance value. SC 50 is defined is the amount of sample required for 50% scavenging of the free radicals. The SC 50 values of the metal oxide samples calculated were 37.98 mg/ml, 64.44 mg/ml and 149.89 mg/ml for iron oxide, nickel oxide and cobalt oxide nanoparticles, respectively. The results show that the antioxidant potency of iron oxide nanoparticles is highest among the three metal oxides tested. Though, macroscopic particles of iron, cobalt and nickel oxides are known oxidants but the result reveals that at nano-scale the oxidant nature of these metal oxides revert to antioxidant. Though the potency of these metal oxide nanoparticles were very less as compared to BHT (SC 50_{BHT} =12.0 mg/l). Out of these the metal oxides iron suits the best as it shows better antioxidant potency compaired to other metal oxides used and is magnetic in nature. Based on the study, it is obvious to use iron oxide nanoparticles in the proposed antioxidant as “magnetic particle”. The observed antioxidant property might be due to the neutralization of free-radical character of DPPH^o by transfer of an electron by these nanomaterials [19].

The antioxidant potency of the proposed grafted antioxidant was also done (figure 5.12). They also showed antioxidant activity. The antioxidant potency of BHT grafted MWCNT is higher than the metal oxides, as evident from the graph. The SC 50 value of the BHT grafted MWCNT is found to be 14.45 mg/ml. Antioxidant properties of BHT grafted MWCNT particles implies feasibility of their use in increasing the longevity of strategic materials (like biodiesel, edible oil, paint, rubber and its composites). The proposed antioxidant was thus found to be potent and was finally tested for biodiesel storage as discussed in the next section.

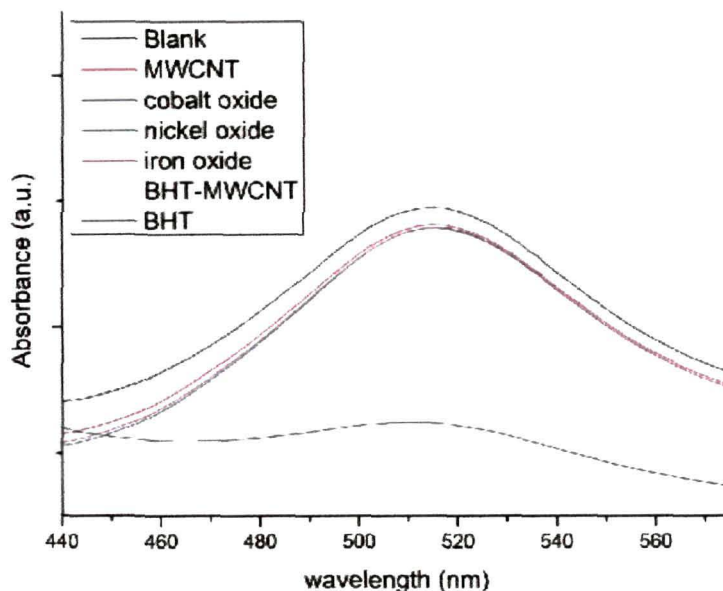


Figure 5.12: Antioxidant potency assay of synthesized nanoparticles and prepared nanocomposite showing absorbance after 45 min. ultrasonication with DPPH.

5.3.3. Oxidation stability analysis

BHT grafted MWCNTs nanoparticles scavenge free radicals in vitro. The antioxidant potency of these nanoparticles were tested long term storage of *Mesua ferrea* biodiesel. During the degradation process (oxidation of biodiesel) volatile organic acids, predominantly formic acid is blown out of the reaction tube which is allowed to pass through the cell and get absorbed in the water. As discussed, this increases the conductivity of water in the conductivity measurement cell and stable oils will result in less conductivity in the conductivity measurement cell in a specific period of time and at a specific temperature and vice versa. Figure 5.13 shows the graphical representation of conductivity-time data obtained from the conductivity measuring cell for the nanoparticles. The rate of degradation (oxidation) of the control and the biodiesel containing BHT grafted MWCNTs mixture is slow at the beginning of the experiment as evident from figure 5.13. With time the degradation

of the oils increases in all the samples. In comparison to the control the oil sample containing BHT grafted MWCNT nanoparticles showed less degradation (oxidation). The nanocomposite containing biodiesel show enhanced stability from the very beginning. The prominent difference in the conductivity in control from the oil samples containing nanoparticles suggests that nanoparticles have significantly increases the stability of the biodiesel. Though, the addition of the nanoparticles could not stop the degradation completely, but, addition of the proposed antioxidant nanocomposite is found to be potent antioxidant as it could enhance the stability of the biodiesel substantially. As the potency of iron oxide nanoparticles is very less, it could not stop the oxidation process.

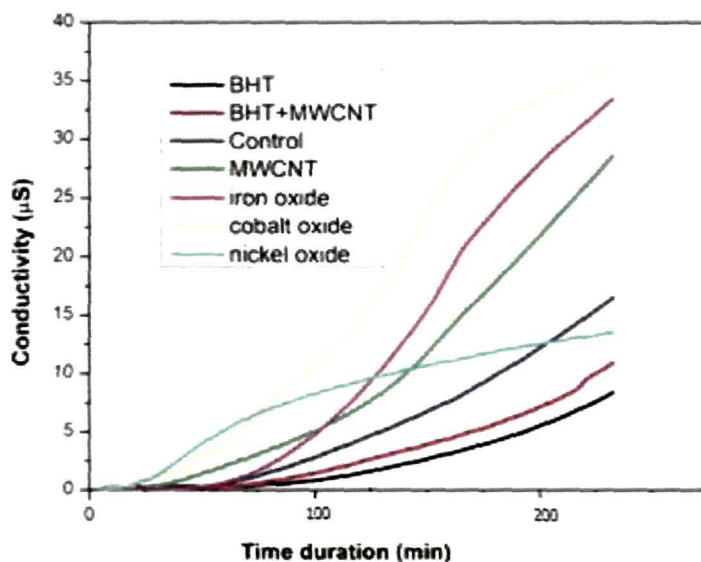


Figure 5.13: Rancimat oxidation stability test of biodiesel, at 110° C.

The induction time (the time that elapses until the start of oxidation) for the samples obtained by Rancimat method were 233.15 min, 187.2 min, 122.01 min, 114.80 min, 60.32 min, 41.20 min, 31.83 min for BHT, BHT grafted MWCNT, Control, MWCNT, iron oxide, nickel oxide and cobalt oxide respectively. The prepared antioxidant showed antioxidant activity and could control oxidation of biodiesel. The potency of the prepared nanoparticle composite is less than the BHT but it could be compensated by adding more amount of nanocomposite in the biodiesel. The enhanced amount of antioxidants may not have any bad effect as it is designed to be

removed before end use. For separating the BHT grafted MWCNT from the oil sample magnetic field may be applied. A test was conducted for this by keeping the samples in ethanol medium. Figure 5.14 (a) and 5.14 (b) respectively show the effect of before and after the application of magnetic field.

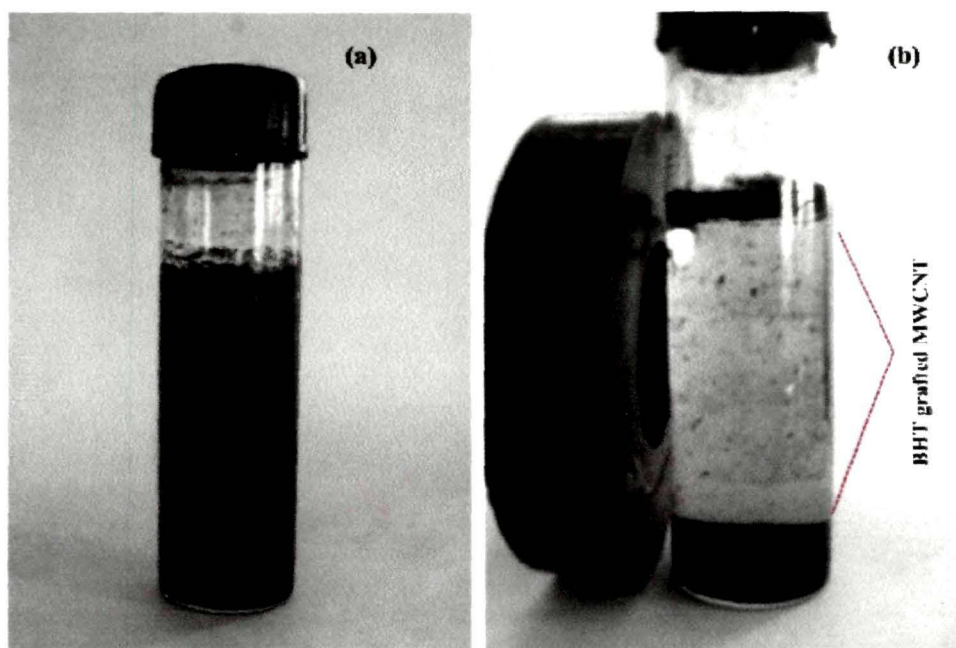


Figure 5.14: BHT grafted MWCNT in ethanol (a) before and (b) after application of magnetic field to demonstrate the magnetic severability of the antioxidants

5.4. Conclusion

The study shows that the metal oxide nanoparticles (iron oxide, nickel oxide and cobalt oxide) scavenge free radicals but, the antioxidant potency of the metal oxide nanoparticles is feeble as compared to BHT. The SC 50 values for the metal oxide nanoparticles obtained were 37.98 mg/ml, 64.44 mg/ml and 149.89 mg/ml for iron oxide, nickel oxide and cobalt oxide nanoparticles, respectively. The variation in surface area due to size of the difference in size of the metal oxide nanoparticles may be ignored because of large differences in the SC 50 values.

The grafting of BHT in MWCNT was successfully demonstrated. The BHT grafted MWCNT showed higher potency compared to the metal oxides with SC 50

value of 14.45 mg/ml. It is established that the proposed nanoparticle may be used as antioxidant. The degradation study of *Mesua ferrea* biodiesel is studied and it is found that BHT grafted MWCNTs is a potent antioxidant and can enhance the shelf life of biodiesels. The potency of BHT grafted MWCNT is less than BHT but, this can be overcome by increasing the amount of the nanoparticle in the biodiesel sample for storage. It has been demonstrated that the nanoparticles can be separated magnetically. This is the primary study where an heterogeneous antioxidant is used, thus there is no result for direct comparison is available.

References

1. Moure, A., et al. Natural antioxidants from residual sources, *Food Chemistry* **72**(2), 145-171, 2001.
2. Ali, S. S., et al. Indian medicinal herbs as sources of antioxidants, *Food Research International*, **41**(1), 1-15 2008.
3. Alía, M., et al. Effect of grape antioxidant dietary fiber on the total antioxidant capacity and the activity of liver antioxidant enzymes in rats, *Nutrition Research* **23**(9), 1251-1267, 2003.
4. Gulçin, I. et al. Radical scavenging and antioxidant activity of tannic acid, *Arabian Journal of Chemistry*, **3** (1), 43-53, 2010.
5. Ozsoy, N., et al. Yanardag, In vitro antioxidant activity of *Amaranthus lividus* L., *Food Chemistry*, **116**(4), 867-872, 2009.
6. Morillas-Ruiz, J.M., et al. Effects of polyphenolic antioxidants on exercise-induced oxidative stress, *Clinical Nutrition* **25**(3), 444-453 2006.
7. Vicente, G., et al. Integrated biodiesel production: a comparison of different homogeneous catalysts systems, *Bioresource Technology* **92**, 297-305, 2004.
8. Bouaid, A., et al. Production of biodiesel from bioethanol and *Brassica carinata* oil: Oxidation stability study, *Bioresource Technology* **100**, 2234-2239, 2009.
9. Guzman, R-de., et al. Synergistic Effects of Antioxidants on the Oxidative Stability of Soybean Oil- and Poultry Fat-Based Biodiese, *J. Am. Oil Chem. Soc.* **86**, 459-467, 2009.
10. Tang, H., et al. The Effect of Natural and Synthetic Antioxidants on the Oxidative Stability of Biodiese, *J. Am. Oil Chem. Soc.* **85**, 373-382, 2008.
11. Kim, S. J. et al. Antimicrobial effects of silver nanoparticles Nanomedicine: Nanotechnology, *Biology and Medicine* **3**(1), 95-101, 2007.
12. Esumi, K., and Takei, N., Antioxidant-potentiality of gold-chitosan nanocomposites, *Colloids and Surfaces B: Biointerfaces* **32**(2), 117-123, 2003.
13. Serpen, A., et al. A New Procedure To Measure the Antioxidant Activity of Insoluble Food Components, *J. Agric. Food Chem* **55**, 7676-7681, 2007.
14. Pouliquen, D., et al. Investigation of the magnetic properties of iron oxide nanoparticles used as contrast agent for MRI, *Magnetic Resonance in Medicine* **24**(1), 75-84, 1992

15. Ahmed, S. R., and Kofinas P. Magnetic properties and morphology of block copolymer-cobalt oxide nanocomposites, *Journal of Magnetism and Magnetic Materials* **288**, 219-223, 2005
16. Ahmad, T. et al. Magnetic and electrochemical properties of nickeloxide nanoparticles obtained by the reverse-micellar route, *Solid State Sciences* **8**(5), 425-430, 2006
17. Sharma, O. P., and Bhat, T. K. DPPH antioxidant assay revisited, *Food Chemistry* **113**(4), 1202-1205, 2009
18. Shahat, A. A. Chemical Composition, Antimicrobial and Antioxidant Activities of Essential Oils from Organically Cultivated Fennel Cultivars *Molecules* **16**, 1366-1377, 2011.
19. Naik, G. H., et al. Comparative antioxidant activity of individual herbal components used in Ayurvedic medicine, *Phytochemistry* **63**, 97-104, 2001

Chapter 6

Conclusion and future work

Chapter 6

Conclusion and future work

6.1. Conclusion

The work reported in the thesis basically pertains to utilize the unique characteristics of one of the highly potent nanomaterial in the form of carbon nanotube synthesized from plant based precursors. For this the synthesis characterization details of the CNT from a range of precursors have been presented. Finally CNTs have been successfully utilized in two important applications: solar photovoltaics and biodiesel storage. Based on the results presented in the thesis following specific conclusion may be drawn.

- i. Out of a number of plant species selected for obtaining plant precursors six could be screened based on oil content. All the six screened plant precursors were found to yield MWCNTs. It is evident from the characterization of the MWCNTs synthesized from plant precursors that the fatty acid composition in the oils affects the morphology and yield of the MWCNT.
- ii. Iron oxide nanoparticles synthesized using solution combustion method (650°C, with an aging time of 1.0 h at 80 °C) was found to be an effective catalyst for MWCNT synthesis using plant precursors too.
- iii. The necessary modification in the CVD setup was effectively incorporated to reduce the energy intensity of the system. The modified setup could enhance the amount of precursor used in each batch. The modified CVD is found to be a more effective design to be used for synthesis of MWCNTs using plant based precursors.
- iv. The parameters for the CNT synthesis using plant precursors were optimized using Taguchi robust method. It was found that the structural features of carbon nanotubes depend on the nature of carbon precursor, catalyst, flowrate, reaction temperature and time. Based on statistical analysis it was found that the

morphology and yield depends on synthesis temperature, flow rate and catalyst had major impact in the yield. The study showed that the precursors having oleic acid yield shorter length MWCNT as compared to those precursors which did not have oleic acid. The quality of CNT tubular structure is found to have minor defects when synthesized with oleic acid bearing precursors. Two precursors, *Sesamum indicum* oil and *Ricinus communis* oil were screened out to be the potent precursors for optimum yield of MWCNTs. The optimized condition of 875° C (synthesis temperature) iron oxide nanoparticles (catalyst), and 150 cc/min (flow rate) was found to be the optimum condition for higher yield. *Sesamum indicum* oil produces MWCNTs of short length but has better quality tubular structures and therefore, these MWCNTs may find application in organic solar cells. *Ricinus communis* oil on the other hand, may be used to develop fuel cell electrodes and as substrate to hold catalysts, as it resulted in high aspect ratio MWCNT compared to MWCNTs synthesized using *Sesamum indicum*.

- v. A modified process for functionalization and cutting of MWCNT was demonstrated. It was found that acid etching at elevated temperature (60° C) along with ultrasonication yielded uniform length cut-MWCNTs. The incorporation of defects due to etching is clearly visible using TEM micrograph. The attachment of functional groups in the walls is confirmed using FTIR analysis.
- vi. The pristine MWCNTs and fc-MWCNTs were successfully utilized in OPV cells showing an increase of 22.22 % and 40.00% in the power conversion efficiency, respectively. This increase is attributable to increase in J_{sc} due to enhanced hole collection and transport along and increase in V_{oc} due to enhancement in shunt resistance. The cutting of the MWCNTs reduced the probability of shorting the electrodes and hence were successfully incorporated in the OPV structure.
- vii. The study on antioxidant activity of different nanomaterials for biodiesel storage reveals that the metal oxide nanoparticles (iron oxide, nickel oxide and cobalt oxide) scavenge free radicals. The antioxidant potency of these metal oxides is feeble as compared to BHT. The grafting of BHT on MWCNT was successfully demonstrated. The BHT grafted MWCNT showed higher

antioxidant potency compared to the metal oxides. It is established that the proposed nanoparticle may be used as antioxidant for biodiesel storage. The degradation study of *Mesua ferrea* biodiesel is studied and it is found that BHT grafted MWCNTs is a potent antioxidant and can enhance the shelf life of biodiesels. The potency of BHT grafted MWCNT is less than BHT but, this can be overcome by increasing the amount of the this nanoparticle in the biodiesel sample for storage. This is the primary study where a heterogeneous antioxidant is used, thus there is no result for direct comparison is available.

- viii. Finally magnetic separation of the BHT grafted MWCNT was demonstrated. Thus separability and possible reutilization of the materials adds a new dimension to biodiesel storage.

6.2. Future work

From the study it is found that renewable plant based oils have great potential as precursors for CNTs. The scope of this thesis could not cover all the available plant species in the region. The first work would be studying more plant species for synthesis of CNTs. The aim and objective of this thesis dwells on synthesis of CNTs from plant sources, but synthesis of other strategic nanoforms of carbon (viz. graphene, nanofibers, nanobeeds) needs to be studied. The optimization of yield of CNTs was only studied in detail, but, the quality also plays important role in some of the applications. A detailed study on the quality of MWCNTs synthesized from these precursors is required. It may be done through Raman study.

The use of fc-MWCNT showed enhancement in performance of OPV devices. Recent reports on the use of highly photoactive materials (viz. P3HT, HDMO-PPV, Tetraphenylporphyrin) has been demonstrated in OPV cells. The use of these photoactive compounds along with fc-MWCNTs could show better results and hence will be studied in future.

The BHT-grafted MWCNT was found to be potent separable and possible reusable antioxidant. The effect of moisture and other ambient parameters during storage also affects the antioxidant potency. The proposed antioxidant is to be tested in real-time situation for bio-diesel storage. Grafting of other antioxidants will be another area of interest.

Appendix I

Synthesis of CNTs from waste Polypropylene and Polyethylene terephthalate products

A process for synthesizing carbon nanotubes from non-biodegradable waste **Polypropylene (PP) and Polyethylene terephthalate (PET)** product is demonstrated. This novel technique has the potential to counter the increasing environmental pollution due to waste plastic products.

A1.1 Introduction

Interest in laboratory – scale synthesis and industrial production of carbon nanotubes (CNTs) has grown enormously in recent years. As numerous new applications of CNTs are being proposed in the areas of power electronics, semiconductor materials, composites, biomedical applications, electrical energy storage, chemical energy storage, microwave applications, etc and so forth the need for large scale production. Many of the precursors (raw material for synthesis of CNTs) and processes hitherto used for CNT synthesis are valuable and environmentally incongruous. As a result, the product and the yield are unacceptable and insufficient in terms of quality and quantity, respectively. The proposed work provides a solution to the adverse environmental impact of generation of large amount of debris in the form of used plastic drinking cups, bottle caps, drinking straws, food trays, outer containers etc. made of PP/PETE for the past few decades. The recycling of these materials for further use aggravates the environmental problem further as the product is considered to be more hazardous than the precursor material itself.

The possibility of use of waste PP and PETE products like - bottles, straws, outer container etc as precursor for synthesis of CNTs is an exciting alternative. Proper and high value addition to waste PP and PETE products provides an alternative route for green development, as well.

The detail of the process and products are presented.

A1.2 Synthesis of CNTs from PP and PETE

The waste PP and PETE products (cups, straw and bottles) were collected. Both PP and PETE wastes were cleaned with warm water (95° C) to remove dirt, dust and organic matter followed by open drying. After this they were cut into small pieces.

The synthesis of CNT was carried out separately for PP and PETE respectively, using iron oxide nanoparticles as catalyst in the basic CVD setup discussed earlier. Nitrogen gas was used as the carrier gas during the synthesis at a flow rate of 150 cc/min while the temperature was varied in a range of 650° C – 1100° C. 10 g of precursor (PP or PETE) was used in each batch for CNT synthesis. The synthesized CNT samples were taken out and kept in 6M NaOH solution for 15 minuits. Thereafter, the CNTs were collected by centrifugation and were washed several times with double distilled water. The process was repeated using 6M HCl for complete removal of catalyst particles.

A1.3 Results and discussion

Synthesis of CNT using PP: The experimental results show that the yield of CNT (from PP) varies with temperature and flow rate for the carrier gas.

The effect of temperature: The synthesis at a temperature bellow 650 °C doesn't yield CNT by the procedure mentioned. At higher temperatures (above 1000 °C) also the yield is affected adversely as it decreases significantly. Thus, during experiment it was found that the economical working temperature for CNT synthesis using PP as a precursor ranged from 650 °C to 1100 °C. The experiments reveals that 800 °C to 900 °C is the best temperature for the synthesis of CNT using PP precursor.

The effect of flow rate: Carrier gas plays a very important role in the synthesis of CNT using CVD technique. As mentioned before, it is not only used to make the atmosphere inert but it is used as a carrier gas to carry evaporated precursor from Furnace I to Furnace II as well. The flow rate controls the rate at which the precursor to be introduced in Furnace II. It flow rates (below 100 cc/min) inadequate amount of precursor is introduced and hence yield becomes very less. Similarly, for higher flow rate of carrier gas (above 200 cc/min) the carrier gas flushes out all the evaporated

precursor and hence yield again reduces. The best flow rate for the synthesis of CNT from PP precursor was found out to be 150 cc/min.

The best condition for CNT synthesis using PP as precursor:

Temperature: 800 °C to 900 °C

Flow rate of carrier gas: 150 cc/min.

The TEM micrograph of CNT synthesized using PP is shown in figure A1.1. The three variants of MWCNT are easily seen - A bamboo type MWCNT of about 40 nm diameter, another high aspect ratio MWCNT of 40 nm diameter and the third MWCNT of 20 nm in diameter. These variations may be ascribed to the variations in the iron oxide nanoparticles used for synthesis.

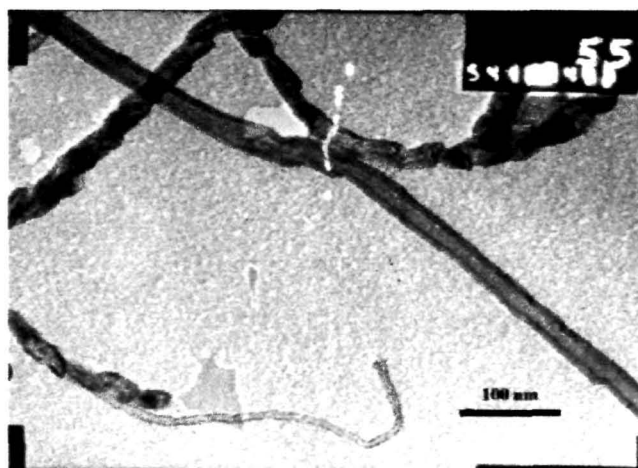


Figure A1.2: TEM micrograph of CNT synthesized using PP at 950°C

Synthesis of CNT using PETE: The variation in yield of CNT from PETE with temperature and flow rate is identical to that of PP.

The effect of temperature: The effect of temperature in the synthesis of CNT from PETE is found to be similar to the results obtained for PP. At both lower temperature (below 600° C) and higher temperature (above 1000 °C) the yield is not significant. Optimum yield for the synthesis of CNT using PETE precursor was found at a temperature range of 800 °C to 900 °C.

The effect of flow rate: The optimum flow rate for the synthesis of CNT using PETE precursor was found out to be 150 cc/min. Similarly, for PETE, the impact of flow rate of gas was found to play major role in the yield of CNTs.

Table AI.1: Experimental data for synthesis of CNTs using PP

For the synthesis of CNTs 10 g of cut PP was placed in the quartz bot.				
Sl/No.	Temperature of the main furnace (°C)	Flow rate of the inert carrier gas (cc/min)	Unpurified CNT Yield (% wt.)	Purified CNT Yield (wt % wrt PP used)
1	650	100	10.0	1.5
2		150	11.5	1.5
3		200	11.9	1.6
4	800	100	29.7	3.9
5		150	31.4	3.9
6		200	30.3	3.1
7	950	100	40.1	4.5
8		150	44.9	4.6
9		200	41.2	4.2
10	1100	100	33.6	4.1
11		150	37.1	3.7
12		200	34.3	3.6

The best condition for CNT synthesis using PETE as precursor:

Temperature: 900 °C

Flow rate of carrier gas: 150 cc/min

The TEM micrograph of CNT synthesized using PETE is shown in figure A1.2. The TEM micrograph reveals the synthesized tubes to be MWCNTs. The synthesized MWCNT have high aspect ratio with a diameter of about 20-30 nm. Some growth on the surface and the trapped catalyst indicate towards need of extended purification.

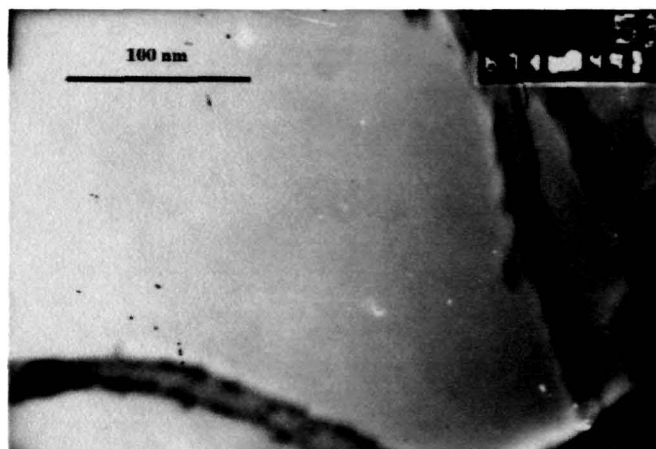


Figure A1.2: TEM micrograph of CNT synthesized using PETE at 950° C

Table-A1.2: Experimental data for CNT synthesis using PETE

For the synthesis of CNTs 10 g of cut PET was placed in the quartz bot.				
Sl/No.	Temperature of the main furnace (°C)	Flow rate of the inert carrier gas (cc/min)	Unpurified CNT Yield (% wt.)	Purified CNT Yield (wt % wrt PETE used)
1	650	100	15.4	1.8
2		150	18.9	1.9
3		200	16.1	1.5
4	800	100	31.2	4.0
5		150	35.1	4.2
6		200	34.9	4.2
7	950	100	45.6	4.5
8		150	48.4	4.6
9		200	43.5	4.5
10	1100	100	39.7	4.1
11		150	40.4	4.3
12		200	38.9	4.1

A1.4 Conclusion

The results show that waste PP and PETE products could be used as potential precursors for CNT synthesis. The process of recycling PP and PETE waste into precious product (in terms of MWCNT) is achieved. The technique is novel with high value addition to waste which is threatening to be environmental menace. It can be adopted by Municipality Corporations to handle environmental problems.

Appendix II

Application of MWCNT in Alkaline fuel cell electrode

The present work aims to develop fuel cell electrodes using MWCNTs synthesized from renewable plant precursor (*Ricinus communis* oil). Through a systematic procedure MWNTs were grown over porous substrate. The electrodes were fabricated with Pt-catalyst and were finally tested for current-voltage characteristics.

A2.1 Introduction

Hydrogen is considered to be the future fuel, because of its high energy density and environment friendly nature. The cleanest method of conversion of chemical energy of hydrogen into electrical energy is through fuel cells. But the fuel cell technology needs improvement. One of the important factors is efficiency due to improper gas diffusion and low surface area for the reaction in the electrodes. The use of CNTs by researchers showed improved performance. The present work is to study the applicability of CNTs synthesized from renewable plant precursor (*Ricinus communis* oil). For better gas diffusion quartz fiber filter paper was selected as substrate. The quartz fiber filter paper is selected for its resistance to high temperature (~1000° C). Thus, it is possible to synthesis CNT on the filter paper without destroying its porous nature.

A2.2 Fabrication of electrode-conducting carbon layer

Quartz fiber filter paper (grade QR-200, Merck India) is insulator and can not conduct electrons from the surface active sites of the electrode to the external connections, conducting carbon thin layer was deposited over it using Chemical Vapour Deposition (CVD) technique at 900° C, followed by deposition of iron oxide nanoparticles detailed as follows.

A2.3 Deposition of catalyst on substrate

Iron oxide nanoparticles were deposited over carbon coated quartz fiber filter paper. The iron oxide nanoparticles would act as catalyst for the synthesis of CNTs. A mixture of iron nitrate and urea (1:3) and was deposited using spray pyrolysis technique. The substrate was finally heated at 450° C for 15 min.

A2.3 Synthesis of CNT on substrate and loading of Pt catalyst

The synthesis of CNT using *Ricinus communis* oil was done using CVD technique at 850° C, as described in Chapter 2. Pt-catalyst was pasted on the CNT grown electrode substrate using Pt-paste (Platisol T, Solaronix, Switzerland) by spray technique. The Pt loaded substrate was heated at 105° C to adhere platinum nanoparticles on the surface of the CNT walls. The fabricated substrates was used is hydrogen as well as oxygen electrode.

A2.4 Results and discussion

The figure A2.1 shows the TEM micrograph of Pt-loaded CNT (scratched out of electrode for TEM analysis). The presence of Pt-catalyst on the CNT surface is evident. In the figure it is evident that some of the Pt particles came out of the CNT surface during sample preparation. The figure A2.1 (inset) reveals that few particles still adhered to the surface of the CNTs. Figure A2.2 shows pictorial view of the electrode substrate, a) electrode substrate after iron oxide coating and b) fabricated electrode substrate after loading of Pt catalyst on CNT.

A cell was constructed using the electrodes fabricated. 30% KOH solution is used as electrolyte in the cell. Hydrogen gas was passed over the Hydrogen –electrode, while air is pumped in to the oxygen–electrode. The voltage-current characteristic of the cell is shown in the figure A2.3. The cell was scanned from 0.0-0.5 A, the open circuit voltage of 0.95 V is evident from the voltage-current curve. A very high activation overvoltage and ohmic overvoltage is observed in the characteristics. It shows a need for substantial refinement in the fabrication procedure.

A2.5 Conclusion

The study shows that the quartz fiber filter paper may be used as a substrate for fuel cell electrode. The porous nature provides uniform gas diffusion for better performance. The growth of CNTs on the filter paper was successfully done. The

loading of catalyst needs to be improved as the Pt-nanoparticles could not adhere properly on the surface of the CNTs.

The V-I characteristics confirms the working of the fabricated cell with the prepared electrode. The porous electrode provides a gas diffusion layer while the MWCNTs provide high surface area for the redox reactions. Thus MWCNT synthesized from *Ricinus communis* oil may be used to fabricate alkaline fuel cell electrode.

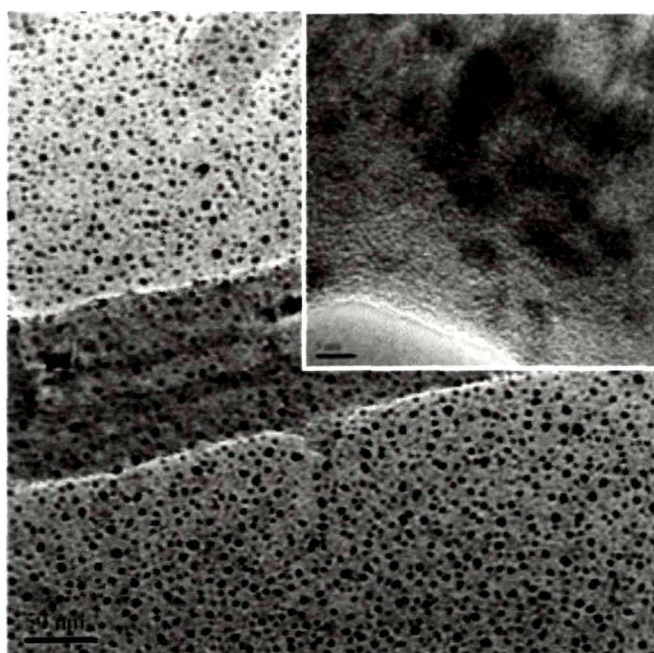


Figure A2.1: The TEM micrograph of Pt-loaded CNT on the electrode substrate

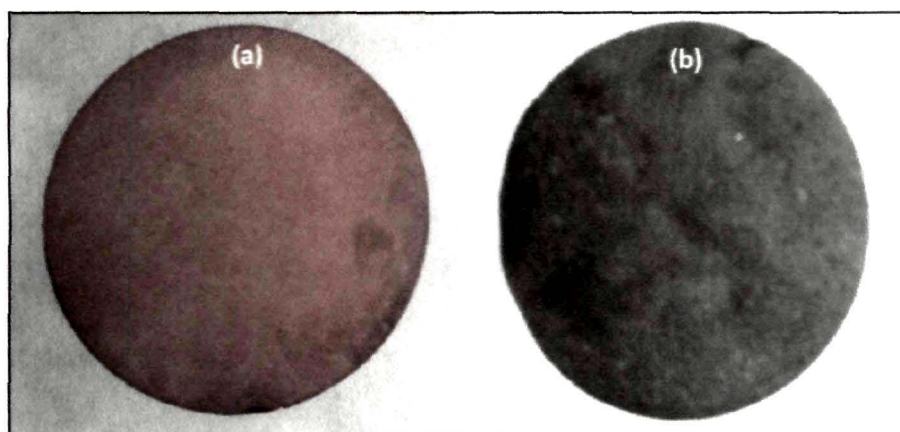


Figure A2.2: Photograph of the electrode substrate, a) electrode substrate after iron oxide coating and b) fabricated electrode substrate after loading of Pt catalyst on CNT.

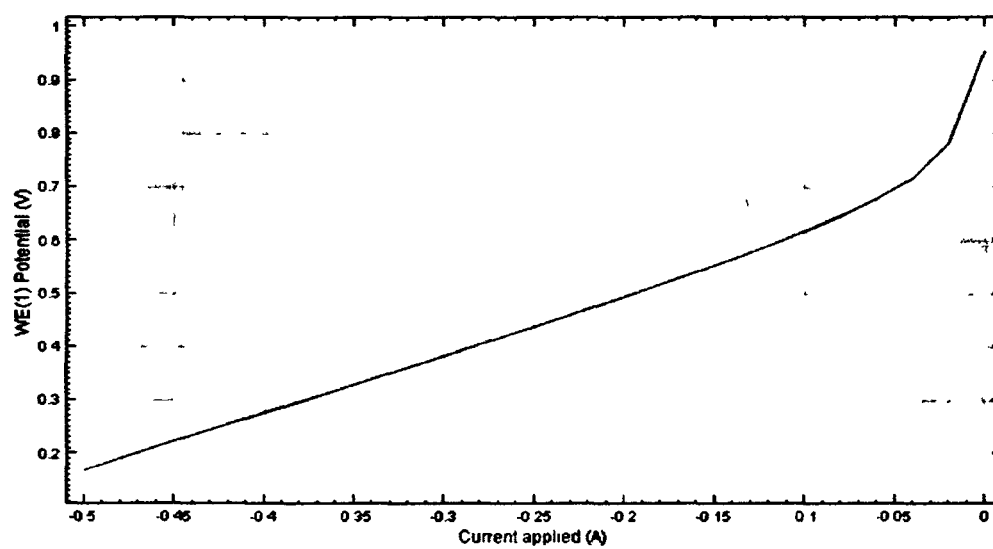


Figure A2.3: Voltage-current characteristics of the fabricated electrode